

NASA/TP-2015-218765



Re-Computation of Numerical Results Contained in NACA Report No. 496

Boyd Perry, III
Langley Research Center, Hampton, Virginia

June 2015

NASA STI Program . . . in Profile

Since its founding, NASA has been dedicated to the advancement of aeronautics and space science. The NASA scientific and technical information (STI) program plays a key part in helping NASA maintain this important role.

The NASA STI program operates under the auspices of the Agency Chief Information Officer. It collects, organizes, provides for archiving, and disseminates NASA's STI. The NASA STI program provides access to the NTRS Registered and its public interface, the NASA Technical Reports Server, thus providing one of the largest collections of aeronautical and space science STI in the world. Results are published in both non-NASA channels and by NASA in the NASA STI Report Series, which includes the following report types:

- **TECHNICAL PUBLICATION.** Reports of completed research or a major significant phase of research that present the results of NASA Programs and include extensive data or theoretical analysis. Includes compilations of significant scientific and technical data and information deemed to be of continuing reference value. NASA counter-part of peer-reviewed formal professional papers but has less stringent limitations on manuscript length and extent of graphic presentations.
- **TECHNICAL MEMORANDUM.** Scientific and technical findings that are preliminary or of specialized interest, e.g., quick release reports, working papers, and bibliographies that contain minimal annotation. Does not contain extensive analysis.
- **CONTRACTOR REPORT.** Scientific and technical findings by NASA-sponsored contractors and grantees.

- **CONFERENCE PUBLICATION.** Collected papers from scientific and technical conferences, symposia, seminars, or other meetings sponsored or co-sponsored by NASA.
- **SPECIAL PUBLICATION.** Scientific, technical, or historical information from NASA programs, projects, and missions, often concerned with subjects having substantial public interest.
- **TECHNICAL TRANSLATION.** English-language translations of foreign scientific and technical material pertinent to NASA's mission.

Specialized services also include organizing and publishing research results, distributing specialized research announcements and feeds, providing information desk and personal search support, and enabling data exchange services.

For more information about the NASA STI program, see the following:

- Access the NASA STI program home page at <http://www.sti.nasa.gov>
- E-mail your question to help@sti.nasa.gov
- Phone the NASA STI Information Desk at 757-864-9658
- Write to:
NASA STI Information Desk
Mail Stop 148
NASA Langley Research Center
Hampton, VA 23681-2199

NASA/TP-2015-218765



Re-Computation of Numerical Results Contained in NACA Report No. 496

Boyd Perry, III
Langley Research Center, Hampton, Virginia

National Aeronautics and
Space Administration

Langley Research Center
Hampton, Virginia 23681-2199

June 2015

Acknowledgments

The author wishes to acknowledge the valuable contributions to this paper made by Mr. Thomas G. Ivanco of the NASA Langley, Aeroelasticity Branch and Mr. G. Lee Pollard of NCI Information Systems, Inc.

Mr. Ivanco is a very talented engineer. While on a one-year active-duty assignment with the U.S. Army Reserve, during his off-duty time, he very generously performed all of the independent flutter calculations used as check cases in this paper.

Mr. Pollard is a very talented graphic designer. He assembled the re-computed results generated by the present author, electronically scanned all the original figures from *NACA 496*, merged the two in figures 5 through 17, and produced all the final figures in this paper.

Mr. Ivanco's and Mr. Pollard's skills and enthusiasm made my interactions with them not only very productive, but also very enjoyable. Many thanks to you both!

<p>The use of trademarks or names of manufacturers in this report is for accurate reporting and does not constitute an official endorsement, either expressed or implied, of such products or manufacturers by the National Aeronautics and Space Administration.</p>

Available from:

NASA STI Program / Mail Stop 148
NASA Langley Research Center
Hampton, VA 23681-2199
Fax: 757-864-6500

ABSTRACT

An extensive examination of NACA Report No. 496 (*NACA 496*), “General Theory of Aerodynamic Instability and the Mechanism of Flutter,” by Theodore Theodorsen, is described. The examination included checking equations and solution methods and re-computing interim quantities and all numerical examples in *NACA 496*. The checks revealed that *NACA 496* contains computational shortcuts (time- and effort-saving devices for engineers of the time) and clever artifices (employed in its solution methods), but, unfortunately, also contains numerous tripping points (aspects of *NACA 496* that have the potential to cause confusion) and some errors. The re-computations were performed employing the methods and procedures described in *NACA 496*, but using modern computational tools. With some exceptions, the magnitudes and trends of the original results were in fair-to-very-good agreement with the re-computed results. The exceptions included what are speculated to be computational errors in the original in some instances and transcription errors in the original in others. Independent flutter calculations were performed and, in all cases, including those where the original and re-computed results differed significantly, were in excellent agreement with the re-computed results. Appendix A contains *NACA 496*; Appendix B contains a Matlab[®] program that performs the re-computation of results; Appendix C presents three alternate solution methods, with examples, for the two-degree-of-freedom solution method of *NACA 496*; Appendix D contains the three-degree-of-freedom solution method (outlined in *NACA 496* but never implemented), with examples.

I. INTRODUCTION

In a year 2000 engineering note, Zeiler [1] pointed out that several of the foundational papers and texts in aeroelastic flutter [2 through 6] contain numerical errors in some of their example problems. It is not surprising that such errors exist because – especially in the cases of references 2, 3, and 4, written in the 1930’s and 40’s – all calculations were performed “by hand” with pencil and paper, slide rules, and, after they were invented, large table-top four-function electro-mechanical calculators.

Because these foundational papers and texts are often used in graduate courses on aeroelasticity, Zeiler recommended that an effort be undertaken to employ the computing resources available today to re-calculate the example problems and to publish the results so as to provide a complete and error-free set of example problems. Following Zeiler’s recommendation, the purpose of this paper is to provide re-computed results for the example problems presented in reference 2: NACA Report No. 496, “General Theory of Aerodynamic Instability and the Mechanism of Flutter,” by Theodore Theodorsen (referred to hereinafter simply as “*NACA 496*”). Future papers will provide re-computed results for references 3 and 4.

In order to perform the re-computation of its numerical examples, an extensive study of *NACA 496* was undertaken by the present author. The study entailed many parts, including reading and re-reading the paper, checking and re-checking its equations, and checking and re-checking its solution method. In the process, the present author discovered in *NACA 496* computational shortcuts (time- and effort-saving devices for engineers of the time) and clever artifices employed in its solution methods. Unfortunately,

the present author also discovered, via tripping, several tripping points (aspects of *NACA 496* that have the potential to cause confusion) and errors. These items are discussed in the present paper.

In reference 1, Zeiler stated “One does not set about lightly to correct the masters ...” Embracing this notion, the present results have been carefully checked and re-checked, and, as a further check, for some of the numerical examples, independent calculations were performed by a colleague. In all cases, including those where the original and present results differed significantly, the independent calculations were in excellent agreement with the present results, providing additional confidence in the present results.

The arrangement of the remainder of the present paper is as follows:

Section II contains preliminaries, which are intended to aid in the understanding of the remainder of this paper.

Section III contains an overview of *NACA 496*, including its theoretical development and solution method.

Section IV describes the checks performed by the present author on the equations and solution method of *NACA 496*.

Section V presents the re-computation of quantities contained in Tables I-IV of *NACA 496*.

Section VI presents the re-computation of the example problems contained in Appendix II of *NACA 496*.

Section VII contains concluding remarks.

Appendix A contains a reproduction of *NACA 496*. (Throughout the present paper the reader will be referred to Appendix A frequently.)

Appendix B contains a Matlab® program that implements the two-degree-of-freedom flutter equations and the two-degree-of-freedom solution method found in Appendix I of *NACA 496*.

Appendix C contains descriptions of, and example problems for, three alternate solution methods for the two-degree-of-freedom flutter equations presented in *NACA 496*.

Appendix D contains a description of, and example problems for, the three-degree-of-freedom flutter equations presented in *NACA 496*.

II. PRELIMINARIES

As stated in the Introduction of the present paper, the information contained in this section is intended to aid in the understanding of the remainder of this paper.

Terminology

The present paper refers to sections and appendices within itself and sections and appendices within *NACA 496*. The present paper also refers to the authors of both papers. To avoid confusion in regard to which paper or author is being referred to, the following (unfortunately but necessarily) awkward-sounding convention is adopted: for the present paper, the terms “present paper,” “this paper,” “main body,” “Appendix A, B, C, or D of the present paper,” and “present author” are used; for *NACA 496*, the terms “*NACA 496*,” “main text,” “Appendix I, II, or III of *NACA 496*,” and “author of *NACA 496*,” are used.

Symbology

The present paper retains the symbology of *NACA 496*. Appendix A of the present paper (the reproduction of *NACA 496*) contains a symbol list (pp. 9 and 10 of *NACA 496*). Symbols not contained in the list are defined as they are used in *NACA 496* and as they are used in the present paper.

Tripping Points and Errors

As used in the present paper, the term “tripping point” is defined to be an aspect of *NACA 496* that has the potential to cause confusion for a reader of *NACA 496*. Tripping points that the present author encountered while reading *NACA 496* are identified throughout the present paper and are collected in Table I of the present paper.

Errors in some of the equations, tables, and figures of *NACA 496* were found by the present author. These errors are identified throughout the present paper and are collected in Table II of the present paper.

Three versions of *NACA 496*

The author of the present paper had access to three different versions of *NACA 496*. At the conclusion of their respective main texts, all three versions contain the following lines of text

“LANGLEY MEMORIAL AERONAUTICAL LABORATORY,
NATIONAL ADVISORY COMMITTEE FOR AERONAUTICS,
LANGLEY FIELD, VA., *May 2, 1934.*”

indicating that all three are “the same” report. This common date is important, as will be seen below.

The first version of *NACA 496* was in hard-copy form and was contained in the bound volume “Twentieth Annual Report of the National Advisory Committee for Aeronautics,” which contains the significant findings of NACA for fiscal year 1934 (July 1933 through June 1934). The page numbering (pages 413 to 433) in this version reflects the fact that *NACA 496* was one of many papers in the bound volume. Errors in some of the equations, tables, and figures were found (by the present author) to exist in this version.

The second version was in electronic form and was acquired from the NASA Technical Report Server website (<http://ntrs.nasa.gov>). This version was a reprint of the first version and was issued as a stand-alone report. The date on the cover of this version is 1949. The page numbering in this version (pages 3 to 23) reflects the fact that it was a stand-alone report. Some of the errors found in the first version are corrected in the second version.

The third version was also a hard-copy version, was also a stand-alone report, and was acquired from the NASA-Langley technical library. Pages 3 to 23 in this version are identical to those in the second version, but the date on the cover of the third version is 1940.

The first tripping point for the present author was the fact that there are three versions of the paper, each with a different publication date. A second tripping point was that some of the errors in the first version were corrected in the second and third versions, but no known errata was issued by NACA, as confirmed by the staffs of the NASA-Langley and NASA-Ames technical libraries. (Errors from the first version that were not corrected in the second and third versions, and therefore remain in the second and third versions, will be discussed throughout the present paper.)

The third version, a corrected version, is contained in Appendix A of the present paper.

Referring to Equations

NACA 496 contains many equations, but only a minority is identified by letters or numbers. In the main text, capital Roman letters and Roman and Arabic numerals, all within parentheses, are used as identifiers. In Appendix I of *NACA 496*, Arabic numerals within parentheses are used as identifiers; in addition, some terms are identified by Arabic numerals, but without parentheses. In what would be very unconventional by today’s report-writing standards, within *NACA 496*, there are multiple instances of different equations being identified using the same equation number.

In the present paper, references to specific equations in *NACA 496* will cite the *NACA 496* page and equation numbers. For example, equation (A) on page 10, equation (XXI) on page 12, and equation (9) on page 14 would be identified herein as “equation (10/A),” “equation (12/XXI),” and “equation (14/9),” respectively.

Equations in the present paper are identified by Arabic numerals within parentheses.

Computational Shortcuts

Given the very rudimentary computational aids of the early 1930's (paper and pencil, slide rules, four-function electro-mechanical calculators), it is natural to deduce that in the construction of their solution methods engineers of the time would have sought ways to minimize the overall number and/or to simplify the complexity of calculations so as to minimize the human time and effort required to obtain a solution. It should not be surprising, then, that such time- and effort-saving techniques are evident in the *NACA 496* solution method. These techniques will be given the general term "computational shortcuts." They will be identified throughout the present paper and are collected in Table III of the present paper.

III. OVERVIEW OF NACA REPORT No. 496

NACA 496 lays out the theoretical development of aeroelastic flutter for a typical section with degrees of freedom in torsion (α), aileron deflection (β), and vertical deflection (at times referred to in *NACA 496* as flexure) (h). *NACA 496* has three appendices: Appendix I presents a detailed description of the steps of the implementation of the solution procedure, including tables of numerical values of quantities required in the solutions; Appendix II presents a number of numerical calculations, including a few comparisons with experimental data; and Appendix III presents integral evaluations for some of the velocity potentials.

Theoretical Development

In *NACA 496*, the theoretical development begins with four simplifying assumptions: (1) the flow is potential and non-stationary; (2) the "wing" is actually a two-dimensional typical section with no thickness and therefore with no airfoil shape; (3) the "wing" motions are sinusoidal and infinitesimal; and (4) the "wing" has no internal or solid friction, resulting in no internal damping forces.

Next, the circulatory and non-circulatory velocity potentials are developed. The magnitude of the circulation, in the form of Theodorsen's circulation function, is developed. After this, the aerodynamic forces and moments are determined via the chordwise integration of the velocity potentials. Then, the aerodynamic forces and moments are combined with the inertia and restraining forces and moments to produce three second-order differential equations in the three unknowns α , β , and h , equations (10/A), (10/B), and (10/C), reproduced here:

$$\begin{aligned}
\text{(A)} \quad & \ddot{\alpha} \left[r_\alpha^2 + \kappa \left(\frac{1}{8} + a^2 \right) \right] + \dot{\alpha} \frac{v}{b} \kappa \left(\frac{1}{2} - a \right) + \alpha \frac{C_\alpha}{Mb^2} + \ddot{\beta} \left[r_\beta^2 + (c-a)x_\beta - \frac{T_7}{\pi} \kappa - (c-a) \frac{T_1}{\pi} \kappa \right] + \frac{1}{\pi} \dot{\beta} \kappa \frac{v}{b} \left[-2p - \left(\frac{1}{2} - a \right) T_4 \right] \\
& + \beta \kappa \frac{v^2}{b^2} \frac{1}{\pi} (T_4 + T_{10}) + \ddot{h} \left(x_\alpha - a\kappa \right) \frac{1}{b} - 2\kappa \left(a + \frac{1}{2} \right) \frac{vC(k)}{b} \left[\frac{v\alpha}{b} + \frac{\dot{h}}{b} + \left(\frac{1}{2} - a \right) \dot{\alpha} + \frac{T_{10}}{\pi} \frac{v}{b} \beta + \frac{T_{11}}{2\pi} \dot{\beta} \right] = 0 \\
\text{(B)} \quad & \ddot{\alpha} \left[r_\beta^2 + (c-a)x_\beta - \kappa \frac{T_7}{\pi} - (c-a) \frac{T_1}{\pi} \kappa \right] + \dot{\alpha} \left(p - T_1 - \frac{1}{2} T_4 \right) \frac{v}{b} \frac{\kappa}{\pi} + \ddot{\beta} \left(r_\beta^2 - \frac{1}{\pi} \kappa T_3 \right) - \frac{1}{2\pi^2} \dot{\beta} T_4 T_{11} \frac{v}{b} \kappa \\
& + \beta \left[\frac{C_\beta}{Mb^2} + \frac{1}{\pi^2} \frac{v^2}{b^2} \kappa (T_5 - T_4 T_{10}) \right] + \ddot{h} \left(x_\beta - \frac{1}{\pi} \kappa T_1 \right) \frac{1}{b} + \frac{T_{12}}{\pi} \kappa \frac{vC(k)}{b} \left[\frac{v\alpha}{b} + \frac{\dot{h}}{b} + \left(\frac{1}{2} - a \right) \dot{\alpha} + \frac{T_{10}}{\pi} \frac{v}{b} \beta + \frac{T_{11}}{2\pi} \dot{\beta} \right] = 0 \\
\text{(C)} \quad & \ddot{\alpha} \left(x_\alpha - \kappa a \right) + \dot{\alpha} \frac{v}{b} \kappa + \ddot{\beta} \left(x_\beta - \frac{1}{\pi} T_1 \kappa \right) - \dot{\beta} \frac{v}{b} T_4 \kappa \frac{1}{\pi} + \ddot{h} (1 + \kappa) \frac{1}{b} + h \frac{C_h}{M} \frac{1}{b} \\
& + 2\kappa \frac{vC(k)}{b} \left[\frac{v\alpha}{b} + \frac{\dot{h}}{b} + \left(\frac{1}{2} - a \right) \dot{\alpha} + \frac{T_{10}}{\pi} \frac{v}{b} \beta + \frac{T_{11}}{2\pi} \dot{\beta} \right] = 0
\end{aligned}$$

where $C(k)$, Theodorsen's circulation function, is a complex function of reduced frequency, k . Equation (10/A) defines the sum of the moments about the elastic axis; equation (10/B), the sum of the moments about the aileron hinge; and equation (10/C), the sum of the forces on the entire "wing" in the vertical direction. Upon examination of equations (10/A) through (10/C) one sees that k appears only implicitly in $C(k)$ while velocity, v , appears multiple times.

Figure 1 in the present paper is a re-drawn figure 2 from *NACA 496*. It illustrates the definitions and positive senses of many of the important physical parameters appearing in the equations of motion.

Assumed forms of the unknowns, α , β , and h . - The assumed forms of the unknowns in equations (10/A) through (10/C) are introduced in *NACA 496* as sine functions of the distance, s , traveled by the wing from the first vortex element. Employing the distance formula, $s = vt$, the sine functions in complex form may be expressed as:

$$\alpha = \alpha_0 e^{ik \frac{v}{b} t} \quad (1a)$$

$$\beta = \beta_0 e^{i(k \frac{v}{b} t + \varphi_1)} \quad (1b)$$

$$h = h_0 e^{i(k \frac{v}{b} t + \varphi_2)} \quad (1c)$$

where α_0 , β_0 , and h_0 are the (infinitesimal) amplitudes of α , β , and h , and φ_1 and φ_2 are phase angles of β and h with respect to α . The first and second time derivatives of α , β , and h are:

$$\dot{\alpha} = ik \frac{v}{b} \alpha \text{ and } \ddot{\alpha} = -\left(k \frac{v}{b}\right)^2 \alpha$$

$$\dot{\beta} = ik \frac{v}{b} \beta \text{ and } \ddot{\beta} = -\left(k \frac{v}{b}\right)^2 \beta$$

$$\dot{h} = ik \frac{v}{b} h \text{ and } \ddot{h} = -\left(k \frac{v}{b}\right)^2 h$$

Substitution of assumed forms into, and normalization of, equations. - Making the substitutions of equations (1a) through (1c) and their time derivatives into equations (10/A) through (10/C) transforms the latter equations from three simultaneous differential equations into three simultaneous algebraic

equations. The algebraic equations are then normalized by the quantity $\kappa \left(\frac{v}{b}k\right)^2$ and by their respective exponentials and amplitudes, resulting in the equations taking the form

$$(A_{a\alpha} + \Omega_\alpha X)\alpha + A_{a\beta}\beta + A_{ah}h = 0 \quad (2a)$$

$$A_{b\alpha}\alpha + (A_{b\beta} + \Omega_\beta X)\beta + A_{bh}h = 0 \quad (2b)$$

$$A_{c\alpha}\alpha + A_{c\beta}\beta + (A_{ch} + \Omega_h X)h = 0 \quad (2c)$$

The physical constants of the problem ($\kappa, a, b, c, x_\alpha, r_\alpha, x_\beta, r_\beta, \omega_\alpha, \omega_\beta$, and ω_h) reside in the coefficients, that is in the A 's and the ΩX terms.

The quantities $A_{a\alpha}$, etc. are complex functions of reduced frequency, k , with real parts $R_{a\alpha}$, etc. and imaginary parts $I_{a\alpha}$, etc. The real parts are defined in equations (12/1) through (12/9) and the imaginary parts in equations (12/11) through (12/19). (There is no equation (12/10). This equation numbering convention was chosen in *NACA 496* so that for any given imaginary part, the second digit in its two-digit equation number would be the same as the single-digit equation number of its corresponding real part.)

The ΩX terms are discussed next.

Products $\Omega_\alpha X$, $\Omega_\beta X$, and $\Omega_h X$. - In equations (2a), (2b), and (2c) the products $\Omega_\alpha X$, $\Omega_\beta X$, and $\Omega_h X$ are real. They are derived from quantities $\frac{C_\alpha}{Mb^2}$ (from eqn. (10/A)), $\frac{C_\beta}{Mb^2}$ (from eqn. (10/B)), and $\frac{C_h}{Mb}$ (from eqn. (10/C)), respectively. Via the substitution and rearrangement of terms and the use of cancelling expressions in the numerator and denominator, from page 12 of *NACA 496* these products are

$$\Omega_\alpha X = \frac{C_\alpha}{k^2 M v^2 \kappa} = \left(\frac{\omega_\alpha r_\alpha}{\omega_r r_r}\right)^2 \frac{1}{\kappa} \left(\frac{b r_r \omega_r}{v k}\right)^2 \quad (3a)$$

$$\Omega_\beta X = \frac{C_\beta}{k^2 M v^2 \kappa} = \left(\frac{\omega_\beta r_\beta}{\omega_r r_r}\right)^2 \frac{1}{\kappa} \left(\frac{b r_r \omega_r}{v k}\right)^2 \quad (3b)$$

$$\Omega_h X = \frac{C_h b^2}{k^2 M v^2 \kappa} = \left(\frac{\omega_h}{\omega_r r_r}\right)^2 \frac{1}{\kappa} \left(\frac{b r_r \omega_r}{v k}\right)^2 \quad (3c)$$

where, to the right of the second equal sign in each equation, X comprises the two right-most terms

$$X = \frac{1}{\kappa} \left(\frac{b r_r \omega_r}{v k}\right)^2 \quad (4)$$

and the respective Ω 's, the remaining terms

$$\Omega_\alpha = \left(\frac{\omega_\alpha r_\alpha}{\omega_r r_r}\right)^2 \quad (5a)$$

$$\Omega_\beta = \left(\frac{\omega_\beta r_\beta}{\omega_r r_r} \right)^2 \quad (5b)$$

$$\Omega_h = \left(\frac{\omega_h}{\omega_r r_r} \right)^2 \quad (5c)$$

The quantities ω_r and r_r are a reference frequency and reference length, which may be conveniently chosen.

Referring back to the normalization that produced equations (2a) through (2c), a critically important result of the normalization is that the quantity X has been conveniently isolated from the other terms in these equations and X is the only quantity in these equations that contains the velocity. The *NACA 496* solution methods take advantage of this result in an ingenious way. As will be seen immediately below, X and the Ω 's are clever artifices created by the author of *NACA 496* to enable the determination of the flutter velocity, v_f , and flutter reduced frequency, k_f . At times X and the Ω 's are treated not as the known quantities expressed in equations (4) and (5), but rather as parameters. At other times X and the Ω 's are treated as the known quantities.

Solution Methods

The solution of equations (2a), (2b), and (2c) is obtained when their determinant is zero

$$\begin{vmatrix} A_{a\alpha} + \Omega_\alpha X & A_{a\beta} & A_{ah} \\ A_{b\alpha} & A_{b\beta} + \Omega_\beta X & A_{bh} \\ A_{c\alpha} & A_{c\beta} & A_{ch} + \Omega_h X \end{vmatrix} = 0 \quad (6)$$

The form of equation (6), $\det(A + X\Omega) = 0$, bears some resemblance to the characteristic polynomial of the eigenvalue problem, $\det(A - \lambda I) = 0$. The quantity X in eqn. (6) would be analogous to λ in the eigenvalue problem and the quantity Ω , a 3x3 diagonal matrix with diagonal elements Ω_α , Ω_β , and Ω_h , would be analogous to the identity matrix. However, in terms of the solution of equation (6), this is where its resemblance to the eigenvalue problem ends.

Expanding the determinant in equation (6) yields equation (12/XXI), re-written here

$$\begin{aligned} &\Omega_\alpha \Omega_\beta \Omega_h X^3 + (\Omega_\alpha \Omega_\beta A_{ch} + \Omega_\beta \Omega_h A_{a\alpha} + \Omega_h \Omega_\alpha A_{b\beta}) X^2 \\ &+ (\Omega_\alpha M_{a\alpha} + \Omega_\beta M_{b\beta} + \Omega_h M_{ch}) X + D = 0 \end{aligned} \quad (7)$$

which is third-order in X with complex coefficients. In equation (7), D is the determinant in equation (6) without the ΩX terms and the M 's are the minors of the determinant without the ΩX terms. Except for Ω_α , Ω_β , and Ω_h , all quantities in equation (7) are functions of reduced frequency, k .

The object of the solution method is to find the values of v and k that cause equation (7) to be satisfied. Such values are then identified as v_f and k_f , the flutter velocity and the flutter reduced frequency, respectively.

Three-degree-of-freedom solution method. – *NACA 496* outlines the method by which the three-degree-of-freedom flutter problem (that it names the “general case”) may be solved.

NACA 496 does not recommend solving directly the third-order equation with complex coefficients (eqn. (7)). Instead, it suggests the computational shortcut of creating two equations, each with real coefficients, by separating the real and imaginary parts of the original. The first equation is cubic in X and is obtained from the real parts of the A ’s, M ’s, and D ; the second is quadratic in X and is obtained from the imaginary parts. The right hand side of both equations is zero. This separation of a complex equation into its real and imaginary parts eliminates complex arithmetic from the solution method.

At this point in the solution method, the artifice of treating X as a parameter, rather than as a known quantity, is employed. The cubic and quadratic equations are each solved for their roots, identified herein as $X_{R_1}, X_{R_2}, X_{R_3}, X_{I_1}$, and X_{I_2} for a large number of reduced frequencies. The X_R ’s and X_I ’s are then plotted on the same set of axes as functions of the inverse of reduced frequency. Intersections of any of the X_R ’s with any of the X_I ’s identify the values of X and the values of reduced frequency, which simultaneously satisfy the cubic and quadratic equations, and therefore also solves the original third-order equation with complex coefficients. These values are the flutter values - X_f and k_f .

With X_f and the k_f known, the artifice of treating X as a parameter is now abandoned and equation (4) is employed, which when re-written to solve for flutter velocity, becomes

$$v_f = \frac{1}{\sqrt{X_f}} \frac{1}{\sqrt{\kappa}} \frac{b\omega_r r_r}{k_f} \quad (8)$$

where κ and b are known constants of the problem and ω_r and r_r are chosen reference values.

Although many illustrative examples are presented in Appendix II of *NACA 496* none are given for the general case, almost certainly due to the difficulty in the early 1930’s of solving “by hand” a cubic equation.

Two-degree-of-freedom solution method. – There are three two-degree-of-freedom subcases available from the three-degree-of-freedom equations: torsion – aileron; aileron – flexure; and flexure – torsion. *NACA 496* lists the subcases in the order just given, but then identifies the first one listed as subcase 3, the second one listed as subcase 2, and the third one listed as subcase 1. No reason is offered in *NACA 496* for this curious pairing of listing order and subcase number.

NACA 496 presents an ingenious solution method for obtaining the flutter velocity and flutter reduced frequency for the three two-degree-of-freedom subcases. This solution method again involves computational shortcuts and the artifices, but, in yet another curiosity, this solution method differs fundamentally from the recommended solution method for three degrees of freedom.

Whereas equation (12/XXI) is the characteristic equation obtained from the expansion of the 3x3 characteristic determinant (eqn. (7) in the present paper), equations (12/XXII), (12/XXIII), and (12/XXIV) are the characteristic equations obtained from the expansion of the three 2x2 minors of the characteristic determinant. The reader is referred to Appendix A of the present paper.

Using the torsion – aileron subcase (subcase 3) as the example, *NACA 496* goes through the algebraic steps of this solution method. The algebraic steps for subcases 2 and 1 mirror those for subcase 3. Equation (12/XXII), a second-order equation in X with complex coefficients, is the starting point. *NACA 496* again employs the computational shortcut of creating two equations, each with real coefficients, by separating the real and imaginary parts of the original. The first equation is quadratic in X and is obtained from the real parts of $A_{a\alpha}$, $A_{b\beta}$, and M_{ch} ; the second is linear in X and is obtained from the imaginary parts. The right hand side of both equations is zero.

At this point the two-degree-of-freedom solution method departs from the three-degree-of-freedom solution method, but like the latter solution method it also employs the artifices: it treats both X and Ω_α as parameters, rather than as the known quantities in equations (4) and (5a). The quadratic and linear equations and parameters X and Ω_α are treated as two equations in two unknowns and are solved conventionally by substitution.

From page 13 in *NACA 496*, the first step is to solve the linear equation for X , yielding

$$X = -\frac{M_{ch}^I}{\Omega_\alpha I_{b\beta} + \Omega_\beta I_{a\alpha}} \quad (9)$$

This expression is then substituted into the quadratic equation in X , thereby eliminating X from that equation and producing, after several steps, equation (13/XXV), which is quadratic in Ω_α and re-written here

$$\begin{aligned} \Omega_\alpha^2 (M_{ch}^R I_{b\beta}^2 - M_{ch}^I R_{b\beta} I_{b\beta}) + \Omega_\alpha [-M_{ch}^I (R_{a\beta} I_{b\alpha} + I_{a\beta} R_{b\alpha}) + 2M_{ch}^R I_{a\alpha} I_{b\beta}] \\ + M_{ch}^R I_{a\alpha}^2 - M_{ch}^I R_{a\alpha} I_{a\alpha} = 0 \end{aligned} \quad (10)$$

Equation (10) is then solved for its two roots, Ω_{α_1} and Ω_{α_2} , for a large number of reduced frequencies.

With the artifice still in place, but recognizing from equation (5a) that Ω_α is defined as the square of a quantity, only the real positive values of Ω_{α_1} and Ω_{α_2} and their corresponding reduced frequencies are retained. A plot of Ω_α as a function of $1/k$, which contains both Ω_{α_1} and Ω_{α_2} , is produced.

Next, values of X are found by substituting the values of Ω_α , just obtained, their corresponding values of reduced frequency, and the values of M_{ch}^I , $I_{a\alpha}$ and $I_{b\beta}$, at corresponding reduced frequencies, into equation (9). *NACA 496* chooses to present the quantity X as a function of Ω_α rather than as a function of $1/k$.

At this point a new quantity, F , the nondimensional flutter factor, is introduced

$$F = \frac{1}{k} \sqrt{\frac{1}{X}} \quad (11)$$

F is also treated as a parameter. Substituting into equation (11) the X 's and their corresponding reduced frequencies produces a plot of F as a function of Ω_α , again containing both Ω_{α_1} and Ω_{α_2} .

The two curves, Ω_α vs. $1/k$, and F vs. Ω_α , represent a family of flutter solutions for a range of Ω_α 's. Each point on the first curve has a corresponding point on the second and each pair of corresponding points represents a unique flutter solution.

To obtain a specific flutter solution from the family of solutions, the artifice is abandoned: quantities Ω_α , X , and F are no longer interpreted as parameters and equations (5a) and (4) are employed. In addition, when the expression in equation (4) is substituted for X in equation (11), the flutter factor becomes

$$F = \frac{\sqrt{\kappa}v}{b\omega_r r_r} \quad (12)$$

When solved for flutter velocity, equation (12) becomes

$$v_f = F \frac{b\omega_r r_r}{\sqrt{\kappa}} \quad (13)$$

Thus, once a family of flutter solutions is obtained, the following simple two-step process for obtaining a specific flutter solution from the family of solutions is performed:

First, problem-specific values of ω_α , r_α , ω_r , and r_r are substituted into equation (5a), yielding a problem-specific value of Ω_α . This value of Ω_α is located in the plot of Ω_α vs. $1/k$. The value of $1/k$ corresponding to this value of Ω_α then yields, via its inverse, the flutter reduced frequency, k_f .

Second, the problem-specific value of Ω_α is located in the plot of F vs. Ω_α . The value of F corresponding to this value of Ω_α and problem-specific values of b , ω_r , r_r , and κ are substituted into equation (13), yielding the flutter velocity, v_f .

IV. CHECKS OF NACA 496 EQUATIONS AND SOLUTION METHOD

Beginning with equations (10/A), (10/B), and (10/C) in the "DIFFERENTIAL EQUATIONS OF MOTION" section of *NACA 496*, the present author checked all of the equations in the main text and Appendix I. With a few exceptions, discussed below, all equations checked.

Missing $1/b$ Factors in Expressions on Page 12

In checking the equations in *NACA 496*, the present author duplicated 12 of the 18 expressions in the left column on page 12. However, as they appear in *NACA 496*, the real expressions in equations (12/3), (12/6) and (12/9) and the imaginary expressions in equations (12/13), (12/16) and (12/19) each lack a factor of $1/b$ compared to what the present author found. These six expressions make up the entirety of equation (10/C) and none of the six appears in either equation (10/A) or equation (10/B).

As it turns out, the missing $1/b$ factors are of no consequence because the left-hand side of an equation whose right-hand side is zero, such as equation (10/C), may be multiplied by any factor without changing the equation. The present author believes that, as a computational shortcut, the author of *NACA 496* multiplied both sides of equation (10/C) by the semi-chord, b , thus eliminating the $1/b$ factor from equations (12/3), (12/6), (12/9), (12/13), (12/16), and (12/19) and thereby relieving engineers of the time of extra, but unnecessary, multiplications in the hand calculations of these expressions.

Comparing Real Expressions in Main Text and Appendix I

The real expressions in the left column on page 12 (main text), the real expressions in the right column on page 14 (Appendix I), and the real expressions in the left column on page 15 (Appendix I), term-by-term, share the same equation numbers. This assignment of equation numbers is a potential tripping point because, term-by-term, the expressions obviously differ from each other. As it turns out, the expressions on page 12 are, term-by-term, equal to the sums of the respective expressions on pages 14 and 15. In checking the equations the present author reproduced all of these expressions.

Table III on page 17 in Appendix I contains a range of values for the expressions in equations (14/1) through (14/9).

Comparing Imaginary Expressions in Main Text and Appendix I

The imaginary expressions in the left column on page 12 (main text) correspond to the imaginary expressions in the right column on page 14 (Appendix I). A cursory examination of these equations suggests the identity of corresponding expressions because: (1) the same symbols for the I 's ($I_{a\alpha}$, $I_{b\beta}$, I_{ch} , etc.) are used in both places; and (2) the same equation numbers are used in both places.

In checking the equations, the present author reproduced the expressions on page 12. However, in comparing the expressions on page 12 with those on page 14, it is seen that each expression on page 12 contains a multiplying factor of $1/k$ while those on page 14 do not. As with the omission of the factor of $1/b$ previously discussed, it turns out that the omission of $1/k$ is also ultimately of no consequence, and for the same reason. As with the $1/b$ omission, the present author believes that the $1/k$ omission was also done deliberately by the author of *NACA 496* as another computational shortcut, again relieving engineers of an extra, but unnecessary, multiplication in the hand calculation of these expressions.

The author of *NACA 496* does alert the reader to these differences in the l 's, but via a whisper, not a shout: a footnote on the bottom of page 14. No explanation is given as to why $1/k$ has been eliminated, yet the elimination has important consequences in the equations employed in the solution method. The differences represented a significant tripping point for the present author, who initially missed the footnote.

Table IV on page 17 in Appendix I contains a range of values for the expressions in equations (14/11) through (14/19) (that is, the expressions without the $1/k$ factor).

Comparing Equations for Solution Method in Main Text and Appendix I

The *NACA 496* solution method is derived beginning at the bottom of the left column on page 12 and continuing through the end of the main text on page 13. The procedure for implementing the solution method is contained in Appendix I on pages 14 through 16. These parts of *NACA 496* will be referred to as the derivation section and the implementation section, respectively.

The solution method involves solving quadratic equations whose coefficients (a , b , and c) contain numerous sums and differences of products of the R 's and l 's and other terms. The other terms are the real and imaginary parts of the minors of the characteristic determinant (M^R_{ch} , M^R_{aa} , M^R_{bb} , and M^I_{ch} , M^I_{aa} , M^I_{bb} , and referred to hereinafter as “real minors” and “imaginary minors”), which also contain sums and differences of products of the R 's and l 's.

As mentioned above, to take advantage of a computational shortcut, all the l 's in the implementation section had their common $1/k$ factor eliminated. For clarity these l 's without the $1/k$ factor will be called “new l 's.” The new l 's and any quantities involving the new l 's (the real and imaginary minors and the quadratic coefficients a , b , and c) are all affected by the elimination of the $1/k$ factor.

This situation would have caused no confusion had new symbols (perhaps original symbols with tildes) been introduced in *NACA 496* to represent the new l 's. The original symbols could have been used in the derivation section; the new symbols in the implementation section. However, the author of *NACA 496* chose not to do this; he chose to retain the original symbols in the implementation section and in so doing assigned each symbol two meanings, with each meaning specific to a given section of the paper.

However, with careful attention to section-specific definitions and by doing a little algebra, it is easy to prove that the quadratic coefficients in the implementation section are proportional, term-by-term, to the quadratic coefficients in the derivation section, with proportionality constant $1/k^2$. Thus, because multiplying either equation (both of whose right-hand sides are zero) by the proper quantity (either k^2 or $1/k^2$) will produce the other, both equations will yield the same roots, and therefore the same values of v_f and k_f .

V. RE-COMPUTATION OF QUANTITIES EMPLOYED IN NACA 496 SOLUTION METHOD

NACA-496 contains four tables of quantities needed in the implementation of the *NACA-496* solution method. For the engineer of the time, these tables, especially the latter two, would have saved valuable human computation time.

Constants Resulting from the Integration of Velocity Potentials

Table I in *NACA 496* contains constants, T_i , associated with integrations of the velocity potentials. These constants are functions of the nondimensional chordwise location of the aileron hinge, c . At the top of the right column on page 5 of *NACA 496* are the integrals in question and it can be seen that there are two types of integrals that produce the T_i 's: those whose limits of integration are c to 1 (integrations over the aileron only) and those whose limits are -1 to 1 (integrations over the entire "wing").

At the bottom of the right column on the same page are the equations for T_1 through T_{14} . However Table I lists only 11 of the 14 T_i 's. The omitted T_i 's (T_9 , T_{13} , and T_{14}) are also functions of a , the elastic axis location.

Figure 2 in the present paper contains comparison plots of the T_i 's listed in Table I and present calculations of the T_i 's. The open circles correspond to the tabular values, which are shown in *NACA 496* for five values of c (-1, -1/2, 0, 1/2, 1). The solid lines correspond to the present calculations, performed in Matlab® and computed from $c = -1$ to $c = 1$ in increments of 0.01. The plots show there is excellent agreement between the original results and the present results.

Theodorsen Circulation Function

Table II in *NACA 496* contains the real part, F , and the negative of the imaginary part, $-G$, of the Theodorsen circulation function and their component Bessel functions. All quantities are functions of reduced frequency, k , and are shown for 16 values of k .

Figure 3 in the present paper contains comparison plots of F and $-G$ listed in Table II and present calculations of F and $-G$. The horizontal axis is logarithmic to more clearly show (compared to what a linear axis would show) the comparisons at low values of $1/k$. A logarithmic axis "spreads out" the values of F and $-G$ at the low values of $1/k$ and compresses them at the high values of $1/k$ in such a way that the distance on the page between $1/k$ of 0.1 and 0.2 is the same as the distance on the page between $1/k$ of 10 and 20. The open circles correspond to the tabular values; the solid lines correspond to the present results, computed in Matlab® from $1/k = 0.1$ to $1/k = 40$ in increments of 0.004.

For values of $1/k$ of 5 and below there is excellent agreement between the original results and the present results. For all values of $1/k$ except 0.1, the original results and the present results differ by less than one percent. For values of $1/k$ of 10 and above the differences vary from 0.2 to 5.6 percent, with

the largest differences occurring at 10 and 40. These largest differences will produce corresponding differences seen in the illustrative examples.

Reduced-Frequency-Dependent Portions of the Elements of the Equations of Motion

Table III in *NACA 496* contains the frequency-dependent portions of the real parts of the coefficients of the equations of motion; Table IV contains the imaginary parts. All quantities in Tables III and IV are functions of reduced frequency, k . Some quantities in Tables III and IV are functions of the nondimensional chordwise location of the elastic axis, a ; other quantities are functions of the nondimensional chordwise location of the aileron hinge, c ; some quantities are functions of both; and two quantities are functions of neither. The quantities in Tables III and IV will be discussed together.

Figure 4 in the present paper contains comparison plots of the real and imaginary parts from Tables III and IV and from present calculations, again performed in Matlab®. As was the case for figure 3, in this figure the horizontal axis is logarithmic to more clearly show (compared to what a linear axis would show) the comparisons at low values of $1/k$. Figure 4(a) contains elements from the pitching moment equation; figure 4(b), from the hinge moment equation; and figure 4(c), from the vertical force equation. For the present calculations the inverse of reduced frequency ranged from $1/k = 0.1$ to $1/k = 40$, in increments of 0.0004.

The plots are for values of a and c of -0.4 and 0.5, respectively. Except for the comparison plot for R''_{ah} , which will be discussed in the next paragraphs, all comparisons show reasonably good agreement. The comparisons at values of $1/k$ of 10, 20, and 40 consistently show differences and are due to the differences in F and $-G$, discussed above.

The comparison plot for R''_{ah} in figure 4(a) shows significant differences between the original and present results. Close examination of the values in Table III reveals that, for $a = -0.4$, R''_{ah} is very nearly directly proportional to $1/k$, that is, is very nearly linear with $1/k$. To more easily see this linearity, R''_{ah} as a function of $1/k$ has been redrawn in figure 4(d) with a linear horizontal axis. A red dashed line has been added to emphasize the linear relationship between R''_{ah} and $1/k$.

If one assumes the values of R''_{ah} in Table III are correct and then employs equation (14/3) to back calculate to find the values of G necessary to produce these values of R''_{ah} , one finds that the resulting G 's are independent of $1/k$ and equal to the value of G at $1/k = 1$. (According to Table II in *NACA 496* and figure 3 in the present paper, G varies from about -0.2 to 0 and clearly is a function of $1/k$.) The R''_{ah} row of Table III corresponding to $a = -0.4$ and $c = 0.5$ is in error.

VI. RE-COMPUTATION OF ILLUSTRATIVE EXAMPLES IN *NACA 496*

This section of the paper presents the re-computation of the illustrative examples contained in Appendix II of *NACA 496*. These examples comprise all three two-degree-of-freedom subcases that may be

derived from the three-degree-of-freedom general case. *NACA 496* presents no examples for the general case.

A brief orientation to figures 5 through 17 in the present paper: figure-by-figure they contain scanned reproductions of the original figures 5 through 17 from *NACA 496*, but with the addition of the present re-computations. In all cases, the original results are in black and the re-computed results are in color. Because of “fuzziness” resulting from the scans, the figure legends for these figures have been re-typed.

Additionally, in figures 5 through 11 and 15 through 17, the colored \circ and $+$ symbols are results from the present implementation, but using the tabular values in Tables I, II, III, and IV of *NACA 496*, and the colored solid and dashed lines are results from the present implementation using present computed values throughout.

As mentioned in Section III of the present paper, the plots of Ω vs $1/k$ and F vs Ω are comprised of two values of Ω , the two quadratic roots obtained from the solution of equation (13/XXV) (as well as two values each from the solutions of eqns. (13/XXVI) and (13/XXVII)). With this in mind, the colored solid lines and the colored \circ symbols correspond to the first quadratic root; the colored dashed lines and the colored $+$ symbols correspond to the second quadratic root.

Implementation of *NACA 496* Solution Method

The implementation of the *NACA 496* solution method was performed by the present author via the writing and execution of m-files in Matlab®. The equations outlined in the main text and Appendix I of *NACA 496* were solved for 100,001 values of the inverse of reduced frequency, beginning at zero, with an increment of 0.0005.

Standard Case

Figures 5 through 10 present what *NACA 496* calls a “standard” case, represented by the quantities:

$$\kappa = 0.1; c = 0.5; a = -0.4; x_\alpha = 0.2; r_\alpha^2 = 0.25; x_\beta = \mathcal{V}_{80}; r_\beta^2 = \mathcal{V}_{160}; \text{ and } \omega_\alpha, \omega_\beta, \omega_h \text{ variable.}$$

Figures 5 and 6 present results for Subcase 3, torsion-aileron; figures 7 and 8 present results for Subcase 2, aileron-flexure; and figures 9 and 10 present results for Subcase 1, flexure-torsion.

For these three subcases, the first figure in each pair shows its respective plot of Ω versus $1/k$; the second figure in each pair shows its respective plot of F versus Ω . However, the quantity F shown in these figures is not the quantity F defined on the bottom of page 15 and the top of page 16 of *NACA 496* (and by eqn. (11) in the present paper). The quantity F shown in figures 6, 8, and 10 is actually the square of the defined quantity. This double use of a symbol to represent not only its original definition, but also the square of its original definition, represented a significant tripping point for the present author.

Subcase 3. – Figures 5 and 6 contain the results for this subcase. While there are some differences between the original and present results in these figures, the overall magnitudes and shapes of the respective curves are very similar. In figure 5, the agreement between original and present results is excellent at values of $1/k$ greater than 0.5, but progressively less so at lower values of $1/k$. In figure 6, the agreement is better at the lower values of Ω_α than at the higher values. In both figures, the present results represented by the colored symbols and colored lines exhibit excellent agreement with each other, reflecting the excellent agreement between the original tabular quantities and the present computed quantities, as illustrated in figure 4.

Subcase 2. - Figures 7 and 8 contain the results for this subcase. In each figure, there are three sets of results, labeled (a), (b), and (c), representing three different values of x_β , the center of gravity of the aileron. The original and present curves (a) and (b) in figure 7 agree fairly well in the overall magnitudes and shapes of the respective curves. However, the original and present curves (c) do not agree well in either magnitude or shape. The original and present curves in figure 8 echo the agreement and disagreement noted for the curves in figure 7. In both figures, the present results represented by the colored symbols and colored lines exhibit excellent agreement with each other, reflecting again the excellent agreement between the original tabular quantities and the present computed quantities, as illustrated in figure 4.

Subcase 1. - Figures 9 and 10 contain the results for this subcase. Once again, in these figures the original and present results are very similar in terms of the overall magnitudes and shapes of the respective curves. In figure 9, the original curve does not “touch” the vertical axis, whereas the present curve does (as did all original and present curves in figures 5 and 7). This trend is repeated in figure 10, but for the horizontal axis. The present results represented by the colored symbols and colored lines do not agree as well in figure 9 and 10 as they did in figures 5 and 6 and figures 7 and 8. These differences are due in part to the errors in R''_{ah} in Table III, and illustrated in figure 4, as previously discussed.

Parameter Variations for Subcase 1

Figures 11 through 14 contain plots of flutter factor, F , as defined on pages 15 and 16 of *NACA 496*, as functions of various parameters. Figure 11 presents results for variation in frequency ratio, ω_1/ω_2 ; figure 12, for variation in the location of the elastic axis, a ; figure 13, for variation in the radius of gyration, r_α ; and figure 14, for variation in the location of the center of gravity, x_α . All results in this subsection of the paper are for Subcase 1, flexure-torsion.

For figures 12, 13, and 14, as a check on the present results, independent calculations were performed by a colleague of the present author who implemented in Matlab® the equations found in reference 5 for a typical section, including unsteady aerodynamics defined by the Theodorsen circulation function. The code loops on velocity. For each velocity, the calculations are run through an iterative loop until the frequencies are converged, followed by an evaluation of damping values to determine if the system is stable or unstable.

To be able to directly compare the independent flutter results with the present flutter results, the independent flutter velocities were converted to flutter factors using equation (12). As will be seen below, in all cases, the present results and the independent results are in excellent agreement, differing in F by no more than 0.5% and in reduced frequency by no more than 3.7%, thereby simultaneously confirming and affording confidence in the present results.

Variation of Frequency Ratio. – The original figure 11 contains theoretical and experimental results, in black. The present results are shown in colored symbols and colored curves. The quantities specific to this example are:

$$\kappa = 1/400; \quad a = -0.4; \quad x_\alpha = 0.2; \quad r_\alpha = 0.5; \quad \omega_1/\omega_2 \text{ variable.}$$

This figure is similar to figure 10, but as already stated, the F in this figure is the as-defined F . In addition, in this figure, equation 5(c) has been employed to convert the units of the abscissa from Ω_h to ω_1/ω_2 (that is, ω_h/ω_α).

Across the limited range of frequency ratio chosen for this figure, the original theoretical results and both sets of present results are in excellent agreement. The colored symbols in the figure correspond to values of $1/k$ of 10, 20, and 40. The re-computed curve in this figure does not “touch” the horizontal axis as did the re-computed curve in figure 10 because the much smaller value of mass ratio, κ , for figure 11 changes the character of the solution.

Variation of Elastic Axis Location. – In addition to containing the dependency of F on elastic axis location, a , figure 12 also contains the dependency of a quantity D on a . According to the sign convention established in figure 2 of *NACA 496*, increasingly negative values of a corresponds to a forward movement of the elastic axis.

The quantities specific to this example are:

$$\kappa = 1/4; \quad \omega_1/\omega_2 = 1/6; \quad x_\alpha = 0.2; \quad r_\alpha = 0.5; \quad a \text{ variable.}$$

In the present effort to re-compute D as a function of a , another tripping point was encountered: D is never defined in *NACA 496*. However, the present author attempted to deduce the definition of D so that a comparison could be made between the original and the re-computed curves.

In the left column on page 16 of *NACA 496*, there is a short discussion that ends with the equations (un-numbered in *NACA 496* but numbered herein)

$$v_D = v_R \frac{1}{\frac{1}{2} + a} \quad (14)$$

$$v_F = v_R F \quad (15)$$

where a and F are defined as above, v_F is the flutter velocity, v_R is a reference velocity defined to be the divergence velocity for the specific case of the elastic axis located at the mid-chord (that occurs when $a = 0$), and v_D is the divergence velocity for other locations of the elastic axis.

Velocity v_R is a proportionality constant in equations (14) and (15). In equation (15), v_R relates the flutter velocity, v_F , to the flutter factor, F . The present author speculated that in equation (14) v_R might relate the divergence velocity, v_D , to a “divergence factor,” D . If this were so, then according to equation (14), quantity D would be equal to the inverse of $(\frac{1}{2} + a)$. As a test of this hypothesis the inverse of $(\frac{1}{2} + a)$ was plotted as a function of a . The hypothesis failed; the curve did not match curve D in figure 12. (Equation (14) is clearly incorrect because, according to the definition of v_R , when a is zero, v_D should be equal to v_R , but under this condition equation (14) predicts v_D to be twice v_R .)

This miss-match led the present author to re-derive the expression relating v_D to D , which resulted not in equation (14), but in the following expression

$$v_D = v_R \frac{1}{\sqrt{1+2a}} \quad (16)$$

When the quantity $\frac{1}{\sqrt{1+2a}}$ is plotted as a function of a , the colored dashed curve in figure 12 results. Except for an area of slight disagreement (less than 5%) between $a = -0.2$ and $a = -0.4$, the original and present curves agree with each other very well. This overall agreement led the present author to conclude that the original curve D in figure 12 represents the expression the author of *NACA 496* knew to be correct (eqn. (16)) and that the expression on page 16 of *NACA 496* (equivalent to eqn. (14)) is a misprint.

The colored circles in figure 12 represent the re-calculation of curve F . Each circle was obtained by selecting a value of a and executing the *NACA 496* solution method for Subcase 1 in which a curve similar to that in figure 10 is used to find the value of F at the following value of Ω_h -

$$\Omega_h = \left(\frac{\omega_h}{\omega_\alpha r_\alpha} \right)^2 = \left(\frac{\omega_1}{\omega_2 r_\alpha} \right)^2 = \left(\frac{\omega_1}{\omega_2} \right)^2 \left(\frac{1}{r_\alpha} \right)^2 = \left(\frac{1}{6} \right)^2 \left(\frac{1}{0.5} \right)^2 = \frac{1}{9}$$

It is obvious that the re-calculation differs markedly from the original. Not only do the numerical values significantly differ from each other, but the trends with increasingly negative values of a are opposite each other. The three large X's at values of a of -0.2, -0.3, and -0.4 are from the independent calculation and are in excellent agreement with the present calculation. The present author can offer no explanation for the significant disagreement between the present calculation and the original.

Variation of Radius of Gyration. – The original figure 13 illustrates the dependency of F on the radius of gyration, r_α , for two different values of frequency ratio, ω_1/ω_2 . Curve A corresponds to $\omega_1/\omega_2 = \frac{1}{6}$; curve B corresponds to $\omega_1/\omega_2 = 1$. Other quantities specific to this example are

$$\kappa = \frac{1}{4}; \quad a = -0.4; \quad x_\alpha = 0.2; \quad r_\alpha \text{ variable}$$

For ease of presentation and in an attempt to preserve the figure numbering convention described at the beginning of this section, this figure is divided into “offspring” figures: 13A and 13B. Further, figure 13B has parts (a), (b), and (c).

Figure 13A contains colored circles representing the re-calculations intended to match the original curve A. Each circle was obtained by selecting a value of r_α and executing the *NACA 496* solution method for Subcase 1. The agreement between the original and present results is very good at values of r_α of 0.75 and greater, but slightly less so at lower values of r_α . If original curve A is extrapolated to the left, the difference between the original and present values of F at $r_\alpha = 0.25$ is about 7.5%. The large X's at values of r_α of 0.50, 0.75, and 1.00 are from the independent calculation and are in excellent agreement with the present calculations.

Figure 13B(a) contains colored squares representing the re-calculations intended to match the original curve B. Each square was also obtained by selecting a value of r_α and executing the *NACA 496* solution method for Subcase 1. The trends of the original and present results agree (F decreases with increasing values of r_α), but in terms of absolute numbers the agreement is very poor: at the higher values of r_α , the magnitudes of the original results are more than a factor of two larger than those of the present results; at the lower values of r_α they approach a factor of two smaller. In fact, the vertical scale of the original figure had to be extended in order to accommodate the present result at $r_\alpha = 0.25$.

N.B.: In the following discussion there are two uses of the word “square.” The first use refers to the product of a quantity and itself; the second use refers to the geometric shape of the colored plotting symbols in figure 13B.

In contemplating the poor agreement between the original and present results, the present author noticed that the values of the present results, represented by the colored squares, at $r_\alpha = 0.375$ and 1.0 (about 1.5 and 0.25, respectively) are approximately equal to the squares of the values of the original curve at the same r_α 's (about 1.25 and 0.5, respectively). This relationship led the present author to compute and plot the squares of the values of the original curve B (curve labeled in the figure as the “square of curve B”).

As can be seen in figure 13B(b), the agreement between the present results and the square of curve B is much better than the agreement between the present results and curve B itself. The better agreement may be quantified by examining the sums of the squared differences between the results: those of the former are less than half those of the latter.

This better agreement suggests that an error occurred in the creation of the original curve B. Because the author of *NACA 496* uses the symbol F to mean, at times, a quantity and, at other times, the square of that quantity, there is ample room for one meaning to be used when the other meaning was intended. The present author believes such an error occurred in the creation of curve B (but not in the creation of curve A).

In figure 13B(c), the large X's at values of r_α of 0.50, 0.75, and 1.00 are from the independent calculation and are in excellent agreement with the present calculations and is supporting evidence that the original curve B was incorrectly plotted.

Variation of Center of Gravity Location. – The original figure 14 illustrates the dependency of F on the location of the center of gravity, x_α , for three different combinations of quantities. Each combination is represented by a different curve, labeled A, B, and C. According to the sign convention established in figure 2 of *NACA 496*, increasingly positive values of x_α corresponds to an aft movement of the center of gravity.

Because of the complexity of the results to be presented for this figure and in an attempt to preserve the figure numbering convention described at the beginning of this section, figure 14 will be divided up into “offspring” figures: 14A, 14B, and 14C. In addition, each offspring figure will have parts (a), (b), and (c).

According to the figure legend in the original figure 14, the quantities specific to this example are

for curve A: $\kappa = 1/400$; $a = -0.4$; $\omega_1/\omega_2 = 1/6$; $r_\alpha = 0.5$; x_α variable
and
for curve B: $\kappa = 1/4$; $a = -0.4$; $\omega_1/\omega_2 = 1/6$; $r_\alpha = 0.5$; x_α variable
and
for curve C: $\kappa = 1/100$; $a = -0.4$; $\omega_1/\omega_2 = 1$; $r_\alpha = 0.5$; x_α variable.

The colored circles in Figures 14A are the result of present calculations intended to match the original curve A; the colored squares in Figures 14B, to match the original curve B; and the colored diamonds in Figures 14C, to match the original curve C. Each present result represented by a symbol was obtained by selecting a value of x_α and executing the *NACA 496* solution method for Subcase 1.

The original figure 14 contains conflicting information regarding curve C. The figure legend defines the quantities listed above; but, within the figure itself is a notation indicating other quantities – “ $\omega_1/\omega_2 = 1$, $4\kappa = .01$ ” – with a leader pointing to curve C. The ratio of frequencies is the same as the ratio specified in the figure legend; however, the value of κ ($= 1/400$) differs from that in the figure legend. Present calculations were performed for both values of κ .

In figure 14A(a), the original results and the present results differ significantly, showing opposite trends with increasing values of x_α . However, the present author observed the following: the present value of F at $x_\alpha = 0$ is very close to the original value of F at $x_\alpha = 0.4$ and vice versa; the present value of F at $x_\alpha = 0.1$ is very close to the original value of F at $x_\alpha = 0.3$ and vice versa; and the present value of F at $x_\alpha = 0.2$ is very close to the original value of F at $x_\alpha = 0.2$.

This observation led to figure 14A(b), in which the original curve A has been rotated about the vertical axis $x_\alpha = 0.2$. The rotated curve A and the colored circles exhibit excellent agreement.

In Figure 14A(c) the large X’s at values of x_α of 0.1, 0.2, and 0.3 are from the independent calculation and are in excellent agreement with the present results and the rotated curve A. This triple agreement suggested to the present author that original curve A was incorrectly plotted.

In the early 1930's, intricate and multi-stepped engineering calculations (such as those required to produce the results in *NACA 496*) were performed by hand; results were recorded and transcribed by hand; and then plotted by hand. It is not unrealistic to consider that with the many steps performed by humans, errors occurred. The present author believes that in the case of curve A, transcription errors occurred – correct values of F were paired with non-corresponding values of x_α – which then led to an incorrect plot.

The trends observed in figures 14A are repeated in figures 14B and 14C: in figures 14B(a) and 14C(a) the original results and the present results (represented now by the colored squares and diamonds) differ significantly, showing opposite trends with increasing values of x_α ; in figures 14B(b) and 14C(b) the original curves B and C have been rotated about the vertical axis $x_\alpha = 0.2$ producing excellent agreement with the present results; and in figures 14B(c) and 14C(c) the large X's from the independent calculation are in excellent agreement with the present results and the rotated curves B and C. Again, this time for curves B and C, the present author believes that transcription errors occurred – correct values of F were paired with non-corresponding values of x_α – which then led to incorrect plots.

Wings A and B

The final three figures in *NACA 496* (figs. 15, 16, and 17) present results for two wings, designated in *NACA 496* as Wing A and Wing B. For each wing, experimental results were obtained. Both wings had symmetrical airfoils with chords of 12.7 centimeters (5 inches) and thickness-to-chord ratios of 0.12. Both wings were tested at zero degrees incidence.

The text of Appendix II of *NACA 496* states that Wing A was constructed of aluminum with quantities:

$$\kappa = 1/416; \quad a = -0.4; \quad x_\alpha = 0.31, 0.173, \text{ and } 0.038; \quad r_\alpha^2 = 0.33; \quad \omega_\alpha = 7 \times 2\pi.$$

The text of Appendix II of *NACA 496* states that Wing B was constructed of wood, with a trailing-edge control surface, with quantities:

$$\kappa = 1/100; \quad c = 0.5; \quad a = -0.4; \quad x_\alpha = 0.192; \quad r_\alpha^2 = 0.178;$$

$$x_\beta = 0.019; \quad r_\beta^2 = 0.0079; \quad \omega_\alpha = 17.6 \times 2\pi.$$

Figure 15 contains Subcase-1 results for Wing A in which flutter velocity is plotted as a function of frequency ratio ω_h/ω_α .

Figure 16 contains Subcase-2 results for Wing B in which flutter velocity is plotted as a function of frequency ratio ω_β/ω_h .

Figure 17 contains Subcase-3 results for Wing B in which flutter velocity is plotted as a function of frequency ratio $\omega_\alpha/\omega_\beta$.

To obtain the curves in these figures, first the appropriate subcase-specific *NACA 496* solution method was executed, resulting in curves of subcase-specific F (as defined) vs. subcase-specific Ω . Next, for each value of F equation (13) was employed, converting the ordinates in these curves from nondimensional F to dimensional v_f . Finally, the equations for the subcase-specific Ω 's from equations (5a), (5b), and (5c) were employed, converting the abscissas from subcase-specific Ω to subcase-specific frequency ratio.

Referring back to equation (13), it can be seen that to obtain the dimensional flutter velocity reference values ω_r and r_r are required, which differ from subcase to subcase. For Subcase 1, values of ω_α and r_α are required; for Subcase 2, a value of ω_h is required; and for Subcase 3, values of ω_β and r_β are required. *NACA 496* supplies values for ω_α , r_α , and r_β , but, in another tripping point, it does not supply values for ω_h and ω_β . Therefore, for the present calculations for Subcases 2 and 3, values of ω_h and ω_β had to be chosen. The choice was based on a trial-and-error investigation of candidate values and the selection criterion for the chosen values of ω_h and ω_β was that there be reasonable agreement between the original and the present curves.

Subcase 1. – Figure 15 contains theoretical and experimental results, in black. The present results are shown in colored O and + symbols and solid and dashed colored curves. Even though three values of x_α are listed above in the quantities for this subcase, $x_\alpha = 0.173$ was chosen for the present calculation because it produced the best agreement with the original curve in figure 15. Over the entire frequency range the trends for original theoretical results and both sets of present results are in very good agreement. The overall agreement over the first half of the range is excellent with maximum differences less than 5 percent; over the second half, less so with maximum differences of about 15 percent.

Subcase 2. – Figure 16 contains theoretical and experimental results, in black. The present results are shown in colored O and + symbols and solid and dashed colored curves. Theoretical results are given for two values of quantity x_b : $x_\beta = 0.019$ and $x_\beta = 0.01$. For this subcase, an assumed value of ω_h of $5.8 \times 2\pi$ was selected because it produced reasonable agreement between the original results and the present results.

In examining the colored curves, it is seen that the upper (corresponding to higher values of v) and lower (lower values of v) extremes of both curves extend to a frequency ratio of zero. Both colored curves are comprised of solid and dashed portions, indicating that two roots of equation (10) are present in each solution. The transition from solid to dashed occurs between frequency ratios of 0.8 and 0.9. The calculations that produced these curves had a range of $1/k$ from 0 to 500.

In examining the black theoretical curves, it is seen that the upper extremes of both curves terminate at a frequency ratio of about 0.75 and the lower extremes terminate at a frequency ratio of about 0.82. The difference in horizontal extent between the black and colored curves suggests to the present author that the calculations that produced the original curves had a very limited range of $1/k$. Further, because the frequency ratio at the lower extremes of the black curves corresponds roughly to the frequency ratio at the transition of the colored curves from solid to dashed, it is possible that the black curves only capture a single root of equation (13/XXVI).

Subcase 3. – Figure 17 contains theoretical and experimental results, in black. The present results are shown in colored \circ and $+$ symbols and solid and dashed colored curves. For this subcase, an assumed value of ω_β of $4.4 \times 2\pi$ was selected because it produced reasonable agreement between the original results and the present results.

As was observed in figure 16 for subcase 2 because the frequency ratio at the lower extreme of the black curve corresponds roughly to the frequency ratio at the transition of the colored curve from solid to dashed, it is possible that the black curve only captures a single root of equation (13/XXV).

VII. CONCLUDING REMARKS

This paper has reported on an extensive study of reference 2, NACA Report No. 496, “General Theory of Aerodynamic Instability and the Mechanism of Flutter,” by Theodore Theodorsen (referred to herein as *NACA 496*), including the re-computation of its numerical results. The study included reading and re-reading the paper, checking its equations, and checking its solution methods. With the few exceptions noted in the present paper, the study revealed the equations and solution methods of *NACA 496* to be correct. Because of the crude (by today’s standards) computational tools available at the time *NACA 496* was written, the author of *NACA 496* conceived of and employed several time- and effort-saving computational shortcuts, pointed out and summarized in a table in the present paper. The study also revealed some “tripping points,” aspects of *NACA 496* that have the potential to cause confusion, and identified some errors in *NACA 496* that were not corrected in the later versions of the paper. Tripping points and errors are also summarized in tables in the present paper.

Appendix II in *NACA 496* contains a number of numerical examples, all of which were re-computed in the present paper. The re-computed results were overlaid on the original figures from *NACA 496*. The re-computations were accomplished by employing the method developed in the original work, but by using modern computational tools. In most instances the overall shapes of the original and re-computed curves are similar, with varying degrees of agreement in magnitude. In some instances, there is significant dissimilarity between the original and re-computed curves. Most dissimilarities are attributed to human computational and transcription errors that are speculated to have occurred during the creation of *NACA 496*. One dissimilarity (namely, that regarding the quantity F in fig. 12) is unattributed. Several of the re-computed results were checked by independent calculations and, in each instance, the re-computed and independent results were in excellent agreement.

Appendix A of the present paper contains *NACA 496*.

Appendix B contains a Matlab® program that implements the two-degree-of-freedom flutter equations and the two-degree-of-freedom solution method found in Appendix I of *NACA 496*. By executing this program, results in figures 5 through 11 and 15 through 17, found in Appendix II of *NACA 496*, may be re-computed directly. This program produces both physical and non-physical solutions. Physical solutions are based on real values of the quantity F and the \mathcal{Q} s; non-physical solutions are based on complex values.

Appendix C of the present paper offers three alternate solution methods, all of which derive from the two-degree-of-freedom flutter equations of *NACA 496*. Compared to the number of computations involved in the *NACA 496* solution method, these alternate solution methods are much more computationally intensive and would have been excluded from consideration in 1934 for that reason. To accuracies within a tenth of a percent, all three alternate solution methods yielded the same value of flutter velocity, v_f , and the same value of flutter reduced frequency, k_f , as those predicted by the solution method of *NACA 496*.

Appendix D of the present paper offers a solution of the three-degree-of-freedom flutter equations following the method proposed in *NACA 496*. This solution method produced an example result for the “standard case.” In addition, for systematic variations in the dimensional modal frequencies, in the limit, the three-degree-of-freedom results (v_f and k_f) approached the two-degree-of-freedom results, including the number of flutter modes predicted.



**NATIONAL ADVISORY COMMITTEE
FOR AERONAUTICS**

REPORT No. 496

**GENERAL THEORY OF AERODYNAMIC INSTABILITY
AND THE MECHANISM OF FLUTTER**

By **THEODORE THEODORSEN**



REPRINT OF REPORT No. 496, ORIGINALLY PUBLISHED APRIL 1935

NACA LIBRARY
LANGLEY MEMORIAL AERONAUTICAL
LABORATORY
Langley Field, Va.

1940

For sale by the Superintendent of Documents, Washington, D. C. - - - - - Price 10 cents
Subscription price, \$3 per year.

AERONAUTIC SYMBOLS

1. FUNDAMENTAL AND DERIVED UNITS

	Symbol	Metric		English	
		Unit	Abbrevia- tion	Unit	Abbrevia- tion
Length.....	l	meter.....	m	foot (or mile).....	ft (or mi)
Time.....	t	second.....	s	second (or hour).....	sec (or hr)
Force.....	F	weight of 1 kilogram.....	kg	weight of 1 pound.....	lb
Power.....	P	horsepower (metric).....		horsepower.....	hp
Speed.....	V	kilometers per hour.....	kph	miles per hour.....	mph
		meters per second.....	mps	feet per second.....	fps

2. GENERAL SYMBOLS

W	Weight= mg	ν	Kinematic viscosity
g	Standard acceleration of gravity= 9.80665 m/s^2 or 32.1740 ft/sec^2	ρ	Density (mass per unit volume)
m	Mass= $\frac{W}{g}$		Standard density of dry air, $0.12497 \text{ kg-m}^{-3}$ at 15° C and 760 mm ; or $0.002378 \text{ lb-ft}^{-3}$
I	Moment of inertia= mk^2 . (Indicate axis of radius of gyration k by proper subscript.)		Specific weight of "standard" air, 1.2255 kg/m^3 or 0.07651 lb/cu ft
μ	Coefficient of viscosity		

3. AERODYNAMIC SYMBOLS

S	Area	i_w	Angle of setting of wings (relative to thrust line)
S_w	Area of wing	i_t	Angle of stabilizer setting (relative to thrust line)
G	Gap	Q	Resultant moment
b	Span	Ω	Resultant angular velocity
c	Chord	R	Reynolds number, $\rho \frac{Vl}{\mu}$ where l is a linear dimen- sion (e.g., for an airfoil of 1.0 ft chord, 100 mph , standard pressure at 15° C , the corresponding Reynolds number is $935,400$; or for an airfoil of 1.0 m chord, 100 mps , the corresponding Reynolds number is $6,865,000$)
A	Aspect ratio, $\frac{b^2}{S}$	α	Angle of attack
V	True air speed	ϵ	Angle of downwash
q	Dynamic pressure, $\frac{1}{2}\rho V^2$	α_0	Angle of attack, infinite aspect ratio
L	Lift, absolute coefficient $C_L = \frac{L}{qS}$	α_i	Angle of attack, induced
D	Drag, absolute coefficient $C_D = \frac{D}{qS}$	α_a	Angle of attack, absolute (measured from zero- lift position)
D_0	Profile drag, absolute coefficient $C_{D_0} = \frac{D_0}{qS}$	γ	Flight-path angle
D_i	Induced drag, absolute coefficient $C_{D_i} = \frac{D_i}{qS}$		
D_p	Parasite drag, absolute coefficient $C_{D_p} = \frac{D_p}{qS}$		
C	Cross-wind force, absolute coefficient $C_c = \frac{C}{qS}$		

2626°

REPORT No. 496

**GENERAL THEORY OF AERODYNAMIC INSTABILITY
AND THE MECHANISM OF FLUTTER**

By THEODORE THEODORSEN
Langley Memorial Aeronautical Laboratory

408269 O—41—1

1

NATIONAL ADVISORY COMMITTEE FOR AERONAUTICS

HEADQUARTERS, NAVY BUILDING, WASHINGTON, D. C.

Created by act of Congress approved March 3, 1915, for the supervision and direction of the scientific study of the problems of flight (U. S. Code, Title 50, Sec. 151). Its membership was increased to 15 by act approved March 2, 1929. The members are appointed by the President, and serve as such without compensation.

VANNEYAR BUSH, Sc. D., *Chairman*,
Washington, D. C.
GEORGE J. MEAD, Sc. D., *Vice Chairman*,
Washington, D. C.
CHARLES G. ABBOT, Sc. D.,
Secretary, Smithsonian Institution.
HENRY H. ARNOLD, Major General, United States Army,
Deputy Chief of Staff, Chief of the Air Corps, War
Department.
GEORGE H. BRETT, Major General, United States Army,
Acting Chief of the Air Corps, War Department.
LYMAN J. BRIGGS, Ph. D.,
Director, National Bureau of Standards.
DONALD H. CONNOLLY, B. S.,
Administrator of Civil Aeronautics.

ROBERT E. DOHERTY, M. S.,
Pittsburgh, Pa.
ROBERT H. HINCKLEY, A. B.,
Assistant Secretary of Commerce.
JEROME C. HUNSAKER, Sc. D.,
Cambridge, Mass.
SYDNEY M. KRAUS, Captain, United States Navy,
Bureau of Aeronautics, Navy Department.
FRANCIS W. REICHELDERFER, Sc. D.,
Chief, United States Weather Bureau.
JOHN H. TOWERS, Rear Admiral, United States Navy,
Chief, Bureau of Aeronautics, Navy Department.
EDWARD WARNER, Sc. D.,
Washington, D. C.
ORVILLE WRIGHT, Sc. D.,
Dayton, Ohio.

GEORGE W. LEWIS, *Director of Aeronautical Research*

S. PAUL JOHNSTON, *Coordinator of Research*

JOHN F. VICTORY, *Secretary*

HENRY J. E. REID, *Engineer-in-Charge, Langley Memorial Aeronautical Laboratory, Langley Field, Va.*

SMITH J. DEFRANCE, *Engineer-in-Charge, Ames Aeronautical Laboratory, Moffett Field, Calif.*

TECHNICAL COMMITTEES

AERODYNAMICS
POWER PLANTS FOR AIRCRAFT
AIRCRAFT MATERIALS

AIRCRAFT STRUCTURES
AIRCRAFT ACCIDENTS
INVENTIONS AND DESIGNS

Coordination of Research Needs of Military and Civil Aviation

Preparation of Research Programs

Allocation of Problems

Prevention of Duplication

Consideration of Inventions

LANGLEY MEMORIAL AERONAUTICAL LABORATORY

AMES AERONAUTICAL LABORATORY

LANGLEY FIELD, VA.

MOFFETT FIELD, CALIF.

Conduct, under unified control, for all agencies, of scientific research on the fundamental problems of flight.

OFFICE OF AERONAUTICAL INTELLIGENCE

WASHINGTON, D. C.

Collection, classification, compilation, and dissemination of
scientific and technical information on aeronautics

REPORT No. 496

GENERAL THEORY OF AERODYNAMIC INSTABILITY AND THE MECHANISM OF FLUTTER

By THEODORE THEODORSEN

SUMMARY

The aerodynamic forces on an oscillating airfoil or airfoil-aileron combination of three independent degrees of freedom have been determined. The problem resolves itself into the solution of certain definite integrals, which have been identified as Bessel functions of the first and second kind and of zero and first order. The theory, being based on potential flow and the Kutta condition, is fundamentally equivalent to the conventional wing-section theory relating to the steady case.

The air forces being known, the mechanism of aerodynamic instability has been analyzed in detail. An exact solution, involving potential flow and the adoption of the Kutta condition, has been arrived at. The solution is of a simple form and is expressed by means of an auxiliary parameter k . The mathematical treatment also provides a convenient cyclic arrangement permitting a uniform treatment of all subcases of two degrees of freedom. The flutter velocity, defined as the air velocity at which flutter starts, and which is treated as the unknown quantity, is determined as a function of a certain ratio of the frequencies in the separate degrees of freedom for any magnitudes and combinations of the airfoil-aileron parameters.

For those interested solely or particularly in the numerical solutions Appendix I has been prepared. The routine procedure in solving numerical examples is put down detached from the theoretical background of the paper. It first is necessary to determine a certain number of constants pertaining to the case, then to perform a few routine calculations as indicated. The result is readily obtained in the form of a plot of flutter velocity against frequency for any values of the other parameters chosen. The numerical work of calculating the constants is simplified by referring to a number of tables, which are included in Appendix I. A number of illustrative examples and experimental results are given in Appendix II.

INTRODUCTION

It has been known that a wing or wing-aileron structurally restrained to a certain position of equilibrium becomes unstable under certain conditions. At least two degrees of freedom are required to create a condition of instability, as it can be shown that vibrations

of a single degree of freedom would be damped out by the air forces. The air forces, defined as the forces due to the air pressure acting on the wing or wing-aileron in an arbitrary oscillatory motion of several degrees of freedom, are in this paper treated on the basis of the theory of nonstationary potential flow. A wing-section theory and, by analogy, a wing theory shall be thus developed that applies to the case of oscillatory motion, not only of the wing as a whole but also to that of an aileron. It is of considerable importance that large oscillations may be neglected; in fact, only infinitely small oscillations about the position of equilibrium need be considered. Large oscillations are of no interest since the sole attempt is to specify one or more conditions of instability. Indeed, no particular type or shape of airfoil shall be of concern, the treatment being restricted to primary effects. The differential equations for the several degrees of freedom will be put down. Each of these equations contains a statement regarding the equilibrium of a system of forces. The forces are of three kinds: (1) The inertia forces, (2) the restraining forces, and (3) the air forces.

There is presumably no necessity of solving a general case of damped or divergent motion, but only the border case of a pure sinusoidal motion, applying to the case of unstable equilibrium. This restriction is particularly important as the expressions for the air force developed for oscillatory motion can thus be employed. Imagine a case that is unstable to a very slight degree; the amplitudes will then increase very slowly and the expressions developed for the air forces will be applicable. It is of interest simply to know under what circumstances this condition may obtain and cases in which the amplitudes are decreasing or increasing at a finite rate need not be treated or specified. Although it is possible to treat the latter cases, they are of no concern in the present problem. Nor is the internal or solid friction of the structure of primary concern. The fortunate situation exists that the effect of the solid friction is *favorable*. Knowledge is desired concerning the condition as existing in the absence of the internal friction, as this case constitutes a sort of lower limit, which it is not always desirable to exceed.

Owing to the rather extensive field covered in the paper it has been considered necessary to omit many elementary proofs, it being left to the reader to verify certain specific statements. In the first part of the paper, the velocity potentials due to the flow around the airfoil-aileron are developed. These potentials are treated in two classes: The noncirculating flow potentials, and those due to the surface of discontinuity behind the wing, referred to as "circulatory" potentials. The magnitude of the circulation for an oscillating wing-aileron is determined next. The

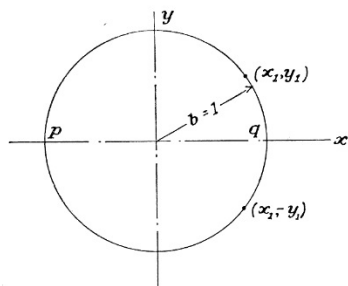


FIGURE 1.—Conformal representation of the wing profile by a circle.

forces and moments acting on the airfoil are then obtained by integration. In the latter part of the paper the differential equations of motion are put down and the particular and important case of unstable equilibrium is treated in detail. The solution of the problem of determining the flutter speed is finally given in the form of an equation expressing a relationship between the various parameters. The three subcases of two degrees of freedom are treated in detail.

The paper proposes to disclose the basic nature of the mechanism of flutter, leaving modifications of the primary results by secondary effects for future investigations.¹ Such secondary effects are: The effects of a finite span, of section shape, of deviations from potential flow, including also modifications of results to include twisting and bending of actual wing sections instead of pure torsion and deflection as considered in this paper.

The supplementary experimental work included in Appendix II similarly refers to well-defined elementary cases, the wing employed being of a large aspect ratio, nondeformable, and given definite degrees of freedom by a supporting mechanism, with external springs maintaining the equilibrium positions of wing or wing-aileron. The experimental work was carried on largely to verify the general shape of and the approximate magnitudes involved in the theoretically predicted response characteristics. As the present report is limited to the mathematical aspects of the flutter problem, specific recommendations in regard to practical applications are not given in this paper.

¹The effect of internal friction is in some cases essential; this subject will be contained in a subsequent paper.

VELOCITY POTENTIALS, FORCES, AND MOMENTS OF THE NONCIRCULATORY FLOW

We shall proceed to calculate the various velocity potentials due to position and velocity of the individual parts in the whole of the wing-aileron system. Let us temporarily represent the wing by a circle (fig. 1). The potential of a source ϵ at the origin is given by

$$\phi = \frac{\epsilon}{4\pi} \log (x^2 + y^2)$$

For a source ϵ at (x_1, y_1) on the circle

$$\phi = \frac{\epsilon}{4\pi} \log \{ (x - x_1)^2 + (y - y_1)^2 \}$$

Putting a double source 2ϵ at (x_1, y_1) and a double negative source -2ϵ at $(x_1, -y_1)$ we obtain for the flow around the circle

$$\phi = \frac{\epsilon}{2\pi} \log \frac{(x - x_1)^2 + (y - y_1)^2}{(x - x_1)^2 + (y + y_1)^2}$$

The function ϕ on the circle gives directly the surface potential of a straight line pq , the projection of the circle on the horizontal diameter. (See fig. 1.) In this case $y = \sqrt{1 - x^2}$ and ϕ is a function of x only.

We shall need the integrals:

$$\int_c^1 \log \frac{(x - x_1)^2 + (y - y_1)^2}{(x - x_1)^2 + (y + y_1)^2} dx_1 = 2(x - c) \log N - 2\sqrt{1 - x^2} \cos^{-1} c$$

and

$$\int_c^1 \log \frac{(x - x_1)^2 + (y - y_1)^2}{(x - x_1)^2 + (y + y_1)^2} (x_1 - c) dx_1 = -\sqrt{1 - c^2} \sqrt{1 - x^2} - \cos^{-1} c (x - 2c) \sqrt{1 - x^2} + (x - c)^2 \log N$$

where

$$N = \frac{1 - cx - \sqrt{1 - x^2} \sqrt{1 - c^2}}{x - c}$$

The location of the center of gravity of the wing-aileron x_a is measured from a , the coordinate of the axis of rotation (fig. 2); x_β the location of the center

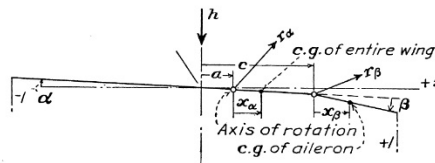


FIGURE 2.—Parameters of the airfoil-aileron combination.

of gravity of the aileron is measured from c , the coordinate of the hinge; and r_α and r_β are the radii of gyration of the wing-aileron referred to a , and of the aileron referred to the hinge. The quantities x_β and r_β are "reduced" values, as defined later in the paper. The quantities a , x_a , c , and x_β are positive toward the rear (right), h is the vertical coordinate of the axis of rotation at a with respect to a fixed reference frame and is positive downward. The angles α and β are positive clockwise (right-hand turn). The wind velocity v is to

the right and horizontal. The angle (of attack) α refers to the direction of v , the aileron angle β refers to the undeflected position and *not* to the wind direction. The quantities r_α and r_β always occur as squares. Observe that the leading edge is located at -1 , the trailing edge at $+1$. The quantities a , c , x_a , x_β , r_α , and r_β , which are repeatedly used in the following treatment, are all dimensionless with the half chord b as reference unit.

The effect of a flap bent down at an angle β (see fig. 2) is seen to give rise to a function φ obtained by substituting $-v\beta b$ for ϵ ; hence

$$\varphi_\beta = \frac{v\beta b}{\pi} [\sqrt{1-x^2} \cos^{-1} c - (x-c) \log N]$$

To obtain the effect of the flap going down at an angular velocity $\dot{\beta}$, we put $\epsilon = -(x_1 - c)\dot{\beta}b^2$ and get

$$\varphi_\beta = \frac{\dot{\beta}b^2}{2\pi} [\sqrt{1-c^2}\sqrt{1-x^2} + \cos^{-1} c(x-2c)\sqrt{1-x^2} - (x-c)^2 \log N]$$

To obtain the effect of an angle α of the entire airfoil, we put $c = -1$ in the expression for φ_β , hence

$$\varphi_\alpha = v\alpha b \sqrt{1-x^2}$$

To depict the airfoil in downward motion with a velocity \dot{h} (+ down), we need only introduce $\frac{\dot{h}}{v}$ instead of α . Thus

$$\varphi_h = \dot{h}b \sqrt{1-x^2}$$

Finally, to describe a rotation around point a at an angular velocity \dot{a} , we notice that this motion may be taken to consist of a rotation around the leading edge $c = -1$ at an angular velocity \dot{a} plus a vertical motion with a velocity $-\dot{a}(1+a)b$. Then

$$\begin{aligned} \varphi_a &= \frac{\dot{a}b^2}{2\pi} \pi(x+2)\sqrt{1-x^2} - \dot{a}(1+a)b^2\sqrt{1-x^2} \\ &= \dot{a}b^2 \left(\frac{1}{2}x - a \right) \sqrt{1-x^2} \end{aligned}$$

The following tables give in succession the velocity potentials and a set of integrals² with associated constants, which we will need in the calculation of the air forces and moments.

VELOCITY POTENTIALS

$$\varphi_\alpha = v\alpha b \sqrt{1-x^2}$$

$$\varphi_h = \dot{h}b \sqrt{1-x^2}$$

$$\varphi_a = \dot{a}b^2 \left(\frac{1}{2}x - a \right) \sqrt{1-x^2}$$

$$\varphi_\beta = \frac{1}{\pi} v\beta b [\sqrt{1-x^2} \cos^{-1} c - (x-c) \log N]$$

$$\begin{aligned} \varphi_{\dot{\beta}} &= \frac{1}{2\pi} \dot{\beta}b^2 [\sqrt{1-c^2}\sqrt{1-x^2} + (x-2c)\sqrt{1-x^2} \cos^{-1} c \\ &\quad - (x-c)^2 \log N] \end{aligned}$$

where

$$N = \frac{1-cx - \sqrt{1-x^2}\sqrt{1-c^2}}{x-c}$$

² Some of the more difficult integral evaluations are given in Appendix III.

INTEGRALS

$$\begin{aligned} \int_c^1 \varphi_\alpha dx &= -\frac{b}{2} v\alpha T_4 & \int_{-1}^{+1} \varphi_\alpha dx &= \frac{b}{2} v\alpha\pi \\ \int_c^1 \varphi_h dx &= -\frac{b}{2} \dot{h} T_4 & \int_{-1}^{+1} \varphi_h dx &= \frac{b}{2} \dot{h}\pi \\ \int_c^1 \varphi_a dx &= \dot{a}b^2 T_9 & \int_{-1}^{+1} \varphi_a dx &= -\dot{a}b^2 \frac{\pi a}{2} \\ \int_c^1 \varphi_\beta dx &= -\frac{b}{2\pi} v\beta T_5 & \int_{-1}^{+1} \varphi_\beta dx &= -\frac{b}{2} v\beta T_4 \\ \int_c^1 \varphi_{\dot{\beta}} dx &= -\frac{b^2}{2\pi} \dot{\beta} T_2 & \int_{-1}^{+1} \varphi_{\dot{\beta}} dx &= -\frac{b^2}{2} \dot{\beta} T_1 \\ \int_c^1 \varphi_\alpha(x-c) dx &= -\frac{b}{2} v\alpha T_1 & \int_{-1}^{+1} \varphi_\alpha(x-c) dx &= -\frac{b}{2} v\alpha c\pi \\ \int_c^1 \varphi_h(x-c) dx &= -\frac{b}{2} \dot{h} T_1 & \int_{-1}^{+1} \varphi_h(x-c) dx &= -\frac{b}{2} \dot{h} c\pi \\ \int_c^1 \varphi_a(x-c) dx &= \dot{a}b^2 T_{13} & \int_{-1}^{+1} \varphi_a(x-c) dx &= \dot{a}b^2 T_{14}\pi \\ \int_c^1 \varphi_\beta(x-c) dx &= -\frac{b}{2\pi} v\beta T_2 & \int_{-1}^{+1} \varphi_\beta(x-c) dx &= -\frac{b}{2} v\beta T_8 \\ \int_c^1 \varphi_{\dot{\beta}}(x-c) dx &= -\frac{b^2}{2\pi} \dot{\beta} T_3 & \int_{-1}^{+1} \varphi_{\dot{\beta}}(x-c) dx &= -\frac{b^2}{2} \dot{\beta} T_7 \end{aligned}$$

CONSTANTS

$$\begin{aligned} T_1 &= -\frac{1}{3} \sqrt{1-c^2} (2+c^2) + c \cos^{-1} c \\ T_2 &= c(1-c^2) - \sqrt{1-c^2} (1+c^2) \cos^{-1} c + c (\cos^{-1} c)^2 \\ T_3 &= -\left(\frac{1}{8} + c^2 \right) (\cos^{-1} c)^2 + \frac{1}{4} c \sqrt{1-c^2} \cos^{-1} c (7+2c^2) \\ &\quad - \frac{1}{8} (1-c^2) (5c^2+4) \\ T_4 &= -\cos^{-1} c + c \sqrt{1-c^2} \\ T_5 &= -(1-c^2) - (\cos^{-1} c)^2 + 2c \sqrt{1-c^2} \cos^{-1} c \\ T_6 &= T_2 \\ T_7 &= -\left(\frac{1}{8} + c^2 \right) \cos^{-1} c + \frac{1}{8} c \sqrt{1-c^2} (7+2c^2) \\ T_8 &= -\frac{1}{3} \sqrt{1-c^2} (2c^2+1) + c \cos^{-1} c \\ T_9 &= \frac{1}{2} \left[\frac{1}{3} (\sqrt{1-c^2}) + a T_4 \right] = \frac{1}{2} (-p + a T_4) \end{aligned}$$

where $p = -\frac{1}{3} (\sqrt{1-c^2})^3$

$$T_{10} = \sqrt{1-c^2} + \cos^{-1} c$$

$$T_{11} = \cos^{-1} c (1-2c) + \sqrt{1-c^2} (2-c)$$

$$T_{12} = \sqrt{1-c^2} (2+c) - \cos^{-1} c (2c+1)$$

$$T_{13} = \frac{1}{2} [-T_7 - (c-a) T_1]$$

$$T_{14} = \frac{1}{16} + \frac{1}{2} ac$$

FORCES AND MOMENTS

The velocity potentials being known, we are able to calculate local pressures and by integration to obtain the forces and moments acting on the airfoil and aileron.

$$p_n = -\rho \left(\frac{w^2}{2} + \frac{\partial \varphi}{\partial t} \right)$$
$$p = -2\rho \left(v \frac{\partial \varphi}{\partial x} + \frac{\partial \varphi}{\partial t} \right)$$
$$P = -2\rho b \int_{-1}^{+1} \dot{\phi} dx$$

$$\begin{aligned}
M_a = & -\rho b^2 \left[-\pi v^2 \alpha + \pi \left(\frac{1}{8} + a^2 \right) b^2 \ddot{\alpha} + v^2 T_1 \beta + \{ T_1 - T \right. \\
& - (c-a) T_4 \} b \dot{\beta} v + \{ -T_7 - (c-a) T_1 \} b^2 \ddot{\beta} \\
& \left. - b a \pi \hbar - \pi v \hbar \right] \quad (III)
\end{aligned}$$

$$\begin{aligned}\varphi_r &= \frac{\Delta\Gamma}{2\pi} \left[\tan^{-1} \frac{Y}{X-X_0} - \tan^{-1} \frac{Y}{X-\frac{1}{X_0}} \right] \\ &= \frac{\Delta\Gamma}{2\pi} \tan^{-1} \frac{\left(-\frac{1}{X_0} + X_0\right)Y}{X^2 - \left(X_0 + \frac{1}{X_0}\right)X + Y^2 + 1}\end{aligned}$$
$$\frac{\partial \varphi}{\partial x} + \frac{\partial \varphi}{\partial x_0} = \frac{\Delta \Gamma}{2\pi} \frac{x_0 + x}{\sqrt{1-x^2} \sqrt{x_0^2-1}}$$

To obtain the force on the aileron, we need the integral

$$\begin{aligned} \int_c^1 \left(\frac{\partial \varphi}{\partial x} + \frac{\partial \varphi}{\partial x_0} \right) dx &= \frac{\Delta \Gamma}{2\pi} \int_c^1 \frac{x_0 + x}{\sqrt{x_0^2 - 1} \sqrt{1 - x^2}} dx \\ &= -\frac{\Delta \Gamma}{2\pi} \left[\frac{x_0}{\sqrt{x_0^2 - 1}} \cos^{-1} x + \frac{\sqrt{1 - x^2}}{\sqrt{x_0^2 - 1}} \right]_c^1 \\ &= \frac{\Delta \Gamma}{2\pi} \left[\frac{x_0}{\sqrt{x_0^2 - 1}} \cos^{-1} c + \frac{\sqrt{1 - c^2}}{\sqrt{x_0^2 - 1}} \right] \end{aligned}$$

Thus, for the force on the aileron

$$\begin{aligned} \Delta P_{cl} &= -\rho v b \frac{\Delta \Gamma}{\pi} \left(\frac{x_0}{\sqrt{x_0^2 - 1}} \cos^{-1} c + \frac{1}{\sqrt{x_0^2 - 1}} \sqrt{1 - c^2} \right) \text{ or} \\ \Delta P_{cl} &= -\rho v b \frac{\Delta \Gamma}{\pi} \left[\frac{x_0}{\sqrt{x_0^2 - 1}} (\cos^{-1} c - \sqrt{1 - c^2}) \right. \\ &\quad \left. + \sqrt{\frac{x_0 + 1}{x_0 - 1}} \sqrt{1 - c^2} \right] \end{aligned}$$

Integrated, with $\Delta \Gamma = U dx_0$

$$\begin{aligned} P_{cl} &= -\frac{\rho v b}{\pi} \left[(\cos^{-1} c - \sqrt{1 - c^2}) \int_1^\infty \frac{x_0}{\sqrt{x_0^2 - 1}} U dx_0 \right. \\ &\quad \left. + \sqrt{1 - c^2} \int_1^\infty \sqrt{\frac{x_0 + 1}{x_0 - 1}} U dx_0 \right] \end{aligned}$$

for $c = -1$ we obtain the expression for P , the force on the whole airfoil

$$P = -\rho v b \int_1^\infty \frac{x_0}{\sqrt{x_0^2 - 1}} U dx_0 \quad (\text{IV})$$

Since U is considered stationary with respect to the fluid elements

$$U = f(vt - x_0)$$

where t is the time since the beginning of the motion. U is thus a function of the distance from the location of the first vortex element or, referred to a system moving with the fluid, U is stationary in value.

Similarly we obtain for the moment on the aileron

$$\begin{aligned} \int_c^1 \left(\frac{\partial \varphi}{\partial x} + \frac{\partial \varphi}{\partial x_0} \right) (x - c) dx &= \frac{\Delta \Gamma}{2\pi} \int_c^1 \frac{(x - c)(x_0 + x)}{\sqrt{1 - x^2} \sqrt{x_0^2 - 1}} dx \\ &= -\frac{\Delta \Gamma}{2\pi} \frac{1}{\sqrt{x_0^2 - 1}} \left[x_0 \sqrt{1 - x^2} + \frac{x \sqrt{1 - x^2}}{2} - c \sqrt{1 - x^2} \right. \\ &\quad \left. + \left(\frac{1}{2} - x_0 c \right) \cos^{-1} x \right]_c^1 \\ &= +\frac{\Delta \Gamma}{2\pi} \frac{1}{\sqrt{x_0^2 - 1}} \left[\left(x_0 + \frac{c}{2} - c \right) \sqrt{1 - c^2} \right. \\ &\quad \left. + \frac{1}{2} (1 - 2x_0 c) \cos^{-1} c \right] \\ &= +\frac{\Delta \Gamma}{2\pi} \left[\frac{x_0}{\sqrt{x_0^2 - 1}} (\sqrt{1 - c^2} - c \cos^{-1} c) \right. \\ &\quad \left. + \frac{1}{\sqrt{x_0^2 - 1}} (\cos^{-1} c - c \sqrt{1 - c^2}) \right] \end{aligned}$$

Finally

$$\begin{aligned} \Delta M_\beta &= -\rho v b^2 \frac{\Delta \Gamma}{\pi} \left[\frac{x_0}{\sqrt{x_0^2 - 1}} \left\{ \sqrt{1 - c^2} \left(1 + \frac{c}{2} \right) \right. \right. \\ &\quad \left. \left. - \cos^{-1} c \left(c + \frac{1}{2} \right) \right\} + \frac{1}{2} \sqrt{\frac{x_0 + 1}{x_0 - 1}} (\cos^{-1} c - c \sqrt{1 - c^2}) \right] \end{aligned}$$

Putting $\Delta \Gamma = U dx_0$ and integrating

$$\begin{aligned} M_\beta &= -\frac{\rho v b^2}{\pi} \left[\left\{ \sqrt{1 - c^2} \left(1 + \frac{c}{2} \right) \right. \right. \\ &\quad \left. \left. - \cos^{-1} c \left(c + \frac{1}{2} \right) \right\} \int_1^\infty \frac{x_0}{\sqrt{x_0^2 - 1}} U dx_0 \right. \\ &\quad \left. + (\cos^{-1} c - c \sqrt{1 - c^2}) \frac{1}{2} \int_1^\infty \sqrt{\frac{x_0 + 1}{x_0 - 1}} U dx_0 \right] \quad (\text{V}) \end{aligned}$$

Further, for the moment on the entire airfoil around a

$$\begin{aligned} \int_{-1}^{+1} \left(\frac{\partial \varphi}{\partial x} + \frac{\partial \varphi}{\partial x_0} \right) (x - a) dx &= -\frac{\Delta \Gamma}{2\pi} \frac{1}{\sqrt{x_0^2 - 1}} \left[\left(x_0 + \frac{x}{2} - a \right) \sqrt{1 - x^2} \right. \\ &\quad \left. + \left(\frac{1}{2} - x_0 a \right) \cos^{-1} x \right]_{-1}^{+1} = +\frac{\Delta \Gamma}{2\pi} \frac{1}{\sqrt{x_0^2 - 1}} \left(\frac{1}{2} - x_0 a \right) \pi \\ &\quad \frac{1}{2} - x_0 a \end{aligned}$$

and

$$\Delta M_\alpha = -\rho v b^2 \Delta \Gamma \frac{1}{\sqrt{x_0^2 - 1}}$$

Integrated, this becomes

$$\begin{aligned} M_\alpha &= -\rho v b^2 \int_1^\infty \frac{1}{2} - x_0 a}{\sqrt{x_0^2 - 1}} U dx_0 \\ &= -\rho v b^2 \int_1^\infty \left[\frac{1}{2} + \frac{1}{2} x_0 - \frac{x_0 \left(a + \frac{1}{2} \right)}{\sqrt{x_0^2 - 1}} \right] U dx_0 \\ &= -\rho v b^2 \int_1^\infty \left[\frac{1}{2} \sqrt{\frac{x_0 + 1}{x_0 - 1}} - \left(a + \frac{1}{2} \right) \frac{x_0}{\sqrt{x_0^2 - 1}} \right] U dx_0 \quad (\text{VI}) \end{aligned}$$

THE MAGNITUDE OF THE CIRCULATION

The magnitude of the circulation is determined by the Kutta condition, which requires that no infinite velocities exist at the trailing edge, or, at $x = 1$

$$\frac{\partial}{\partial x} (\varphi_1 + \varphi_a + \varphi_h + \varphi_{\dot{a}} + \varphi_\beta + \varphi_{\dot{\beta}}) = \text{finite}$$

Introducing the values of φ_α , etc. from page 5 and

φ_1 from $\frac{\partial \varphi}{\partial x}$ page 6 gives the important relation:

$$\begin{aligned} \frac{1}{2\pi} \int_1^\infty \frac{\sqrt{x_0 + 1}}{\sqrt{x_0 - 1}} U dx_0 &= v\alpha + \dot{h} + b \left(\frac{1}{2} - a \right) \dot{\alpha} \\ &\quad + \frac{T_{10}}{\pi} \rho \beta + b \frac{T_{11}}{2\pi} \dot{\beta} \quad (\text{VII}) \end{aligned}$$

This relation must be satisfied to comply with the Kutta condition, which states that the flow shall leave the airfoil at the trailing edge.

It is observed that the relation reduces to that of the Kutta condition for stationary flow on putting $x_0 = \infty$,

and in subsequence omitting the variable parameters α , β , and h .

Let us write

$$\frac{1}{2\pi} \int_1^\infty \sqrt{\frac{x_0+1}{x_0-1}} U dx_0 = v\alpha + h + b \left(\frac{1}{2} - \alpha \right) \\ + \frac{T_{10}}{\pi} v\beta + b \frac{T_{11}}{2\pi} \dot{\beta} = Q$$

Introduced in (IV)

$$P = -2\pi\rho vbQ \frac{\int_1^\infty \frac{x_0}{\sqrt{x_0^2-1}} U dx_0}{\int_1^\infty \sqrt{\frac{x_0+1}{x_0-1}} U dx_0}$$

from (V)

$$M_\beta = -2\rho vb^2 \left[\left(\sqrt{1-c^2} \left(1 + \frac{c}{2} \right) - \cos^{-1} c \left(c + \frac{1}{2} \right) \right) \times \right. \\ \left. \frac{\int_1^\infty \frac{x_0}{\sqrt{x_0^2-1}} U dx_0}{\int_1^\infty \sqrt{\frac{x_0+1}{x_0-1}} U dx_0} + \frac{1}{2} \left(\cos^{-1} c - c\sqrt{1-c^2} \right) \right] Q$$

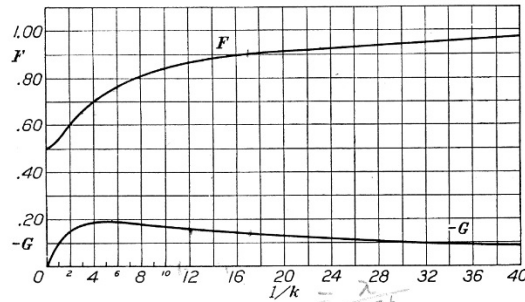


FIGURE 4.—The functions F and G against $\frac{1}{k}$.

and from (VI)

$$M_\alpha = -2\pi\rho vb^2 \left[\frac{1}{2} - \left(a + \frac{1}{2} \right) \frac{\int_1^\infty \frac{x_0}{\sqrt{x_0^2-1}} U dx_0}{\int_1^\infty \sqrt{\frac{x_0+1}{x_0-1}} U dx_0} \right] Q$$

Introducing

$$C = \frac{\int_1^\infty \frac{x_0}{\sqrt{x_0^2-1}} U dx_0}{\int_1^\infty \sqrt{\frac{x_0+1}{x_0-1}} U dx_0}$$

we obtain finally

$$P = -2\rho vb\pi CQ \quad (\text{VIII})$$

$$M_\beta = -2\rho vb^2 \left[\left(\sqrt{1-c^2} \left(1 + \frac{c}{2} \right) - \cos^{-1} c \left(c + \frac{1}{2} \right) \right) C \right. \\ \left. + \frac{1}{2} \left(\cos^{-1} c - c\sqrt{1-c^2} \right) \right] Q = -\rho vb^2 (T_{12}C - T_4)Q \quad (\text{IX})$$

$$M_\alpha = 2\pi\rho vb^2 \left[\left(a + \frac{1}{2} \right) C - \frac{1}{2} \right] Q \quad (\text{X})$$

where Q is given above and $C = C(k)$ will be treated in the following section.

VALUE OF THE FUNCTION $C(k)$

Put $U = U_0 e^{i \left[k \left(\frac{s}{b} - x_0 \right) + \varphi \right]}$

where $s = vt$ ($s \rightarrow \infty$), the distance from the first vortex element to the airfoil, and k a positive constant determining the wave length, then

$$C(k) = \frac{\int_1^\infty \frac{x_0}{\sqrt{x_0^2-1}} e^{-ikx_0} dx_0}{\int_1^\infty \sqrt{\frac{x_0+1}{x_0-1}} e^{-ikx_0} dx_0} \quad (\text{XI})$$

These integrals are known, see next part, formulas (XIV)–(XVII) and we obtain³

$$C(k) = \frac{-\frac{\pi}{2} J_1 + i \frac{\pi}{2} Y_1}{-\frac{\pi}{2} J_1 - \frac{\pi}{2} Y_0 + i \frac{\pi}{2} Y_1 - i \frac{\pi}{2} J_0} = \frac{-J_1 + i Y_1}{-(J_1 + Y_0) + i(Y_1 - J_0)} \\ = \frac{(-J_1 + i Y_1)[- (J_1 + Y_0) - i(Y_1 - J_0)]}{(J_1 + Y_0)^2 + (Y_1 - J_0)^2} \\ = \frac{J_1(J_1 + Y_0) + Y_1(Y_1 - J_0)}{(J_1 + Y_0)^2 + (Y_1 - J_0)^2} \\ - i \frac{Y_1(J_1 + Y_0) - J_1(Y_1 - J_0)}{(J_1 + Y_0)^2 + (Y_1 - J_0)^2} = F + iG$$

where

$$F = \frac{J_1(J_1 + Y_0) + Y_1(Y_1 - J_0)}{(J_1 + Y_0)^2 + (Y_1 - J_0)^2} \quad (\text{XII})$$

$$G = -\frac{Y_1 Y_0 + J_1 J_0}{(J_1 + Y_0)^2 + (Y_1 - J_0)^2} \quad (\text{XIII})$$

These functions, which are of fundamental importance in the theory of the oscillating airfoil are given graphically against the argument $\frac{1}{k}$ in figure 4.

SOLUTION OF THE DEFINITE INTEGRALS IN C BY MEANS OF BESSEL FUNCTIONS

We have

$$K_n(z) = \int_0^\infty e^{-z \cosh t} \cosh nt \, dt$$

(Formula (34), p. 51—Gray, Mathews & MacRobert: Treatise on Bessel Functions. London, 1922)

where

$$K_n(t) = e^{\frac{in\pi}{2}} G_n(it)$$

(Eq. (28), sec. 3, p. 23, same reference)

and

$$G_n(x) = -\overline{Y}_n(x) + \left[\log 2 - \gamma + \frac{i\pi}{2} \right] J_n(x)$$

but

$$\overline{Y}_n(x) = \frac{\pi}{2} Y_n(x) + (\log 2 - \gamma) J_n(x)$$

(where $Y_n(x)$ is from N. Nielsen: Handbuch der Theorie der Cylinderfunktionen. Leipzig, 1904).

³ This may also be expressed in Hänkel functions, $C = \frac{H_1^{(2)}}{H_0^{(2)} + i H_0^{(1)}}$

Thus,

$$G_n(x) = -\frac{\pi}{2}[Y_n(x) - iJ_n(x)]$$

We have

$$K_0(-ik) = \int_0^\infty e^{ik \cosh t} dt = \int_1^\infty \frac{e^{ikx}}{\sqrt{x^2-1}} dx$$

or

$$-\frac{\pi}{2}Y_0(k) + i\frac{\pi}{2}J_0(k) = \int_1^\infty \frac{\cos kx dx}{\sqrt{x^2-1}} + i \int_1^\infty \frac{\sin kx dx}{\sqrt{x^2-1}}$$

Thus,

$$\int_1^\infty \frac{\cos kx dx}{\sqrt{x^2-1}} = -\frac{\pi}{2}Y_0(k) \quad (\text{XIV})$$

$$\int_1^\infty \frac{\sin kx dx}{\sqrt{x^2-1}} = \frac{\pi}{2}J_0(k) \quad (\text{XV})$$

Further,

$$K_1(-ik) = \int_0^\infty e^{ik \cosh t} \cosh t dt = \int_1^\infty \frac{e^{ikx} x dx}{\sqrt{x^2-1}}$$

$$iG_1(k) = -i\frac{\pi}{2}Y_1(k) - \frac{\pi}{2}J_1(k)$$

$$= \int_1^\infty \frac{x}{\sqrt{x^2-1}} (\cos kx + i \sin kx) dx$$

Thus,

$$\int_1^\infty \frac{x \cos kx dx}{\sqrt{x^2-1}} = -\frac{\pi}{2}J_1(k) \quad (\text{XVI})$$

$$\int_1^\infty \frac{x \sin kx dx}{\sqrt{x^2-1}} = -\frac{\pi}{2}Y_1(k) \quad (\text{XVII})$$

TOTAL AERODYNAMIC FORCES AND MOMENTS

TOTAL FORCE

From equations (I) and (VIII) we obtain

$$\begin{aligned} P = & -\rho b^2(v\pi\dot{\alpha} + \pi\ddot{h} - \pi b a \ddot{\alpha} - vT_4\dot{\beta} - T_1b\ddot{\beta}) \\ & - 2\pi\rho v b C \left\{ v\alpha + \dot{h} + b\left(\frac{1}{2} - a\right)\dot{\alpha} + \frac{1}{\pi}T_{10}v\beta \right. \\ & \left. + b\frac{1}{2\pi}T_{11}\dot{\beta} \right\} \end{aligned} \quad (\text{XVIII})$$

TOTAL MOMENTS

From equations (II) and (IX) we obtain similarly

$$\begin{aligned} M_\beta = & -\rho b^2 \left[\left(-2T_9 - T_1 + T_4\left(a - \frac{1}{2}\right) \right) v b \dot{\alpha} + 2T_{13}b^2\ddot{\alpha} \right. \\ & + \frac{1}{\pi}v^2\beta(T_9 - T_4T_{10}) - \frac{1}{2\pi}v b \dot{\beta}T_4T_{11} - \frac{1}{\pi}T_3b^2\ddot{\beta} \\ & \left. - T_1b\ddot{h} \right] - \rho v b^2 T_{12} C \left\{ v\alpha + \dot{h} + b\left(\frac{1}{2} - a\right)\dot{\alpha} \right. \\ & \left. + \frac{1}{\pi}T_{10}v\beta + b\frac{1}{2\pi}T_{11}\dot{\beta} \right\} \end{aligned} \quad (\text{XIX})$$

From equations (III) and (X)

$$\begin{aligned} M_\alpha = & -\rho b^2 \left[\pi\left(\frac{1}{2} - a\right) v b \dot{\alpha} + \pi b^2\left(\frac{1}{8} + a^2\right)\ddot{\alpha} \right. \\ & + (T_4 + T_{10})v^2\beta \\ & + \left(T_1 - T_9 - (c-a)T_4 + \frac{1}{2}T_{11} \right) v b \dot{\beta} \\ & - \left(T_7 + (c-a)T_1 \right) b^2\ddot{\beta} - a\pi b \ddot{h} \\ & + 2\rho v b^2 \pi \left(a + \frac{1}{2} \right) C \left\{ v\alpha + \dot{h} + b\left(\frac{1}{2} - a\right)\dot{\alpha} \right. \\ & \left. + \frac{1}{\pi}T_{10}v\beta + b\frac{1}{2\pi}T_{11}\dot{\beta} \right\} \end{aligned} \quad (\text{XX})$$

DIFFERENTIAL EQUATIONS OF MOTION

Expressing the equilibrium of the moments about a of the entire airfoil, of the moments on the aileron about c , and of the vertical forces, we obtain, respectively, the following three equations:

$$\begin{aligned} \alpha: & -I_\alpha\ddot{\alpha} - I_\beta\ddot{\beta} - b(c-a)S_\beta\ddot{\beta} - S_\alpha\ddot{h} - \alpha C_\alpha + M_\alpha = 0 \\ \beta: & -I_\beta\ddot{\beta} - I_\alpha\ddot{\alpha} - b(c-a)\ddot{\alpha}S_\beta - \ddot{h}S_\beta - \beta C_\beta + M_\beta = 0 \\ h: & -\ddot{h}M - \ddot{\alpha}S_\alpha - \ddot{\beta}S_\beta - \ddot{h}C_h + P = 0 \end{aligned}$$

Rearranged:

$$\begin{aligned} \alpha: & \ddot{\alpha}I_\alpha + \ddot{\beta}(I_\beta + b(c-a)S_\beta) + \ddot{h}S_\alpha + \alpha C_\alpha - M_\alpha = 0 \\ \beta: & \ddot{\alpha}(I_\beta + b(c-a)S_\beta) + \ddot{\beta}I_\beta + \ddot{h}S_\beta + \beta C_\beta - M_\beta = 0 \\ h: & \ddot{\alpha}S_\alpha + \ddot{\beta}S_\beta + \ddot{h}M + hC_h - P = 0 \end{aligned}$$

The constants are defined as follows:

ρ ,	mass of air per unit of volume.
b ,	half chord of wing.
M ,	mass of wing per unit of length.
S_α, S_β ,	static moments of wing (in slugs-feet) per unit length of wing-aileron and aileron, respectively. The former is referred to the axis a ; the latter, to the hinge c .
I_α, I_β ,	moments of inertia per unit length of wing-aileron and aileron about a and c , respectively.
C_α ,	torsional stiffness of wing around a , corresponding to unit length.
C_β ,	torsional stiffness of aileron around c , corresponding to unit length.
C_h ,	stiffness of wing in deflection, corresponding to unit length.

DEFINITION OF PARAMETERS USED IN EQUATIONS

$$\kappa = \frac{\pi\rho b^2}{M}, \quad \text{the ratio of the mass of a cylinder of air of a diameter equal to the chord of the wing to the mass of the wing, both taken for equal length along span.}$$

$r_\alpha = \sqrt{\frac{I_\alpha}{Mb^2}}$, the radius of gyration divided by b .
 $x_\alpha = \frac{S_\alpha}{Mb}$, the center of gravity distance of the wing from a , divided by b .
 $\omega_\alpha = \sqrt{\frac{C_\alpha}{I_\alpha}}$, the frequency of torsional vibration around a .
 $r_\beta = \sqrt{\frac{I_\beta}{Mb^2}}$, reduced radius of gyration of aileron divided by b , that is, the radius at which the entire mass of the airfoil would have to be concentrated to give the moment of inertia of the aileron I_β .

$x_\beta = \frac{S_\beta}{Mb}$, reduced center of gravity distance from c .
 $\omega_\beta = \sqrt{\frac{C_\beta}{I_\beta}}$, frequency of torsional vibration of aileron around c .
 $\omega_h = \sqrt{\frac{C_h}{M}}$, frequency of wing in deflection.

FINAL EQUATIONS IN NONDIMENSIONAL FORM

On introducing the quantities M_α , M_β , and P , replacing T_0 and T_{13} from page 5, and reducing to nondimensional form, we obtain the following system of equations:

$$\begin{aligned}
 \text{(A)} \quad & \ddot{\alpha} \left[r_\alpha^2 + \kappa \left(\frac{1}{8} + a^2 \right) \right] + \dot{\alpha} \frac{v}{b} \kappa \left(\frac{1}{2} - a \right) + \alpha \frac{C_\alpha}{Mb^2} + \ddot{\beta} \left[r_\beta^2 + (c-a)x_\beta - \frac{T_7}{\pi} \kappa - (c-a) \frac{T_1}{\pi} \kappa \right] + \frac{1}{\pi} \dot{\beta} \kappa \frac{v}{b} \left[-2p - \left(\frac{1}{2} - a \right) T_4 \right] \\
 & + \beta \kappa \frac{v^2}{b^2} \frac{1}{\pi} (T_4 + T_{10}) + \ddot{h} \left(x_\alpha - a\kappa \right) \frac{1}{b} - 2\kappa \left(a + \frac{1}{2} \right) \frac{vC(k)}{b} \left[\frac{v\alpha}{b} + \frac{\dot{h}}{b} + \left(\frac{1}{2} - a \right) \dot{\alpha} + \frac{T_{10}}{\pi} \frac{v}{b} \beta + \frac{T_{11}}{2\pi} \dot{\beta} \right] = 0 \\
 \text{(B)} \quad & \ddot{\alpha} \left[r_\beta^2 + (c-a)x_\beta - \kappa \frac{T_7}{\pi} - (c-a) \frac{T_1}{\pi} \kappa \right] + \dot{\alpha} \left(p - T_1 - \frac{1}{2} T_4 \right) \frac{v}{b} \kappa + \ddot{\beta} \left(r_\beta^2 - \frac{1}{\pi} \kappa T_3 \right) - \frac{1}{2\pi^2} \dot{\beta} T_4 T_{11} \frac{v}{b} \kappa \\
 & + \beta \left[\frac{C_\beta}{Mb^2} + \frac{1}{\pi^2} \frac{v^2}{b^2} \kappa (T_5 - T_4 T_{10}) \right] + \ddot{h} \left(x_\beta - \frac{1}{\pi} \kappa T_1 \right) \frac{1}{b} + \frac{T_{12}}{\pi} \kappa \frac{vC(k)}{b} \left[\frac{v\alpha}{b} + \frac{\dot{h}}{b} + \left(\frac{1}{2} - a \right) \dot{\alpha} + \frac{T_{10}}{\pi} \frac{v}{b} \beta + \frac{T_{11}}{2\pi} \dot{\beta} \right] = 0 \\
 \text{(C)} \quad & \ddot{\alpha} \left(x_\alpha - \kappa a \right) + \dot{\alpha} \frac{v}{b} \kappa + \ddot{\beta} \left(x_\beta - \frac{1}{\pi} T_1 \kappa \right) - \dot{\beta} \frac{v}{b} T_4 \kappa \frac{1}{\pi} + \ddot{h} (1 + \kappa) \frac{1}{b} + h \frac{C_h}{M} \frac{1}{b} \\
 & + 2\kappa \frac{vC(k)}{b} \left[\frac{v\alpha}{b} + \frac{\dot{h}}{b} + \left(\frac{1}{2} - a \right) \dot{\alpha} + \frac{T_{10}}{\pi} \frac{v}{b} \beta + \frac{T_{11}}{2\pi} \dot{\beta} \right] = 0
 \end{aligned}$$

SOLUTION OF EQUATIONS

As mentioned in the introduction, we shall only have to specify the conditions under which an unstable equilibrium may exist, no general solution being needed. We shall therefore introduce the variables at once as sine functions of the distance s or, in complex form with $\frac{1}{k}$ as an auxiliary parameter, giving the ratio of the wave length to 2π times the half chord b :

$$\alpha = \alpha_0 e^{ik \frac{s}{b}}$$

$$\beta = \beta_0 e^{i \left(k \frac{s}{b} + \varphi_1 \right)}$$

and

$$h = h_0 e^{i \left(k \frac{s}{b} + \varphi_2 \right)}$$

where s is the distance from the airfoil to the first vortex element, $\frac{ds}{dt} = v$, and φ_1 and φ_2 are phase angles of β and h with respect to α .

Having introduced these quantities in our system of equations, we shall divide through by $\left(\frac{v}{b} k \right)^2 \kappa$.

We observe that the velocity v is then contained in only one term of each equation. We shall consider this term containing v as the unknown parameter ΩX . To distinguish terms containing X we shall employ a bar; terms without bars do not contain X .

We shall resort to the following notation, taking care to retain a perfectly cyclic arrangement. Let the letter A refer to the coefficients in the first equation not containing $C(k)$ or X , B to similar coefficients of the second equation, and C to those in the third equation. Let the first subscript α refer to the first variable α , the subscript β to the second, and h to the third. Let the second subscripts 1, 2, 3 refer to the second derivative, the first derivative, and the argument of each variable, respectively. $A_{\alpha 1}$ thus refers to the coefficient in the first equation associated with the second derivative of α and not containing $C(k)$ or

X ; C_{h3} to the constant in the third equation attached to h , etc. These coefficients⁴ are as follows:

$$A_{a1} = \frac{r_{\alpha}^2}{\kappa} + \left(\frac{1}{8} + a^2\right)$$

$$A_{a2} = \left(\frac{1}{2} - a\right)$$

$$A_{a3} = 0$$

$$A_{\beta 1} = \frac{r_{\beta}^2}{\kappa} - \frac{T_7}{\pi} + (c-a) \left(\frac{x_{\beta}}{\kappa} - \frac{T_1}{\pi}\right)$$

$$A_{\beta 2} = \frac{1}{\pi} \left[-2p - \left(\frac{1}{2} - a\right) T_4\right]$$

$$A_{\beta 3} = \frac{1}{\pi} (T_4 + T_{10})$$

$$A_{h1} = \frac{x_{\alpha}}{\kappa} - a$$

$$A_{h2} = 0$$

$$A_{h3} = 0$$

$$B_{a1} = \frac{r_{\beta}^2}{\kappa} - \frac{T_7}{\pi} + (c-a) \left(\frac{x_{\beta}}{\kappa} - \frac{T_1}{\pi}\right) \quad (=A_{\beta 1})$$

$$B_{a2} = \frac{1}{\pi} \left(p - T_1 - \frac{1}{2} T_4\right)$$

$$B_{a3} = 0$$

$$B_{\beta 1} = \frac{r_{\beta}^2}{\kappa} - \frac{1}{\pi^2} T_3$$

$$B_{\beta 2} = -\frac{1}{2\pi^2} T_4 T_{11}$$

$$B_{\beta 3} = \frac{1}{\pi^2} (T_5 - T_4 T_{10})$$

$$B_{h1} = \frac{x_{\beta}}{\kappa} - \frac{1}{\pi} T_1$$

$$B_{h2} = 0$$

$$B_{h3} = 0$$

$$C_{a1} = \frac{x_{\alpha}}{\kappa} - a \quad (=A_{h1})$$

$$C_{a2} = 1$$

$$C_{a3} = 0$$

$$C_{\beta 1} = \frac{x_{\beta}}{\kappa} - \frac{1}{\pi} T_1 \quad (=B_{h1})$$

$$C_{\beta 2} = -\frac{1}{\pi} T_4$$

$$C_{\beta 3} = 0$$

$$C_{h1} = \frac{1}{\kappa} + 1$$

$$C_{h2} = 0$$

$$C_{h3} = 0$$

⁴The factor $\frac{1}{k}$ or $\frac{1}{k^2}$ is not included in these constants. See the expressions for the R 's and I 's on next page.

The solution of the instability problem as contained in the system of three equations A, B, and C is given by the vanishing of a third-order determinant of complex numbers representing the coefficients. The solution of particular subcases of two degrees of freedom is given by the minors involving the particular coefficients. We shall denote the case *torsion-aileron* (α, β) as case 3, *aileron-deflection* (β, h) as case 2, and *deflection-torsion* (h, α) as case 1. The determinant form of the solution is given in the major case and in the three possible subcases, respectively, by:

$$\bar{D} = \begin{vmatrix} \bar{R}_{a\alpha} + iI_{a\alpha}, & \bar{R}_{a\beta} + iI_{a\beta}, & \bar{R}_{ah} + iI_{ah} \\ \bar{R}_{b\alpha} + iI_{b\alpha}, & \bar{R}_{b\beta} + iI_{b\beta}, & \bar{R}_{bh} + iI_{bh} \\ \bar{R}_{c\alpha} + iI_{c\alpha}, & \bar{R}_{c\beta} + iI_{c\beta}, & \bar{R}_{ch} + iI_{ch} \end{vmatrix} = 0$$

and

$$\bar{M}_{ch} = \begin{vmatrix} \bar{R}_{a\alpha} + iI_{a\alpha}, & \bar{R}_{a\beta} + iI_{a\beta} \\ \bar{R}_{b\alpha} + iI_{b\alpha}, & \bar{R}_{b\beta} + iI_{b\beta} \end{vmatrix} = 0 \quad \text{Case 3}$$

$$\bar{M}_{a\alpha} = \begin{vmatrix} \bar{R}_{b\beta} + iI_{b\beta}, & \bar{R}_{bh} + iI_{bh} \\ \bar{R}_{c\beta} + iI_{c\beta}, & \bar{R}_{ch} + iI_{ch} \end{vmatrix} = 0 \quad \text{Case 2}$$

$$\bar{M}_{b\beta} = \begin{vmatrix} \bar{R}_{ch} + iI_{ch}, & \bar{R}_{c\alpha} + iI_{c\alpha} \\ \bar{R}_{ah} + iI_{ah}, & \bar{R}_{a\alpha} + iI_{a\alpha} \end{vmatrix} = 0 \quad \text{Case 1}$$

REAL EQUATIONS

IMAGINARY EQUATIONS

$$\begin{vmatrix} \bar{R}_{a\alpha} \bar{R}_{a\beta} \\ \bar{R}_{b\alpha} \bar{R}_{b\beta} \end{vmatrix} - \begin{vmatrix} I_{a\alpha} I_{a\beta} \\ I_{b\alpha} I_{b\beta} \end{vmatrix} = 0 \quad \begin{vmatrix} \bar{R}_{a\alpha} \bar{R}_{a\beta} \\ I_{b\alpha} I_{b\beta} \end{vmatrix} + \begin{vmatrix} I_{a\alpha} I_{a\beta} \\ \bar{R}_{b\alpha} \bar{R}_{b\beta} \end{vmatrix} = 0 \quad \text{Case 3}$$

$$\begin{vmatrix} \bar{R}_{b\beta} \bar{R}_{bh} \\ \bar{R}_{c\beta} \bar{R}_{ch} \end{vmatrix} - \begin{vmatrix} I_{b\beta} I_{bh} \\ I_{c\beta} I_{ch} \end{vmatrix} = 0 \quad \begin{vmatrix} \bar{R}_{b\beta} \bar{R}_{bh} \\ I_{c\beta} I_{ch} \end{vmatrix} + \begin{vmatrix} I_{b\beta} I_{bh} \\ \bar{R}_{c\beta} \bar{R}_{ch} \end{vmatrix} = 0 \quad \text{Case 2}$$

$$\begin{vmatrix} \bar{R}_{ch} \bar{R}_{c\alpha} \\ \bar{R}_{ah} \bar{R}_{a\alpha} \end{vmatrix} - \begin{vmatrix} I_{ch} I_{c\alpha} \\ I_{ah} I_{a\alpha} \end{vmatrix} = 0 \quad \begin{vmatrix} \bar{R}_{ch} \bar{R}_{c\alpha} \\ I_{ah} I_{a\alpha} \end{vmatrix} + \begin{vmatrix} I_{ch} I_{c\alpha} \\ \bar{R}_{ah} \bar{R}_{a\alpha} \end{vmatrix} = 0 \quad \text{Case 1}$$

NOTE.—Terms with bars contain X ; terms without bars do not contain X .

The 9 quantities $R_{a\alpha}, R_{a\beta}$, etc., refer to the real parts and the 9 quantities $I_{a\alpha}, I_{a\beta}$, etc., to the imaginary parts of the coefficients of the 3 variables α, β , and h in the 3 equations A, B, C on page 10. Denoting the coefficients of $\ddot{\alpha}, \dot{\alpha}$, and α in the first equation by p, q , and r ,

$$R_{a\alpha} + iI_{a\alpha} = \frac{1}{\kappa} \left[-p + iq \frac{b}{kv} + r \left(\frac{b}{kv} \right)^2 \right]$$

which, separated in real and imaginary parts, gives the quantities $R_{a\alpha}$ and $I_{a\alpha}$. Similarly, the remaining quantities R and I are obtained. They are all functions of k or $C(k)$. The terms with bars $\bar{R}_{a\alpha}, \bar{R}_{b\beta}$, and \bar{R}_{ch} are seen to be the only ones containing the unknown X . The quantities Ω and X will be defined shortly. The quantities R and I are given in the following list:

$$\left\{ \begin{aligned} \bar{R}_{a\alpha} &= -A_{\alpha 1} + \Omega_{\alpha} X + \frac{1}{k} 2 \left(\frac{1}{2} + a \right) \left[\left(\frac{1}{2} - a \right) G - \frac{1}{k} F \right] \end{aligned} \right. \quad (1)$$

$$\left\{ \begin{aligned} \bar{R}_{a\beta} &= -A_{\beta 1} + \frac{1}{k^2} A_{\beta 3} + \frac{1}{k} \frac{1}{\pi} \left(a + \frac{1}{2} \right) \left[T_{11} G - 2 \frac{1}{k} T_{10} F \right] \end{aligned} \right. \quad (2)$$

$$\left\{ \begin{aligned} \bar{R}_{a h} &= -A_{h 1} + \frac{1}{k} 2 \left(a + \frac{1}{2} \right) G \end{aligned} \right. \quad (3)$$

$$\left\{ \begin{aligned} \bar{R}_{b\alpha} &= -B_{\alpha 1} - \frac{1}{k} \frac{T_{12}}{\pi} \left[\left(\frac{1}{2} - a \right) G - \frac{1}{k} F \right] \end{aligned} \right. \quad (4)$$

$$\left\{ \begin{aligned} \bar{R}_{b\beta} &= -B_{\beta 1} + \frac{1}{k^2} B_{\beta 3} + \Omega_{\beta} X - \frac{1}{k^2} \frac{T_{12}}{\pi^2} \left[T_{11} G - 2 T_{10} \frac{1}{k} F \right] \end{aligned} \right. \quad (5)$$

$$\left\{ \begin{aligned} \bar{R}_{b h} &= -B_{h 1} - \frac{1}{k} \frac{T_{12}}{\pi} G \end{aligned} \right. \quad (6)$$

$$\left\{ \begin{aligned} \bar{R}_{c\alpha} &= -C_{\alpha 1} - \frac{1}{k} 2 \left[\left(\frac{1}{2} - a \right) G - \frac{1}{k} F \right] \end{aligned} \right. \quad (7)$$

$$\left\{ \begin{aligned} \bar{R}_{c\beta} &= -C_{\beta 1} - \frac{1}{k} \frac{1}{\pi} \left[T_{11} G - 2 T_{10} \frac{1}{k} F \right] \end{aligned} \right. \quad (8)$$

$$\left\{ \begin{aligned} \bar{R}_{c h} &= -C_{h 1} + \Omega_h X - \frac{1}{k} 2 G \end{aligned} \right. \quad (9)$$

$$\left\{ \begin{aligned} I_{a\alpha} &= -\frac{1}{k} \left[2 \left(a + \frac{1}{2} \right) \left\{ \left(\frac{1}{2} - a \right) F + \frac{1}{k} G \right\} - A_{\alpha 2} \right] \end{aligned} \right. \quad (11)$$

$$\left\{ \begin{aligned} I_{a\beta} &= -\frac{1}{k} \left[\frac{1}{\pi} \left(a + \frac{1}{2} \right) \left(T_{11} F + 2 \frac{1}{k} T_{10} G \right) - A_{\beta 2} \right] \end{aligned} \right. \quad (12)$$

$$\left\{ \begin{aligned} I_{a h} &= -\frac{1}{k} 2 \left(a + \frac{1}{2} \right) F \end{aligned} \right. \quad (13)$$

$$\left\{ \begin{aligned} I_{b\alpha} &= \frac{1}{k} \left[\frac{T_{12}}{\pi} \left\{ \left(\frac{1}{2} - a \right) F + \frac{1}{k} G \right\} + B_{\alpha 2} \right] \end{aligned} \right. \quad (14)$$

$$\left\{ \begin{aligned} I_{b\beta} &= \frac{1}{k} \left[\frac{T_{12}}{2\pi^2} \left(T_{11} F + 2 \frac{1}{k} T_{10} G \right) + B_{\beta 2} \right] \end{aligned} \right. \quad (15)$$

$$\left\{ \begin{aligned} I_{b h} &= \frac{1}{k} \frac{T_{12}}{\pi} F \end{aligned} \right. \quad (16)$$

$$\left\{ \begin{aligned} I_{c\alpha} &= \frac{1}{k} \left[2 \left\{ \left(\frac{1}{2} - a \right) F + \frac{1}{k} G \right\} + C_{\alpha 2} \right] \end{aligned} \right. \quad (17)$$

$$\left\{ \begin{aligned} I_{c\beta} &= \frac{1}{k} \left[\frac{1}{\pi} \left(T_{11} F + 2 \frac{1}{k} T_{10} G \right) + C_{\beta 2} \right] \end{aligned} \right. \quad (18)$$

$$\left\{ \begin{aligned} I_{c h} &= \frac{1}{k} 2 F \end{aligned} \right. \quad (19)$$

The solution as given by the three-row determinant shall be written explicitly in X . We are immediately able to put down for the general case a cubic equation in X with complex coefficients and can easily segregate the three subcases. The quantity D is as before the value of the determinant, but with the term containing X missing. The quantities $M_{a\alpha}$, $M_{b\beta}$, and M_{ch} are the minors of the elements in the diagonal squares $a\alpha$, $b\beta$, and ch , respectively. They are expressed explicitly in terms of R and I under the subcases treated in the following paragraphs.

$$\bar{D} = \begin{vmatrix} A_{a\alpha} + \Omega_{\alpha} X & A_{a\beta} & A_{a h} \\ A_{b\alpha} & A_{b\beta} + \Omega_{\beta} X & A_{b h} \\ A_{c\alpha} & A_{c\beta} & A_{c h} + \Omega_h X \end{vmatrix} = 0$$

where $A_{a\alpha} = R_{a\alpha} + iI_{a\alpha}$ etc.

Complex cubic equation in X :

$$\Omega_{\alpha} \Omega_{\beta} \Omega_h X^3 + (\Omega_{\alpha} \Omega_{\beta} A_{ch} + \Omega_{\beta} \Omega_h A_{a\alpha} + \Omega_h \Omega_{\alpha} A_{b\beta}) X^2 + (\Omega_{\alpha} M_{a\alpha} + \Omega_{\beta} M_{b\beta} + \Omega_h M_{ch}) X + D = 0 \quad (XXI)$$

Case 3, (α , β):

$$\Omega_{\alpha} \Omega_{\beta} X^2 + (\Omega_{\alpha} A_{b\beta} + \Omega_{\beta} A_{a\alpha}) X + M_{ch} = 0 \quad (XXII)$$

Case 2, (β , h):

$$\Omega_{\beta} \Omega_h X^2 + (\Omega_{\beta} A_{ch} + \Omega_h A_{b\beta}) X + M_{a\alpha} = 0 \quad (XXIII)$$

Case 1, (h , α):

$$\Omega_h \Omega_{\alpha} X^2 + (\Omega_h A_{a\alpha} + \Omega_{\alpha} A_{ch}) X + M_{b\beta} = 0 \quad (XXIV)$$

$$\Omega_{\alpha} X = \frac{C_{\alpha}}{k^2 M v^2 \kappa} = \left(\frac{\omega_{\alpha} r_{\alpha}}{\omega_r r_r} \right)^2 \frac{1}{\kappa} \left(\frac{b r_r \omega_r}{v k} \right)^2$$

$$\Omega_{\beta} X = \frac{C_{\beta}}{k^2 M v^2 \kappa} = \left(\frac{\omega_{\beta} r_{\beta}}{\omega_r r_r} \right)^2 \frac{1}{\kappa} \left(\frac{b r_r \omega_r}{v k} \right)^2$$

$$\Omega_h X = \frac{C_h b^2}{k^2 M v^2 \kappa} = \left(\frac{\omega_h}{\omega_r r_r} \right)^2 \frac{1}{\kappa} \left(\frac{b r_r \omega_r}{v k} \right)^2$$

and finally

$$X = \frac{1}{\kappa} \left(\frac{b r_r \omega_r}{v k} \right)^2$$

We are at liberty to introduce the reference parameters ω_r and r_r , and the convention adopted is: ω_r is the last ω in cyclic order in each of the subcases 3, 2, and 1.

Then $\Omega_n = \left(\frac{\omega_n r_n}{\omega_{n+1} r_{n+1}} \right)^2$ and $\Omega_{n+1} = 1$, thus for

$$\text{Case 3, } \Omega_{\alpha} = \left(\frac{\omega_{\alpha} r_{\alpha}}{\omega_{\beta} r_{\beta}} \right)^2 \text{ and } \Omega_{\beta} = 1$$

$$\text{Case 2, } \Omega_{\beta} = \left(\frac{\omega_{\beta} r_{\beta}}{\omega_h} \right)^2 \text{ and } \Omega_h = 1$$

$$\text{Case 1, } \Omega_h = \left(\frac{\omega_h}{\omega_{\alpha} r_{\alpha}} \right)^2 \text{ and } \Omega_{\alpha} = 1$$

To treat the general case of three degrees of freedom (equation (XXI)), it is observed that the real part of the equation is of third degree while the imaginary part furnishes an equation of second degree. The problem is to find values of X satisfying both equations. We shall adopt the following procedure: Plot graphically X against $\frac{1}{k}$ for both equations. The points of intersection are the solutions. We are only concerned with positive values of $\frac{1}{k}$ and positive values of X . Observe that we do not have to solve for k , but may reverse the process by choosing a number of values of k and solve for X . The plotting of X against $\frac{1}{k}$ for the second-degree equation is simple

enough, whereas the task of course is somewhat more laborious for the third-degree equation. However, the general case is of less practical importance than are the three subcases. The equation simplifies considerably, becoming of second degree in X .

We shall now proceed to consider these three subcases. By virtue of the cyclic arrangement, we need only consider the first case (α, β) . The complex quadratic equations (XXII)–(XXIV) all resolve themselves into two independent statements, which we shall for convenience denote "Imaginary equation" and "Real equation", the former being of first and the latter of second degree in X . All constants are to be resolved into their real and imaginary parts, denoted by an upper index R or I , respectively.

Let $M_{aa} = M_{aa}^R + iM_{aa}^I$ and let similar expressions denote M_{bb} and M_{ch} .

Case 3, (α, β) . Separating equation (XXII) we obtain.
(1) Imaginary equation:

$$(\Omega_a I_{b\beta} + \Omega_\beta I_{a\alpha})X + M_{ch}^I = 0$$

$$X = -\frac{M_{ch}^I}{\Omega_a I_{b\beta} + \Omega_\beta I_{a\alpha}}$$

(2) Real equation:

$$\Omega_a \Omega_\beta X^2 + (\Omega_a R_{b\beta} + \Omega_\beta R_{a\alpha})X + M_{ch}^R = 0$$

Eliminating X we get

$$\Omega_a \Omega_\beta (M_{ch}^I)^2 - (\Omega_a R_{b\beta} + \Omega_\beta R_{a\alpha})(\Omega_a I_{b\beta} + \Omega_\beta I_{a\alpha})M_{ch}^I + M_{ch}^R (\Omega_a I_{b\beta} + \Omega_\beta I_{a\alpha})^2 = 0$$

By the convention adopted we have in this case:

$$\omega_r = \omega_\beta, \quad \Omega_\alpha = \left(\frac{\omega_\alpha}{\omega_\beta}\right)^2 \left(\frac{r_\alpha}{r_\beta}\right)^2, \quad \text{and } \Omega_\beta = 1$$

Arranging the equation in powers of Ω_α we have:

$$\begin{aligned} \Omega_\alpha^2 [-M_{ch}^I (R_{b\beta} I_{b\beta}) + M_{ch}^R I_{b\beta}^2] + \Omega_\alpha [(M_{ch}^I)^2 \\ - M_{ch}^I (R_{a\alpha} I_{b\beta} + I_{a\alpha} R_{b\beta}) + 2M_{ch}^R I_{a\alpha} I_{b\beta}] \\ + [-M_{ch}^I R_{a\alpha} I_{a\alpha} + M_{ch}^R I_{a\alpha}^2] = 0 \end{aligned}$$

But we have

$$\begin{aligned} (M_{ch}^I)^2 - M_{ch}^I (R_{a\alpha} I_{b\beta} + I_{a\alpha} R_{b\beta}) \\ = M_{ch}^I [R_{a\alpha} I_{b\beta} - R_{a\beta} I_{b\alpha} + R_{b\beta} I_{a\alpha} - R_{b\alpha} I_{a\beta} - R_{a\alpha} I_{b\beta} - R_{b\beta} I_{a\alpha}] \\ = -M_{ch}^I (R_{a\beta} I_{b\alpha} + I_{a\beta} R_{b\alpha}) \end{aligned}$$

Finally, the equation for Case 3 (α, β) becomes:

$$\begin{aligned} \Omega_\alpha^2 (M_{ch}^R I_{b\beta}^2 - M_{ch}^I R_{b\beta} I_{b\beta}) + \Omega_\alpha [-M_{ch}^I (R_{a\beta} I_{b\alpha} + I_{a\beta} R_{b\alpha}) \\ + 2M_{ch}^R I_{a\alpha} I_{b\beta}] + M_{ch}^R I_{a\alpha}^2 - M_{ch}^I R_{a\alpha} I_{a\alpha} = 0 \quad (XXV) \end{aligned}$$

where

$$\begin{aligned} M_{ch}^R &= R_{a\alpha} R_{b\beta} - R_{a\beta} R_{b\alpha} - I_{a\alpha} I_{b\beta} + I_{a\beta} I_{b\alpha} \\ M_{ch}^I &= R_{a\alpha} I_{b\beta} - R_{a\beta} I_{b\alpha} + I_{a\alpha} R_{b\beta} - I_{a\beta} R_{b\alpha} \end{aligned}$$

The remaining cases may be obtained by cyclic rearrangement:

$$\text{Case 2, } (\beta, h) \quad \omega_r = \omega_h \quad \Omega_\beta = \left(\frac{\omega_\beta}{\omega_h}\right)^2 r_\beta^2 \quad \Omega_h = 1$$

$$\begin{aligned} \Omega_\beta^2 (M_{aa}^R I_{ch}^2 - M_{aa}^I R_{ch} I_{ch}) + \Omega_\beta [-M_{aa}^I (R_{bh} I_{c\beta} + I_{bh} R_{c\beta}) \\ + 2M_{aa}^R I_{b\beta} I_{ch}] + M_{aa}^R I_{b\beta}^2 - M_{aa}^I R_{b\beta} I_{b\beta} = 0 \quad (XXVI) \end{aligned}$$

$$\begin{aligned} \text{where } M_{aa}^R &= R_{b\beta} R_{ch} - R_{bh} R_{c\beta} - I_{b\beta} I_{ch} + I_{bh} I_{c\beta} \\ M_{aa}^I &= R_{b\beta} I_{ch} - R_{bh} I_{c\beta} + I_{b\beta} R_{ch} - I_{bh} R_{c\beta} \end{aligned}$$

$$\text{Case 1, } (h, \alpha) \quad \omega_r = \omega_\alpha \quad \Omega_h = \left(\frac{\omega_h}{\omega_\alpha}\right)^2 \frac{1}{r_\alpha^2} \quad \Omega_\alpha = 1$$

$$\begin{aligned} \Omega_h^2 (M_{bb}^R I_{aa}^2 - M_{bb}^I R_{aa} I_{aa}) + \Omega_h [-M_{bb}^I (R_{ca} I_{ah} + I_{ca} R_{ah}) \\ + 2M_{bb}^R I_{ch} I_{aa}] + M_{bb}^R I_{ch}^2 - M_{bb}^I R_{ch} I_{ch} = 0 \quad (XXVII) \end{aligned}$$

$$\begin{aligned} \text{where } M_{bb}^R &= R_{ch} R_{aa} - R_{ca} R_{ah} - I_{ch} I_{aa} + I_{ca} I_{ah} \\ M_{bb}^I &= R_{ch} I_{aa} - R_{ca} I_{ah} + I_{ch} R_{aa} - I_{ca} R_{ah} \end{aligned}$$

Equations (XXV), (XXVI), and (XXVII) thus give the solutions of the cases: *torsion-aileron*, *aileron-deflection*, and *deflection-torsion*, respectively. The quantity Ω may immediately be plotted against

$\frac{1}{k}$ for any value of the independent parameters.

The coefficients in the equations are all given in terms of R and I , which quantities have been defined above. Routine calculations and graphs giving Ω against $\frac{1}{k}$ are contained in Appendix I and Appendix II.

Knowing related values of Ω and $\frac{1}{k}$, X is immediately

expressed as a function of Ω by means of the first-degree equation. The definition of X and Ω for each subcase is given above. The cyclic arrangement of all quantities is very convenient as it permits identical treatment of the three subcases.

It shall finally be repeated that the above solutions represent the *border case* of unstable equilibrium. The plot of X against Ω gives a boundary curve between the stable and the unstable regions in the $X\Omega$ plane.

It is preferable, however, to plot the quantity $\frac{1}{k^2} \frac{1}{X}$

instead of X , since this quantity is proportional to the square of the flutter speed. The stable area can easily be identified by inspection as it will contain the axis $\frac{1}{k^2} \frac{1}{X} = 0$, if the combination is stable for zero velocity.

LANGLEY MEMORIAL AERONAUTICAL LABORATORY,
NATIONAL ADVISORY COMMITTEE FOR AERONAUTICS,
LANGLEY FIELD, VA., May 2, 1934.

APPENDIX I

PROCEDURE IN SOLVING NUMERICAL EXAMPLES

(1) Determine the R 's and I 's, nine of each for a major case of three degrees of freedom, or those pertaining to a particular subcase, 4 R 's and 4 I 's. Refer to the following for the R 's and I 's involved in each case:

The numerals 1 to 9 and 11 to 19 are used for convenience.

(Major case) Three degrees of freedom

1	$R_{a\alpha}$	$I_{a\alpha}$	11
2	$R_{a\beta}$	$I_{a\beta}$	12
3	R_{ah}	I_{ah}	13
4	$R_{b\alpha}$	$I_{b\alpha}$	14
5	$R_{b\beta}$	$I_{b\beta}$	15
6	R_{bh}	I_{bh}	16
7	$R_{c\alpha}$	$I_{c\alpha}$	17
8	$R_{c\beta}$	$I_{c\beta}$	18
9	R_{ch}	I_{ch}	19

(Case 3) Torsional-aileron (α, β)

1	$R_{a\alpha}$	$I_{a\alpha}$	11
2	$R_{a\beta}$	$I_{a\beta}$	12
4	$R_{b\alpha}$	$I_{b\alpha}$	14
5	$R_{b\beta}$	$I_{b\beta}$	15

(Case 2) Aileron-deflection (β, h)

5	$R_{b\beta}$	$I_{b\beta}$	15
6	R_{bh}	I_{bh}	16
8	$R_{c\beta}$	$I_{c\beta}$	18
9	R_{ch}	I_{ch}	19

(Case 1) Deflection-torsion (h, α)

7	$R_{c\alpha}$	$I_{c\alpha}$	17
9	R_{ch}	I_{ch}	19
1	$R_{a\alpha}$	$I_{a\alpha}$	11
3	R_{ah}	I_{ah}	13

It has been found convenient to split the R 's in two parts $R=R'+R''$, the former being independent of the argument $\frac{1}{k}$. The quantities I and R'' are func-

tions of the two independent parameters a and c only.⁵ The formulas are given in the following list.

$$R''_{a\alpha} = \frac{1}{k} 2 \left(a + \frac{1}{2} \right) \left(\left(\frac{1}{2} - a \right) G - \frac{F}{k} \right) \quad (1)$$

$$R''_{a\beta} = \frac{1}{k} \frac{1}{\pi} \left\{ (T_4 + T_{10}) \frac{1}{k} + \left(a + \frac{1}{2} \right) \left(T_{11} G - \frac{2}{k} T_{10} F \right) \right\} \quad (2)$$

$$R''_{ah} = \frac{1}{k} 2 \left(a + \frac{1}{2} \right) G \quad (3)$$

$$R''_{b\alpha} = -\frac{1}{k} \frac{T_{12}}{\pi} \left\{ \left(\frac{1}{2} - a \right) G - \frac{F}{k} \right\} \quad (4)$$

$$R''_{b\beta} = -\frac{1}{k} \frac{1}{\pi^2} \left\{ \frac{T_{12}}{2} \left(T_{11} G - \frac{2}{k} T_{10} F \right) - \frac{1}{k} (T_5 - T_4 T_{10}) \right\} \quad (5)$$

$$R''_{bh} = -\frac{1}{k} \frac{T_{12}}{\pi} G \quad (6)$$

$$R''_{c\alpha} = -\frac{1}{k} 2 \left(\left(\frac{1}{2} - a \right) G - \frac{F}{k} \right) \quad (7)$$

$$R''_{c\beta} = -\frac{1}{k} \frac{1}{\pi} \left(T_{11} G - 2 T_{10} \frac{F}{k} \right) \quad (8)$$

$$R''_{ch} = -\frac{1}{k} 2 G \quad (9)$$

$$I_{a\alpha} = -2 \left(a + \frac{1}{2} \right) \left\{ \left(\frac{1}{2} - a \right) F + \frac{1}{k} G \right\} + \frac{1}{2} - a \quad (11)$$

$$I_{a\beta} = -\frac{1}{\pi} \left\{ \left(a + \frac{1}{2} \right) \left(T_{11} F + \frac{2}{k} T_{10} G \right) + 2p + \left(\frac{1}{2} - a \right) T_4 \right\} \quad (12)$$

$$I_{ah} = -2 \left(a + \frac{1}{2} \right) F \quad (13)$$

$$I_{b\alpha} = \frac{T_{12}}{\pi} \left\{ \left(\frac{1}{2} - a \right) F + \frac{1}{k} G \right\} + \frac{1}{\pi} \left(p - T_1 - \frac{1}{2} T_4 \right) \quad (14)$$

Where $p = -\frac{1}{3} (1 - c^2)^{3/2}$

$$I_{b\beta} = \frac{1}{2\pi^2} \left\{ T_{12} \left(T_{11} F + \frac{2}{k} T_{10} G \right) - T_4 T_{11} \right\} \quad (15)$$

$$I_{bh} = \frac{T_{12}}{\pi} F \quad (16)$$

$$I_{c\alpha} = 2 \left\{ \left(\frac{1}{2} - a \right) F + \frac{1}{k} G \right\} + 1 \quad (17)$$

$$I_{c\beta} = \frac{1}{\pi} \left\{ \left(T_{11} F + \frac{2}{k} T_{10} G \right) - T_4 \right\} \quad (18)$$

$$I_{ch} = 2F \quad (19)$$

⁵ The quantities I given in the appendix and used in the following calculations are seen to differ from the I 's given in the body of the paper by the factor $\frac{1}{k}$. It may be noticed that this factor drops out in the first-degree equations.

Choosing certain values of a and c and employing the values of the T 's given by the formulas of the report (p. 5) or in table I and also using the values of F and G (formulas (XII) and (XIII)) or table II, we evaluate the quantities I and R'' for a certain number of $\frac{1}{k}$ values. The results of this evaluation are given in tables III and IV, which have been worked out for $a=0, -0.2$, and -0.4 , and for $c=0.5$ and $c=0$. The range of $\frac{1}{k}$ is from 0 to 40. These tables save the work of calculating the I 's and R'' 's for almost all cases of practical importance. Interpolation may be used for intermediate values. This leaves the quantities R' to be determined. These, being independent of $\frac{1}{k}$, are as a result easy to obtain. Their values, using the same system of numbers for identification, and referring to the definition of the original independent variables on pages 9 and 10, are given as follows:

$$R'_{aa} = -\frac{r_a^2}{\kappa} - \left(\frac{1}{8} + a^2\right) \quad (1)$$

$$R'_{ab} = -\frac{r_b^2}{\kappa} - (c-a)\frac{x_\beta}{\kappa} + \frac{T_7}{\pi} + (c-a)\frac{T_1}{\pi} \quad (2)$$

$$R'_{ah} = -\frac{x_a}{\kappa} + a \quad (3)$$

$$R'_{ba} = \text{same as } R'_{ab} \quad (4)$$

$$R'_{bb} = -\frac{r_b^2}{\kappa} + \frac{1}{\pi^2} T_3 \quad (5)$$

$$R'_{bh} = -\frac{x_\beta}{\kappa} + \frac{1}{\pi} T_1 \quad (6)$$

$$R'_{ca} = \text{same as } R'_{ah} \quad (7)$$

$$R'_{cb} = \text{same as } R'_{bh} \quad (8)$$

$$R'_{ch} = -\frac{1}{\kappa} - 1 \quad (9)$$

Because of the symmetrical arrangement in the determinant, the 9 quantities are seen to reduce to 6 quantities to be calculated. It is very fortunate, indeed, that all the remaining variables segregate themselves in the 6 values of R' which are independent of $\frac{1}{k}$, while the more complicated I and R'' are functions solely of c and a . In order to solve any problem it is therefore only necessary to refer to tables III and IV and then to calculate the 6 values of R' .

The quantities (1) to (9) and (11) to (19) thus having been determined, the plot of Ω against $\frac{1}{k}$, which constitutes our method of solution, is obtained by solving the equation $a\Omega^2 + b\Omega + c = 0$. The constants a , b , and c are obtained automatically by computation according to the following scheme:

Case 3

Find products 1.5 2.4 11.15 12.14

$$\text{Then } M^R_{ch} = 1.5 - 2.4 - \frac{1}{k^2}(11.15 - 12.14)$$

Find products 1.15 2.14 11.5 12.4

$$\text{Then } M^I_{ch} = 1.15 - 2.14 + 11.5 - 12.4$$

$$\text{and } a = M^R_{ch}(15)^2 - M^I_{ch}(5.15)$$

$$b = -M^I_{ch}(2.14 + 12.4) + 2M^R_{ch}(11.15)$$

$$c = M^R_{ch}(11)^2 - M^I_{ch}(1.11) \quad \text{Find } \Omega_a$$

$$\text{Solution: } \frac{1}{X} = -\frac{\Omega_a(15) + 11}{M^I_{ch}}$$

Similarly

Case 2

5.9 6.8 15.19 16.18

$$M^R_{aa} = 5.9 - 6.8 - \frac{1}{k^2}(15.19 - 16.18)$$

5.19 6.18 15.9 16.8

$$M^I_{aa} = 5.19 - 6.18 + 15.9 - 16.8$$

$$a = M^R_{aa}(19)^2 - M^I_{aa}(9.19)$$

$$b = -M^I_{aa}(6.18 + 16.8)$$

$$+ 2M^R_{aa}(6.18 + 16.8)$$

$$c = M^R_{aa}(15)^2 - M^I_{aa}(5.15) \quad \text{Find } \Omega_\beta$$

$$\frac{1}{X} = \frac{\Omega_\beta(19) + 15}{M^I_{aa}}$$

and

Case 1

9.1 7.3 19.11 17.13

$$M^R_{b\beta} = 9.1 - 7.3 - \frac{1}{k^2}(19.11 - 17.13)$$

9.11 7.13 19.1 17.3

$$M^I_{b\beta} = 9.11 - 7.13 + 19.1 - 17.3$$

$$a = M^R_{b\beta}(11)^2 - M^I_{b\beta}(1.11)$$

$$b = -M^I_{b\beta}(7.13 + 17.3) + 2M^R_{b\beta}(19.11)$$

$$c = M^R_{b\beta}(19)^2 - M^I_{b\beta}(9.19) \quad \text{Find } \Omega_h$$

$$\frac{1}{X} = \frac{\Omega_h(11) + 19}{M^I_{b\beta}}$$

Ω_a is defined as $\left(\frac{\omega_a r_a}{\omega_\beta r_\beta}\right)^2$ for case 3;

Ω_β is defined as $\left(\frac{\omega_\beta r_\beta}{\omega_h}\right)^2$ for case 2; and

Ω_h is defined as $\left(\frac{\omega_h}{\omega_a r_a}\right)^2$ for case 1.

The quantity $\frac{1}{X}$ is $\kappa \left(\frac{vk}{b\omega_r r_r}\right)^2$ by definition.

Since both Ω and $\frac{1}{X}$ are calculated for each value of $\frac{1}{k}$, we may plot $\frac{1}{k^2} \frac{1}{X}$ directly as a function of Ω . This quantity, which is proportional to the square of the flutter speed, represents the solution.

We shall sometimes use the square root of the above quantity, viz, $\frac{1}{k} \sqrt{\frac{1}{X}} = \frac{\sqrt{\kappa} v}{b\omega_r r_r}$, and will denote this

quantity by F , which we shall term the "flutter factor." The flutter velocity is consequently obtained as

$$v = F \frac{b\omega_r r_r}{\sqrt{\kappa}}$$

Since F is nondimensional, the quantity $\frac{b\omega_r r_r}{\sqrt{\kappa}}$ must obviously be a velocity. It is useful to establish the significance of this velocity, with reference to which the flutter speed, so to speak, is measured. Observing that $\kappa = \frac{\pi \rho b^2}{M}$ and that the stiffness in case 1 is given by

$\omega_\alpha = \sqrt{\frac{C_\alpha}{Mb^2 r_\alpha^2}}$ this reference velocity may be written:

$$v_R = \frac{b\omega_\alpha r_\alpha}{\sqrt{\kappa}} = \frac{1}{b} \sqrt{\frac{C_\alpha}{\pi \rho}} \text{ or } \pi \rho v_R^2 b^2 = C_\alpha$$

The velocity v_R is thus the velocity at which the total force on the airfoil $\pi \rho v_R^2 b$ attacking with an arm $\frac{b}{2}$ equals the torsional stiffness C_α of the wing. This statement means, in case 1, that the reference velocity used is equal to the "divergence" velocity obtained with the torsional axis in the middle of the chord. This velocity is considerably smaller than the usual divergence velocity, which may be expressed as

$$v_D = v_R \frac{1}{\frac{1}{2} + a}$$

where a ranges from 0 to $-\frac{1}{2}$. We may thus express the flutter velocity as

$$v_F = v_R F$$

In case 3 the reference velocity has a similar significance, that is, it is the velocity at which the entire lift of the airfoil attacking with a leverage $\frac{1}{2} b$ equals numerically the torsional stiffness C_β of the aileron or movable tail surface.

In case 2, no suitable or useful significance of the reference velocity is available.

TABLE I.—VALUES OF T

	$c=1$	$c=\frac{1}{2}$	$c=0$	$c=-\frac{1}{2}$	$c=-1$
T_1	0	-0.1259	-0.6967	-1.6967	-3.1416
T_2	0	-0.2103	-1.5707	-4.8356	-9.8697
T_3	0	-.05313	-.8084	-3.8375	-11.1034
T_4	0	-.6142	-1.5708	-1.6614	-3.1416
T_5	0	-.9398	-3.4674	-6.9503	-9.8697
T_6	0	-0.2103	-1.5707	-4.8356	-9.8697
T_7	0	.0132	-.1964	-1.1913	-3.5343
T_8	0	.0903	-.3333	-1.4805	-3.1416
T_{10}	0	1.9152	2.5708	2.9604	3.1416
T_{11}	0	1.2990	3.5708	6.5538	9.4248
T_{12}	0	.07066	.4292	1.2990	3.1416

TABLE II.—TABLE OF THE BESSEL FUNCTIONS J_0, J_1, Y_0, Y_1 AND THE FUNCTIONS F AND G

$$F(k) = \frac{J_1(J_1+Y_0)+Y_1(Y_1-J_0)}{(J_1+Y_0)^2+(Y_1-J_0)^2}$$

$$-G(k) = \frac{Y_1(J_1+Y_0)-J_1(Y_1-J_0)}{(J_1+Y_0)^2+(Y_1-J_0)^2}$$

k	$\frac{1}{k}$	J_0	J_1	Y_0	Y_1	F	$-G$
∞	0	0.5000	0
10	$\frac{1}{10}$	-0.2459	0.0435	0.0557	0.2490	.5006	0.0126
6	$\frac{1}{6}$.1506	-.2767	-.2882	-.1750	.5018	.0207
4	$\frac{1}{4}$	-.3972	-.0690	-.0170	.3979	.5037	.0305
2	$\frac{1}{2}$.2239	.5767	.5104	-.1071	.5129	.0577
1	1	.7652	.4401	.0882	-.7813	.5395	.1003
.8	$\frac{1}{14}$.8463	.3688	-.0868	-.9780	.5541	.1165
.6	$\frac{1}{15}$.9120	.2867	-.3085	-1.2004	.5788	.1378
.5	2	.9385	.2423	-.4444	-1.4714	.6030	.151
.4	$\frac{2}{5}$.9604	.1960	-.6060	-1.7808	.6245	.166
.3	$\frac{3}{10}$.9776	.1483	-.8072	-2.2929	.6650	.180
.2	$\frac{1}{5}$.9900	.0995	-1.0810	-3.3235	.7276	.1886
.1	10	.9975	.0499	-1.5342	-7.0317	.8457	.1626
.05	20911	.132
.025	40965	.090
0	∞	1.000	0

TABLE III.—VALUES OF R

$\frac{1}{k}$			0	$\frac{1}{4}a$	$\frac{1}{2}a$	$\frac{3}{4}a$	a	1	$1\frac{1}{4}$	$1\frac{1}{2}$	2	$2\frac{1}{4}$	$2\frac{1}{2}$	3	5	10	20	40
R''_{aa}	c	a	0	0	0	0	0	0	0	0	0	0	0	0	0	0	0	0
			0	0	0	0	0	0	0	0	0	0	0	0	0	0	0	0
R''_{aa}	(1)	0	0	0	0	0	0	0	0	0	0	0	0	0	0	0	0	0
		0	0	0	0	0	0	0	0	0	0	0	0	0	0	0	0	0
		0	0	0	0	0	0	0	0	0	0	0	0	0	0	0	0	0
$R''_{a\beta}$	0	0	0	0	0	0	0	0	0	0	0	0	0	0	0	0	0	0
		0	0	0	0	0	0	0	0	0	0	0	0	0	0	0	0	0
		0	0	0	0	0	0	0	0	0	0	0	0	0	0	0	0	0
R''_{ab}	(1)	0	0	0	0	0	0	0	0	0	0	0	0	0	0	0	0	0
		0	0	0	0	0	0	0	0	0	0	0	0	0	0	0	0	0
		0	0	0	0	0	0	0	0	0	0	0	0	0	0	0	0	0
R''_{ba}	0	0	0	0	0	0	0	0	0	0	0	0	0	0	0	0	0	0
		0	0	0	0	0	0	0	0	0	0	0	0	0	0	0	0	0
		0	0	0	0	0	0	0	0	0	0	0	0	0	0	0	0	0
R''_{bb}	(1)	0	0	0	0	0	0	0	0	0	0	0	0	0	0	0	0	0
		0	0	0	0	0	0	0	0	0	0	0	0	0	0	0	0	0
		0	0	0	0	0	0	0	0	0	0	0	0	0	0	0	0	0
R''_{ca}	(1)	0	0	0	0	0	0	0	0	0	0	0	0	0	0	0	0	0
		0	0	0	0	0	0	0	0	0	0	0	0	0	0	0	0	0
		0	0	0	0	0	0	0	0	0	0	0	0	0	0	0	0	0
R''_{cb}	(1)	0	0	0	0	0	0	0	0	0	0	0	0	0	0	0	0	0
		0	0	0	0	0	0	0	0	0	0	0	0	0	0	0	0	0
		0	0	0	0	0	0	0	0	0	0	0	0	0	0	0	0	0

¹ Independent of c .² Independent of a .

TABLE IV.—VALUES OF I

$\frac{1}{k}$			0	$\frac{1}{4}a$	$\frac{1}{2}a$	$\frac{3}{4}a$	a	1	$1\frac{1}{4}$	$1\frac{1}{2}$	2	$2\frac{1}{4}$	$2\frac{1}{2}$	3	5	10	20	40
I_{aa}	c	a	0	0	0	0	0	0	0	0	0	0	0	0	0	0	0	0
			0	0	0	0	0	0	0	0	0	0	0	0	0	0	0	0
I_{aa}	(1)	0	0	0	0	0	0	0	0	0	0	0	0	0	0	0	0	0
		0	0	0	0	0	0	0	0	0	0	0	0	0	0	0	0	0
		0	0	0	0	0	0	0	0	0	0	0	0	0	0	0	0	0
I_{ab}	0	0	0	0	0	0	0	0	0	0	0	0	0	0	0	0	0	0
		0	0	0	0	0	0	0	0	0	0	0	0	0	0	0	0	0
		0	0	0	0	0	0	0	0	0	0	0	0	0	0	0	0	0
I_{ba}	(1)	0	0	0	0	0	0	0	0	0	0	0	0	0	0	0	0	0
		0	0	0	0	0	0	0	0	0	0	0	0	0	0	0	0	0
		0	0	0	0	0	0	0	0	0	0	0	0	0	0	0	0	0
I_{bb}	0	0	0	0	0	0	0	0	0	0	0	0	0	0	0	0	0	0
		0	0	0	0	0	0	0	0	0	0	0	0	0	0	0	0	0
		0	0	0	0	0	0	0	0	0	0	0	0	0	0	0	0	0
I_{ca}	(1)	0	0	0	0	0	0	0	0	0	0	0	0	0	0	0	0	0
		0	0	0	0	0	0	0	0	0	0	0	0	0	0	0	0	0
		0	0	0	0	0	0	0	0	0	0	0	0	0	0	0	0	0
I_{cb}	(1)	0	0	0	0	0	0	0	0	0	0	0	0	0	0	0	0	0
		0	0	0	0	0	0	0	0	0	0	0	0	0	0	0	0	0
		0	0	0	0	0	0	0	0	0	0	0	0	0	0	0	0	0

¹ Independent of c .² Independent of a .

APPENDIX II

NUMERICAL CALCULATIONS

A number of routine examples have been worked out to illustrate typical results. A "standard" case has been chosen, represented by the following constants:

$$\kappa=0.1, c=0.5, a=-0.4, x_a=0.2,$$

$$r_a^2=0.25, x_\beta=\frac{1}{80}, r_\beta^2=\frac{1}{160}$$

$$\omega_\alpha, \omega_\beta, \omega_h \text{ variable.}$$

We will show the results of a numerical computation of the three possible subcases in succession.

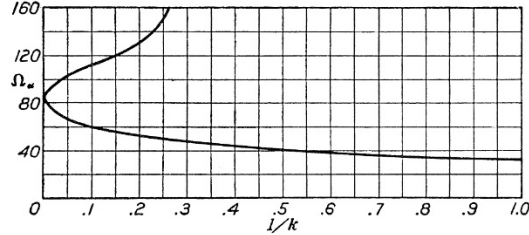


FIGURE 5.—Case 3, Torsion-aileron (α, β): Standard case. Showing Ω_α against $\frac{1}{k}$.

Case 3, Torsion-aileron (α, β): Figure 5 shows the Ω_α against $\frac{1}{k}$ relation and figure 6 the final curve

$$F = \kappa \left(\frac{v}{\omega_\beta r_\beta b} \right)^2 \text{ against } \Omega_\alpha = \left(\frac{\omega_\alpha r_\alpha}{\omega_\beta r_\beta} \right)^2 = 40 \left(\frac{\omega_\alpha}{\omega_\beta} \right)^2$$

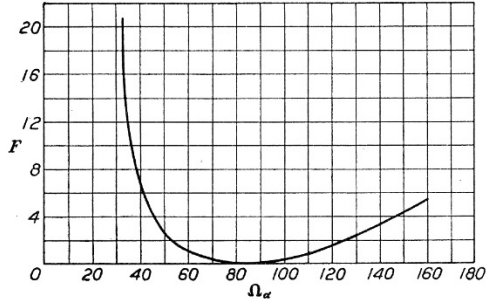


FIGURE 6.—Case 3, Torsion-aileron (α, β): Standard case. Showing flutter factor F against Ω_α .

Case 2, Aileron-flexure (β, h): Figure 7 shows the Ω_β against $\frac{1}{k}$ relation⁶ and figure 8 the final curve $\kappa \left(\frac{v}{\omega_h b} \right)^2$

$$\text{against } \Omega_\beta = \left(\frac{\omega_\beta r_\beta}{\omega_h} \right)^2 = \frac{1}{160} \left(\frac{\omega_\beta}{\omega_h} \right)^2$$

⁶ It is realized that considerable care must be exercised to get these curves reasonably accurate.

The heavy line shows the standard case, while the remaining curves show the effect of a change in the value of x_β to $\frac{1}{40}$ and $\frac{1}{160}$.

Case 1, Flexure-torsion (h, α): Figure 9 shows again

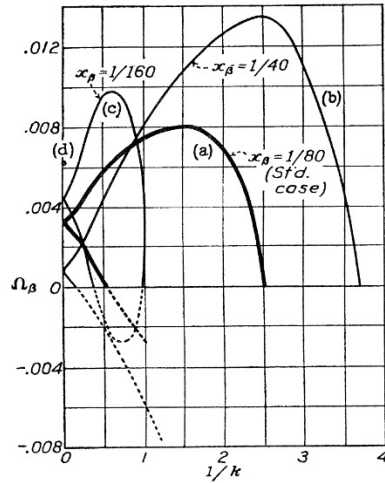


FIGURE 7.—Case 2, Aileron-deflection (β, h): (a) Standard case. (b), (c), (d) indicate dependency on x_β . Case (d), $x_\beta = -0.004$, reduces to a point.

the Ω_h against $\frac{1}{k}$ relation and figure 10 the final result

$$\kappa \left(\frac{v}{\omega_\alpha r_\alpha b} \right)^2 \text{ against } \Omega_h = \left(\frac{\omega_h}{\omega_\alpha r_\alpha} \right)^2 = 4 \left(\frac{\omega_h}{\omega_\alpha} \right)^2$$

Case 1, which is of importance in the propeller theory, has been treated in more detail. The quantity F shown

in the figures is $\sqrt{\kappa} \frac{v}{\omega_\alpha r_\alpha b}$.

Figure 11 shows the dependency on $\frac{\omega_h}{\omega_\alpha} = \frac{\omega_1}{\omega_2}$;

figure 12 shows the dependency on the location of the axis a ; figure 13 shows the dependency on the radius of gyration $r_a = r$; and figure 14 shows the dependency on the location of the center of gravity x , for three different combinations of constants.

EXPERIMENTAL RESULTS

Detailed discussion of the experimental work will not be given in this paper, but shall be reserved for a later report. The experiments given in the following are

restricted to wings of a large aspect ratio, arranged with two or three degrees of freedom in accordance with the

able springs restrain the wing to its equilibrium position.

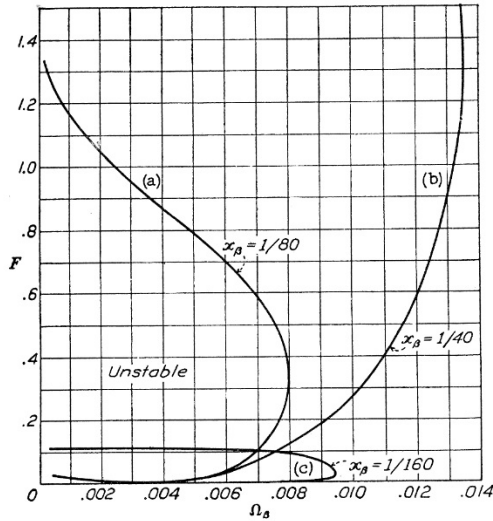


FIGURE 8.—Case 2, Aileron-deflection (β , h): Final curves giving flutter factor F against Ω_h corresponding to cases shown in figure 7.

theoretical cases. The wing is free to move parallel to itself in a vertical direction (h); is equipped with an

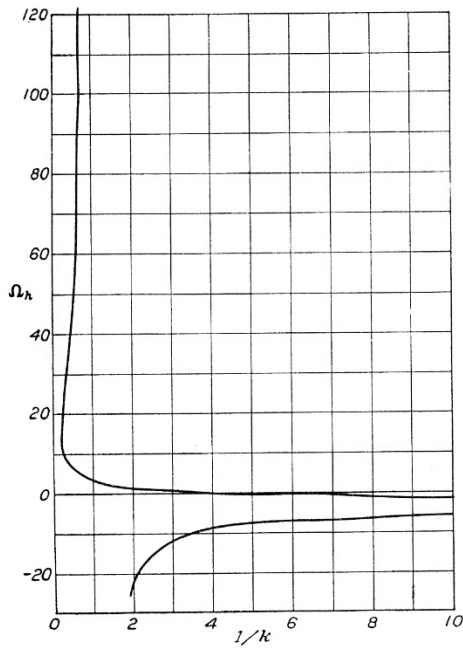


FIGURE 9.—Case 1, Flexure-torsion (h , α): Standard case. Showing Ω_h against $\frac{1}{k}$.

axis in roller bearings at (a) (fig. 2) for torsion, and with an aileron hinged at (c). Variable or exchange-

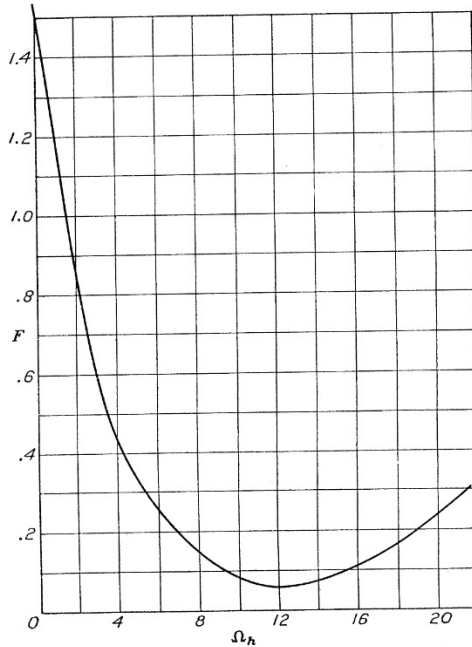


FIGURE 10.—Case 1, Flexure-torsion (h , α): Standard case. Showing flutter factor F against Ω_h .

We shall present results obtained on two wings, both of symmetrical cross section 12 percent thick, and with chord $2b=12.7$ cm, tested at 0° .

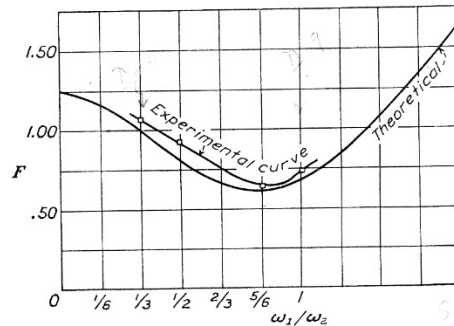


FIGURE 11.—Case 1, Flexure-torsion (h , α): Showing dependency of F on $\frac{\omega_1}{\omega_2}$. The upper curve is experimental. Airfoil with $r = \frac{1}{2}$; $a = -0.4$; $x = 0.2$; $4\kappa = 0.1$; $\frac{\omega_1}{\omega_2}$ variable.

Wing A, aluminum, with the following constants:

$$\kappa = \frac{1}{416}, a = -0.4, x_a = 0.31, 0.173, \text{ and } 0.038,$$

respectively;

$$r_a^2 = 0.33 \text{ and } \omega_a = 7 \times 2\pi$$

Wing B, wood, with flap, and the constants:

$$\kappa = \frac{1}{100}, \quad c = 0.5, \quad a = -0.4, \quad x_a = 0.192, \quad r_a^2 = 0.178, \\ x_\beta = 0.019, \quad r_\beta^2 = 0.0079, \quad \text{and } \omega_a \text{ kept constant} \\ = 17.6 \times 2\pi$$

The results for wing A, case 1, are given in figure 15; and those for wing B, cases 2 and 3, are given in figures 16 and 17, respectively. The abscissas are the frequency ratios and the ordinates are the velocities in cm/sec. Compared with the theoretical results calculated for the three test cases, there is an almost perfect

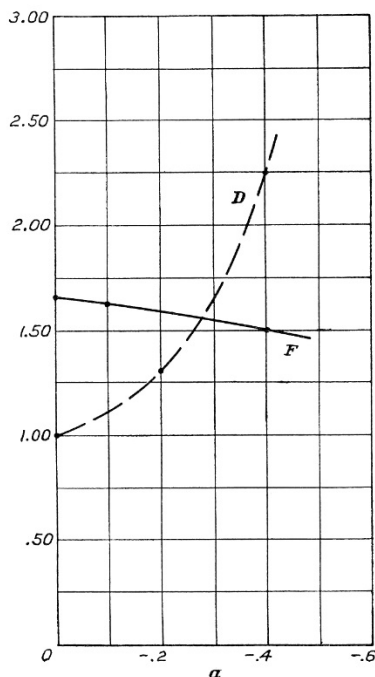


FIGURE 12.—Case 1, Flexure-torsion (h, α): Showing dependency of F on location of axis of rotation α . Airfoil with $r = \frac{1}{2}$; $x = 0.2$; $\kappa = \frac{1}{4}$; $\frac{\omega_1}{\omega_2} = \frac{1}{6}$; a variable.

agreement in case 1 (fig. 15). Not only is the minimum velocity found near the same frequency ratio, but the experimental and theoretical values are, furthermore, very nearly alike. Very important is also the fact that the peculiar shape of the response curve in case 2, predicted by the theory, repeats itself experimentally. The theory predicts a range of instabilities extending from a small value of the velocity to a definite upper limit. It was very gratifying to observe that the upper branch of the curve not only existed but that it was remarkably definite. A small increase in speed near this upper limit would suffice to change the condition from violent flutter to complete rest, no range of transition being observed. The experimental cases 2 and 3 are compared with theoretical results given by the dotted lines in both figures (figs. 16 and 17).

The conclusion from the experiments is briefly that the general shapes of the predicted response curves re-

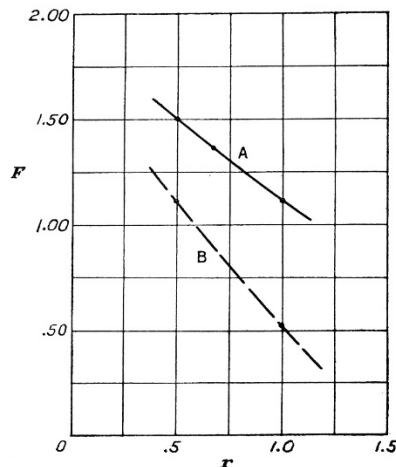


FIGURE 13.—Case 1, Flexure-torsion (h, α): Showing dependency of F on the radius of gyration $r_a = r$.

A, airfoil with $a = -0.4$; $\kappa = \frac{1}{4}$; $x = 0.2$; $\frac{\omega_1}{\omega_2} = \frac{1}{6}$; r variable.

B, airfoil with $a = -0.4$; $\kappa = \frac{1}{4}$; $x = 0.2$; $\frac{\omega_1}{\omega_2} = 1.00$; r variable.

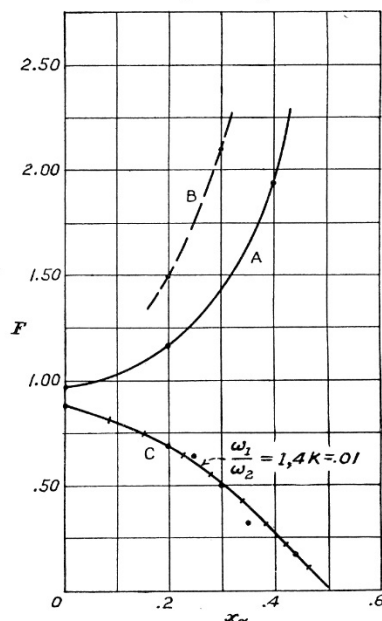


FIGURE 14.—Case 1, Flexure-torsion (h, α): Showing dependency of F on x_a , the location of the center of gravity.

A, airfoil with $r = \frac{1}{2}$; $a = -0.4$; $\kappa = \frac{1}{400}$; $\frac{\omega_1}{\omega_2} = \frac{1}{6}$; x variable.

B, airfoil with $r = \frac{1}{2}$; $a = -0.4$; $\kappa = \frac{1}{4}$; $\frac{\omega_1}{\omega_2} = \frac{1}{6}$; x variable.

C, airfoil with $r = \frac{1}{2}$; $a = -0.4$; $\kappa = \frac{1}{100}$; $\frac{\omega_1}{\omega_2} = 1$; x variable.

peat themselves satisfactorily. Next, that the influence of the internal friction⁷ obviously is quite appreci-

⁷ This matter is the subject of a paper now in preparation.

able in case 3. This could have been expected since the predicted velocities and thus also the air forces on the aileron are very low, and no steps were taken to eliminate the friction in the hinge. The outline of the stable region is rather vague, and the wing is subject

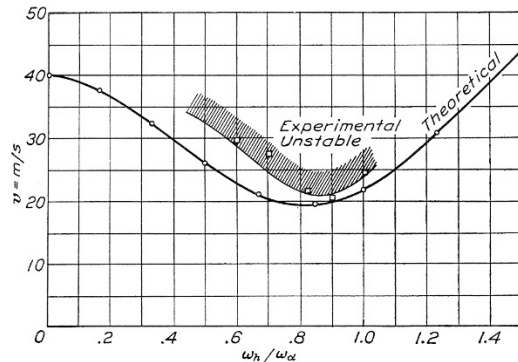


FIGURE 15.—Case 1. Wing A. Theoretical and experimental curves giving flutter velocity v against frequency ratio $\frac{\omega_h}{\omega_\alpha}$. Deflection-torsion.

to temporary vibrations at much lower speeds than that at which the violent flutter starts. The above experiments are seen to refer to cases of exaggerated unbalance, and therefore of low flutter speeds. It is evident that the internal friction is less important at larger velocities. The friction does in all cases *increase* the speed at which flutter starts.

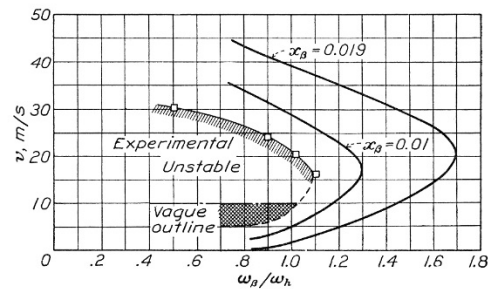


FIGURE 16.—Case 2. Wing B. Theoretical and experimental curves giving flutter velocity v against frequency ratio $\frac{\omega_\beta}{\omega_h}$. Aileron-deflection (β, h).

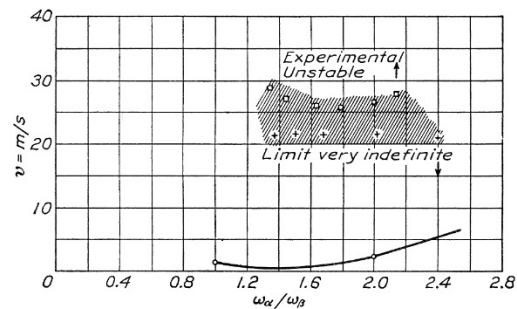


FIGURE 17.—Case 3. Theoretical curve giving flutter velocity against the frequency ratio $\frac{\omega_\alpha}{\omega_\beta}$. The experimental unstable area is indefinite due to the importance of internal friction at very small velocities. Torsion-aileron (α, β).

APPENDIX III

EVALUATION OF φ_β

$$\begin{aligned}
 & \int_c^1 \log \frac{(x-x_1)^2 + (y-y_1)^2}{(x-x_1)^2 + (y+y_1)^2} dx_1 \\
 &= \left[x_1 \log \frac{(x-x_1)^2 + (y-y_1)^2}{(x-x_1)^2 + (y+y_1)^2} \right]_c^1 - 2y \int_c^1 \frac{x_1 dx_1}{y_1(x-x_1)} \\
 &= -2c \log \frac{1-cx-y\sqrt{1-c^2}}{(x-c)} - 2y \int_c^1 \frac{x_1 dx_1}{\sqrt{1-x_1^2}(x-x_1)} \\
 &+ \int_c^1 \frac{x_1 dx_1}{\sqrt{1-x_1^2}(x-x_1)} = \int_c^1 \frac{dx_1}{\sqrt{1-x_1^2}} \\
 &+ x \int_c^1 \frac{dx_1}{(x_1-x)\sqrt{1-x_1^2}} \text{ [Putting } x_1 = \cos \theta \text{]} \\
 &= -\theta - \frac{x}{\sqrt{1-x^2}} \log \frac{1-x \cos \theta + \sqrt{1-x^2} \sin \theta}{\cos \theta - x} \Big|_{\cos \theta=c}^{\cos \theta=1} \\
 &= \cos^{-1} c + \frac{x}{\sqrt{1-x^2}} \log \frac{1-cx + \sqrt{1-x^2} \sqrt{1-c^2}}{c-x} \\
 &= \cos^{-1} c + \frac{x}{\sqrt{1-x^2}} \log \frac{c-x}{1-cx - \sqrt{1-x^2} \sqrt{1-c^2}} \\
 \varphi \frac{2\pi}{\epsilon} &= -2c \log (1-cx - \sqrt{1-x^2} \sqrt{1-c^2}) + 2c \log (x-c) \\
 &- 2\sqrt{1-x^2} \cos^{-1} c - 2x \log (c-x) \\
 &+ 2x \log (1-cx - \sqrt{1-x^2} \sqrt{1-c^2}) \\
 &= 2(x-c) \log \left(\frac{1-cx - \sqrt{1-x^2} \sqrt{1-c^2}}{x-c} \right) \\
 &- 2\sqrt{1-x^2} \cos^{-1} c
 \end{aligned}$$

EVALUATION OF φ_β

$$\begin{aligned}
 \varphi_x &= \int_c^1 \{ \log[(x-x_1)^2 + (y-y_1)^2] \\
 &- \log[(x-x_1)^2 + (y+y_1)^2] \} (x_1-c) dx_1 \\
 &= \frac{(x_1-c)^2}{2} \{ \log[(x-x_1)^2 + (y-y_1)^2] \\
 &- \log[(x-x_1)^2 + (y+y_1)^2] \} \Big|_c^1 \\
 &+ y \int_c^1 (x_1-c)^2 \frac{dx_1}{y_1(x-x_1)} \\
 &\int_c^1 \frac{(x_1-c)^2 dx_1}{y_1(x-x_1)} = \int_c^1 \frac{(x_1-c)^2 dx_1}{1-x_1^2(x-x_1)} = - \int_c^1 \frac{(\cos \theta - c)^2 d\theta}{x - \cos \theta} \\
 &x_1 = \cos \theta, y_1 = \sin \theta, dx_1 = -\sin \theta d\theta \\
 &\int_c^1 \frac{(x_1-c)^2 dx_1}{y_1(x-x_1)} = \sin \theta + (x-2c)\theta - (x-c)^2 \int_c^1 \frac{d\theta}{x - \cos \theta} \\
 &\int_c^1 \frac{d\theta}{x - \cos \theta} = \int_c^1 \frac{d(\pi + \theta)}{x + \cos(\pi + \theta)}
 \end{aligned}$$

22

$$\begin{aligned}
 &= \frac{1}{\sqrt{1-x^2}} \log \frac{1-x \cos \theta - \sqrt{1-x^2} \sin \theta}{x - \cos \theta} \Big|_{\cos \theta=c}^{\cos \theta=1} \\
 &= \frac{1}{\sqrt{1-x^2}} \left[\log \frac{1-x}{x-1} - \log \frac{1-cx - \sqrt{1-x^2} \sqrt{1-c^2}}{x-c} \right] \\
 &= -\frac{1}{\sqrt{1-x^2}} \log (1-cx - \sqrt{1-x^2} \sqrt{1-c^2}) \\
 &+ \frac{1}{\sqrt{1-x^2}} \log (x-c) \\
 \frac{2\pi}{\epsilon} \varphi_x &= \sqrt{1-x^2} \left[-\sqrt{1-c^2} - (x-2c) \cos^{-1} c \right. \\
 &+ \frac{(x-c)^2}{\sqrt{1-x^2}} \log (1-cx - \sqrt{1-x^2} \sqrt{1-c^2}) \\
 &\left. - \frac{(x-c)^2}{\sqrt{1-x^2}} \log (x-c) \right] \\
 \frac{2\pi}{\epsilon} \varphi_x &= -\sqrt{1-c^2} \sqrt{1-x^2} - \cos^{-1} c (x-2c) \sqrt{1-x^2} \\
 &+ (x-c)^2 \log (1-cx - \sqrt{1-x^2} \sqrt{1-c^2}) \\
 &- (x-c)^2 \log (x-c)
 \end{aligned}$$

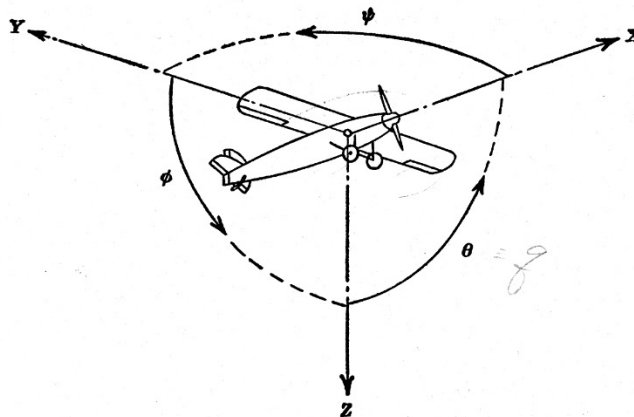
EVALUATION OF T_3

$$\begin{aligned}
 \int_c^1 \frac{2\pi}{\epsilon} \varphi_x(x-c) dx &= -\sqrt{1-c^2} \int_c^1 (x-c) \sqrt{1-x^2} dx \\
 &- \cos^{-1} c \int_c^1 (x-c) (x-2c) \sqrt{1-x^2} dx \\
 &+ \frac{(x-c)^4}{4} \log (1-cx - \sqrt{1-x^2} \sqrt{1-c^2}) \\
 &- \frac{1}{4} \int_c^1 (x-c)^3 dx - \sqrt{\frac{1-c^2}{4}} \frac{(x-c)^3}{\sqrt{1-x^2}} dx \\
 &- \int_c^1 (x-c)^3 \log (x-c) dx; x = \cos \theta, dx = -\sin \theta d\theta \\
 \frac{2\pi}{\epsilon} \int_c^1 \varphi_x(x-c) dx &= \sqrt{1-c^2} \int (\cos \theta - c) \sin^2 \theta d\theta \\
 &+ \cos^{-1} c \int (\cos \theta - c) (\cos \theta - 2c) \sin^2 \theta d\theta \\
 &+ \frac{(x-c)^4}{4} \log (1-cx - \sqrt{1-x^2} \sqrt{1-c^2}) \\
 &- \frac{1}{4} \int_c^1 (x-c)^3 dx + \frac{\sqrt{1-c^2}}{4} \int (\cos \theta - c)^3 d\theta \\
 &- \frac{(x-c)^4}{4} \log (x-c) + \frac{1}{4} \int_c^1 (x-c)^3 dx \\
 \frac{2\pi}{\epsilon} \int_c^1 \varphi_x(x-c) dx &= -\cos^{-1} c \int \cos^4 \theta d\theta \\
 &+ \left(3c \cos^{-1} c - \sqrt{1-c^2} + \frac{\sqrt{1-c^2}}{4} \right) \int \cos^3 \theta d\theta \\
 &+ \left(\cos^{-1} c - 2c^2 \cos^{-1} c + c\sqrt{1-c^2} - \frac{3}{4} c\sqrt{1-c^2} \right) \int \cos^2 \theta d\theta \\
 &+ \left(-3c \cos^{-1} c + \sqrt{1-c^2} + \frac{3c^2 \sqrt{1-c^2}}{4} \right) \int \cos \theta d\theta \\
 &+ \left(2c^2 \cos^{-1} c - c\sqrt{1-c^2} - \frac{c^3 \sqrt{1-c^2}}{4} \right) \int d\theta
 \end{aligned}$$

$$\begin{aligned}
&= -\cos^{-1}c \left[\frac{\cos^3 \theta \sin \theta}{4} + \frac{3}{4} \left(\frac{\theta}{2} + \frac{\sin \theta \cos \theta}{2} \right) \right] \\
&+ \frac{1}{3} \left(3c \cos^{-1}c - \frac{3}{4} \sqrt{1-c^2} \right) \sin \theta (\cos^2 \theta + 2) \\
&+ \left(\cos^{-1}c - 2c^2 \cos^{-1}c + \frac{c\sqrt{1-c^2}}{4} \right) \left(\frac{\theta}{2} + \frac{\sin \theta \cos \theta}{2} \right) \\
&+ \left(-3c \cos^{-1}c + \sqrt{1-c^2} + \frac{3c^2\sqrt{1-c^2}}{4} \right) \sin \theta \\
&+ \left(2c^2 \cos^{-1}c - c\sqrt{1-c^2} - \frac{c^3\sqrt{1-c^2}}{4} \right) \theta \\
&= \cos^{-1}c \left(\frac{3}{8} \pi + \frac{\pi}{2} - 3\pi \right) = -\frac{9}{8} \pi \cos^{-1}c \\
&\frac{2\pi}{\epsilon} \int_c^1 \varphi_z(x-c) dx \\
&= \cos^{-1}c \left[\frac{c^3\sqrt{1-c^2}}{4} + \frac{3}{8} \cos^{-1}c + \frac{3c\sqrt{1-c^2}}{8} \right] \\
&- \left[c \cos^{-1}c - \frac{\sqrt{1-c^2}}{4} \right] (c^2\sqrt{1-c^2} + 2\sqrt{1-c^2}) \\
&- \left(\cos^{-1}c - 2c^2 \cos^{-1}c + \frac{c\sqrt{1-c^2}}{4} \right) \left(\frac{\cos^{-1}c + c\sqrt{1-c^2}}{2} \right) \\
&- \left(-3c \cos^{-1}c + \sqrt{1-c^2} + \frac{3c^2\sqrt{1-c^2}}{4} \right) \sqrt{1-c^2} \\
&- \left(2c^2 \cos^{-1}c - c\sqrt{1-c^2} - \frac{c^3\sqrt{1-c^2}}{4} \right) \cos^{-1}c \\
&= \cos^{-1}c \left[\frac{3}{8} - \frac{1}{2} + c^2 - 2c^2 \right] \\
&+ \sqrt{1-c^2} \cos^{-1}c \left[\frac{c^3}{4} + \frac{3c}{8} - c^3 - 2c - \frac{c}{2} + c^3 + 3c + c \right. \\
&\left. + \frac{c^3}{4} - \frac{c}{8} \right] + \frac{c^2(1-c^2)}{4} + \frac{(1-c^2)}{2} - \frac{c^2(1-c^2)}{8} \\
&- (1-c^2) - \frac{3c^2(1-c^2)}{4} = -\left(\frac{1}{8} + c^2 \right) (\cos^{-1}c)^2 \\
&+ \frac{c\sqrt{1-c^2} \cos^{-1}c}{4} (7+2c^2) - \frac{(1-c^2)}{8} (5c^2+4) (=T_3)
\end{aligned}$$

EVALUATION OF T_3

$$\begin{aligned}
&\int_c^1 \left\{ 2(x-c) \log \frac{1-cx-\sqrt{1-x^2}\sqrt{1-c^2}}{x-c} \right. \\
&\quad \left. - 2\sqrt{1-x^2} \cos^{-1}c \right\} dx = T_3 = -2 \int (x-c) \log (x-c) dx \\
&+ 2 \int (x-c) \log (1-cx-\sqrt{1-x^2}\sqrt{1-c^2}) dx \\
&- 2 \cos^{-1}c \int \sqrt{1-x^2} dx = -\frac{2(x-c)^2}{2} \log (x-c) \\
&+ \int (x-c) dx + 2 \cos^{-1}c \int \sin^2 \theta d\theta \\
&+ (x-c)^2 \log (1-cx-\sqrt{1-x^2}\sqrt{1-c^2}) \\
&\quad - c + x \frac{\sqrt{1-c^2}}{\sqrt{1-x^2}} \\
&- \int (x-c)^2 \frac{1}{1-cx-\sqrt{1-x^2}\sqrt{1-c^2}} dx \\
\text{Now} &\quad -c + x \frac{\sqrt{1-c^2}}{\sqrt{1-x^2}} \\
&\int (x-c)^2 \frac{1}{1-cx-\sqrt{1-x^2}\sqrt{1-c^2}} dx \\
&= \int \left\{ -c + c^2x - c\sqrt{1-c^2}\sqrt{1-x^2} + x \frac{\sqrt{1-c^2}}{\sqrt{1-x^2}} - cx^2 \frac{\sqrt{1-c^2}}{\sqrt{1-x^2}} \right. \\
&\quad \left. + (1-c^2)x \right\} dx = \int \frac{(x-c)\sqrt{1-x^2} + (x-c)\sqrt{1-c^2}}{\sqrt{1-x^2}} dx \\
&= \int (x-c) dx + \sqrt{1-c^2} \int \frac{(x-c)}{\sqrt{1-x^2}} dx \\
T_3 &= -(x-c)^2 \log (x-c) + 2 \cos^{-1}c \int \sin^2 \theta d\theta \\
&+ (x-c)^2 \log (1-cx-\sqrt{1-x^2}\sqrt{1-c^2}) \\
&+ \sqrt{1-c^2} \int (\cos \theta - c) d\theta \\
&= \frac{2 \cos^{-1}c}{2} (\theta - \sin \theta \cos \theta) + \sqrt{1-c^2} \sin \theta \\
&- c \sqrt{1-c^2} \theta \Big|_{\cos \theta=c}^{\cos \theta=1} \\
&= -(1-c^2) - (\cos^{-1}c)^2 + 2c \sqrt{1-c^2} \cos^{-1}c
\end{aligned}$$



Positive directions of axes and angles (forces and moments) are shown by arrows

Axis			Moment about axis			Angle		Velocities	
Designation	Sym- bol	Force (parallel to axis) symbol	Designation	Sym- bol	Positive direction	Designa- tion	Sym- bol	Linear (compo- nent along axis)	Angular
Longitudinal.....	X	X	Rolling.....	L	Y→Z	Roll.....	φ	u	p
Lateral.....	Y	Y	Pitching.....	M	Z→X	Pitch.....	θ	v	q
Normal.....	Z	Z	Yawing.....	N	X→Y	Yaw.....	ψ	w	r

Absolute coefficients of moment

$$C_l = \frac{L}{qbS} \quad C_m = \frac{M}{qcS} \quad C_n = \frac{N}{qbS}$$

(rolling) (pitching) (yawing)

Angle of set of control surface (relative to neutral position), δ . (Indicate surface by proper subscript.)

4. PROPELLER SYMBOLS

D Diameter
 p Geometric pitch
 p/D Pitch ratio
 V' Inflow velocity
 V_s Slipstream velocity

T Thrust, absolute coefficient $C_T = \frac{T}{\rho n^2 D^4}$

Q Torque, absolute coefficient $C_Q = \frac{Q}{\rho n^2 D^5}$

P Power, absolute coefficient $C_P = \frac{P}{\rho n^3 D^5}$

C_s Speed-power coefficient $= \sqrt[5]{\frac{\rho V_s^6}{P n^2}}$

η Efficiency

n Revolutions per second, rps

Φ Effective helix angle $= \tan^{-1}\left(\frac{V}{2\pi r n}\right)$

5. NUMERICAL RELATIONS

1 hp = 76.04 kg-m/s = 550 ft-lb/sec

1 metric horsepower = 0.9863 hp

1 mph = 0.4470 mps

1 mps = 2.2369 mph

1 lb = 0.4536 kg

1 kg = 2.2046 lb

1 mi = 1,609.35 m = 5,280 ft

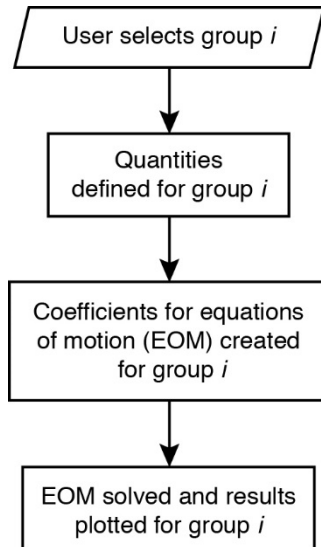
1 m = 3.2808 ft

APPENDIX B

MATLAB® PROGRAM FOR RE-COMPUTING RESULTS IN NACA 496

This appendix contains a Matlab® program that implements the two-degree-of-freedom flutter equations and the two-degree-of-freedom solution method found in Appendix I of *NACA 496*. By executing this program, results in figures 5 through 11 and 15 through 17, found in Appendix II of *NACA 496*, may be re-computed directly. The re-computation of results in figures 12 through 14 is discussed below.

The program is structured as depicted in the simplified flow chart, below, on the left. There are four “groups” of re-computed figures that may be chosen, according to the table, below, on the right. The user inputs an integer from 1 to 4, thereby specifying a group. Then, based on the integer, the program selects a set of quantities (κ , X_{α} , r_{α} , X_{β} , r_{β} , etc.), computes the coefficients of the equations of motion, solves the equations of motion and plots the results. The “cases” in the table are consistent with subsection titles in section VI of the main body of the present paper.



Group Number, <i>i</i>	Quantities for Case -	NACA 496 Figures Reproduced
1	Standard	5 thru 10
2	Parameter Variation	11
3	Wing A	15
4	Wing B	16 & 17

The re-computation of results in figures 12 through 14 requires multiple executions of the program, with the user selecting group number 2 and supplying appropriately modified sets of quantities (see figure legends of figs. 12 through 14) for this group.

During the normal execution of the solution method, the computed quantity F and the computed \mathcal{Q} s may be, at times, real and, at other times, complex. Only real values of F and the \mathcal{Q} s represent physical solutions; complex values of F and the \mathcal{Q} s represent non-physical solutions.

The Matlab® program in this appendix produces both physical and non-physical solutions. When plotting, Matlab® does not distinguish between real quantities and complex quantities and, if a quantity is complex, Matlab® will plot its real part and issue a warning message in the command window. The user is cautioned to check the command window for such messages, and if present, carefully examine the variable F and the \mathcal{Q} s to discern which values in the solution are real and which are complex. By so

doing the user may determine if a particular locus of points in a figure represents a physical solution or a non-physical solution.

```
-----

%% This program reproduces figs 5 --> 11 and 15 --> 17 from NACA 496
% Figs 12 --> 14 require multiple executions of group number 2 with
% appropriately modified input quantities
%
% Implemented using NACA 496 equations and 2DOF solution method
% Boyd Perry, III
% NASA-Langley Research Center
% May 2015

clc
clear
close all

%% Define k and kinv

N = 10001;
oneoverkmax = 100;
deltaoneoverk = oneoverkmax/(N-1);

for i=1:N
    kinv(i) = (i-1)*deltaoneoverk;
    k(i) = 1/kinv(i);
end

%% Define Quantities
a = [0 -0.2 -0.4];
c = [0 0.5];

% For all calculations a = -0.4 and c = 0.5

group = input('Enter group number (1, 2, 3, or 4) ');

% Group number may be 1, 2, 3, or 4
% Group number 1 is for the Standard Case and reproduces figs 5 --> 10
% Group number 2 is for the Standard Case and reproduces fig 11
% Group number 3 is for Wing A and reproduces fig 15
% Group number 4 is for Wing B and reproduces figs 16 & 17

% Input quantities for group number 1
if group == 1
    kappa = 0.1;
    xa = 0.2;
    ra2 = 0.25;
    xb = 1/80; % Corresponds to curve (a) in figs 7 & 8
    %xb = 1/40; % Corresponds to curve (b) in figs 7 & 8
    %xb = 1/160; % Corresponds to curve (c) in figs 7 & 8
    rb2 = 1/160;
end
```

```

% Input quantitie for group number 2
if group == 2
kappa = 1/400;
xa = 0.2;
ra2 = 0.25;
xb = 1/80;
rb2 = 1/160;
end

% Input quantitie for group number 3
if group == 3
kappa = 1/416;
%xa = 0.31;
xa = 0.173;
%xa = 0.038;
ra2 = 0.33;
xb = 1/80;
rb2 = 1/160;
omegaa = 7*2*pi;
b = 2.5/12;
end

% Input quantitie for group number 4
if group == 4
kappa = 1/100;
xa = 0.192;
ra2 = 0.178;
xb = 0.019;
%xb = 0.01;
rb2 = 0.0079;
omegaa = 17.6*2*pi;
omegah = 5.8*2*pi;
omegab = 4.4*2*pi;
b = 2.5/12;
end

% Other relationships

ra = sqrt(ra2);
rb = sqrt(rb2);

%% Define array indices
%
% For Ti constants:
% Ti(kk)
% kk ~ variation of quantity c
%
% For R' arrays:
% R'(j,kk)
% j ~ variation of quantity a
% kk ~ variation of quantity c
%
% For F and G, real and imag parts of Theodorsen Function:
% F(i) and G(i)

```

```

% i ~ variation of reduced frequency
%
% For R" and I arrays:
% R"(i,j,kk) and I(i,j,kk)
% i ~ variation of reduced frequency
% j ~ variation of quantity a
% kk ~ variation of quantity c
%

%% Define Ti
for kk=1:2 % loop on quantity c [0, 0.5]
    c2(kk) = c(kk)*c(kk);
    TiTerm1 = 1 + c2(kk);
    TiTerm2 = 1 - c2(kk);
    TiTerm3 = sqrt(TiTerm2);
    TiTerm4 = acos(c(kk));
    TiTerm5 = 1/8 + c2(kk);
    TiTerm6 = 7 + 2*c2(kk);
    T1(kk) = -(1/3)*TiTerm3*(2+c2(kk)) + c(kk)*TiTerm4;
    T2(kk) = c(kk)*TiTerm2 - TiTerm3*TiTerm1*TiTerm4 + c(kk)*TiTerm4*TiTerm4;
    T3(kk) = -TiTerm5*TiTerm4*TiTerm4 +
(1/4)*c(kk)*TiTerm3*acos(c(kk))*TiTerm6 - (1/8)*TiTerm2*(5*c2(kk)+4);
    T4(kk) = -TiTerm4 + c(kk)*TiTerm3;
    T5(kk) = -TiTerm2-TiTerm4*TiTerm4 + 2*c(kk)*TiTerm3*TiTerm4;
    T6(kk) = T2(kk);
    T7(kk) = -TiTerm5*TiTerm4 + (1/8)*c(kk)*TiTerm3*TiTerm6;
    T8(kk) = -(1/3)*TiTerm3*(2*c2(kk)+1) + c(kk)*TiTerm4;
    T10(kk) = TiTerm3 + TiTerm4;
    T11(kk) = TiTerm4*(1-2*c(kk)) + TiTerm3*(2-c(kk));
    T12(kk) = TiTerm3*(2+c(kk)) - acos(c(kk))*(2*c(kk)+1);
end

%% Define F and G
for i=1:N
    J0(i) = besselj(0,k(i));
    J1(i) = besselj(1,k(i));
    Y0(i) = bessely(0,k(i));
    Y1(i) = bessely(1,k(i));

    TheoTerm1(i) = J1(i) + Y0(i);
    TheoTerm2(i) = Y1(i) - J0(i);

    Fnumer(i) = J1(i)*TheoTerm1(i) + Y1(i)*TheoTerm2(i);
    Gnumer(i) = Y1(i)*Y0(i) + J1(i)*J0(i);

    denom(i) = TheoTerm1(i)^2 + TheoTerm2(i)^2;

    F(i) = Fnumer(i)/denom(i);
    G(i) = -Gnumer(i)/denom(i);
end

%% Define R' Terms
for kk=1:2 % loop on quantity c [0, 0.5]
    for j=1:3 % loop on quantity a [0 -0.2 -0.4]

```

```

Raap(j, kk) = -ra2/kappa - (1/8 + a(j)*a(j));
Rabp(j, kk) = -rb2/kappa - (c(kk)-a(j))*xb/kappa + T7(kk)/pi + (c(kk)-
a(j))*T1(kk)/pi;
Rahp(j, kk) = -xa/kappa + a(j);

Rbap(j, kk) = Rabp(j, kk);
Rbbp(j, kk) = -rb2/kappa + T3(kk)/(pi*pi);
Rbhp(j, kk) = -xb/kappa + T1(kk)/pi;

Rcap(j, kk) = Rahp(j, kk);
Rcbp(j, kk) = Rbhp(j, kk);
Rchp(j, kk) = -1/kappa - 1;

end
end

%% Define R" and I Terms
% Equations (1)-(9) and (11)-(19) on p. 14

for kk=1:2 % loop on quantity c [0, 0.5]
    p = -(1/3)*(1-c(kk)*c(kk))^(3/2);
    for j=1:3 % loop on quantity a [0 -0.2 -0.4]
        for i=1:N % loop on reduced frequency

            RITerm1 = (a(j)+0.5);
            RITerm2 = (0.5-a(j))*G(i) - kinv(i)*F(i);
            RITerm3 = T11(kk)*G(i)-2*kinv(i)*T10(kk)*F(i);

            Raapp(i, j, kk) = kinv(i)*2*RITerm1*RITerm2;
            Rabpp(i, j, kk) =
kinv(i)*(1/pi)*((T4(kk)+T10(kk))*kinv(i)+RITerm1*RITerm3);
            Rahpp(i, j, kk) = kinv(i)*2*RITerm1*G(i);

            Rbapp(i, j, kk) = -kinv(i)*(T12(kk)/pi)*RITerm2;
            Rbbpp(i, j, kk) = -kinv(i)*(1/pi)*(1/pi)*((T12(kk)/2)*RITerm3-
kinv(i)*(T5(kk)-T4(kk)*T10(kk)));
            Rbhpp(i, j, kk) = -kinv(i)*(T12(kk)/pi)*G(i);

            Rcapp(i, j, kk) = -kinv(i)*2*RITerm2;
            Rcbpp(i, j, kk) = -kinv(i)*(1/pi)*RITerm3;
            Rchpp(i, j, kk) = -kinv(i)*2*G(i);

            RITerm4 = (0.5-a(j))*F(i) + kinv(i)*G(i);
            RITerm5 = T11(kk)*F(i)+2*kinv(i)*T10(kk)*G(i);

            Iaa(i, j, kk) = -2*RITerm1*RITerm4 + (0.5-a(j));
            Iab(i, j, kk) = -(1/pi)*(RITerm1*RITerm5 + 2*p + (0.5-
a(j))*T4(kk));
            Iah(i, j, kk) = -2*RITerm1*F(i);

            Iba(i, j, kk) = (T12(kk)/pi)*RITerm4 +(1/pi)*(p-T1(kk)-0.5*T4(kk));
            Ibb(i, j, kk) = (0.5/(pi*pi))*((T12(kk)*RITerm5-T4(kk)*T11(kk)));
            Ibh(i, j, kk) = (T12(kk)/pi)*F(i);

```

```

        Ica(i,j,kk) = 2*RIterm4 + 1;
        Icb(i,j,kk) = (1/pi)*(RIterm5-T4(kk));
        Ich(i,j,kk) = 2*F(i);

    end
end
end

%% Create R's and I's for j=3 (a=-0.4) and kk=2 (c=0.5)

j = 3;
kk = 2;

for i=1:N

    R1(i) = Raap(j,kk) + Raapp(i,j,kk);
    R2(i) = Rabp(j,kk) + Rabpp(i,j,kk);
    R3(i) = Rahp(j,kk) + Rahpp(i,j,kk);

    R4(i) = Rbap(j,kk) + Rbapp(i,j,kk);
    R5(i) = Rbbp(j,kk) + Rbbpp(i,j,kk);
    R6(i) = Rbhp(j,kk) + Rbhpp(i,j,kk);

    R7(i) = Rcap(j,kk) + Rcapp(i,j,kk);
    R8(i) = Rcbp(j,kk) + Rcbpp(i,j,kk);
    R9(i) = Rchp(j,kk) + Rchpp(i,j,kk);

    I11(i) = Iaa(i,j,kk);
    I12(i) = Iab(i,j,kk);
    I13(i) = Iah(i,j,kk);

    I14(i) = Iba(i,j,kk);
    I15(i) = Ibb(i,j,kk);
    I16(i) = Ibh(i,j,kk);

    I17(i) = Ica(i,j,kk);
    I18(i) = Icb(i,j,kk);
    I19(i) = Ich(i,j,kk);

end

%% Solve Case 3 Example Using Equations from Appendix I (Figs 5 & 6)

if group == 1

% Compute quadratic coefficients
for i=1:N

MRch(i) = R1(i)*R5(i) - R2(i)*R4(i) - kinv(i)*kinv(i)*(I11(i)*I15(i)-
I12(i)*I14(i));
MIch(i) = R1(i)*I15(i) - R2(i)*I14(i) + I11(i)*R5(i) - I12(i)*R4(i);

```

```

A(i) = MRch(i)*I15(i)*I15(i) - MICH(i)*R5(i)*I15(i);
B(i) = -MICH(i)*(R2(i)*I14(i)+ I12(i)*R4(i)) + 2*MRch(i)*I11(i)*I15(i);
C(i) = MRch(i)*I11(i)*I11(i) - MICH(i)*R1(i)*I11(i);

end

% Solve quadratic equation
for i=2:N

    Quad = [A(i) B(i) C(i)];
    r = roots(Quad);
    OmegaAlpha1(i) = r(1);
    OmegaAlpha2(i) = r(2);
    X1(i) = -MICH(i)/(OmegaAlpha1(i)*I15(i)+I11(i));
    X2(i) = -MICH(i)/(OmegaAlpha2(i)*I15(i)+I11(i));

    F1(i) = kinv(i)*kinv(i)/X1(i); % This is actually the square of F
    F2(i) = kinv(i)*kinv(i)/X2(i); % This is actually the square of F

end

figure(5)
plot(kinv, OmegaAlpha1, 'r.', kinv, OmegaAlpha2, 'b. ');
grid
axis([0 1 0 160])
xlabel('1/k', 'FontWeight', 'bold');
ylabel('Omega-Alpha', 'FontWeight', 'bold');
title('Fig 5, Case 3, Standard Case', 'FontWeight', 'bold');

figure(6)
plot(OmegaAlpha1, F1, 'r.', OmegaAlpha2, F2, 'b. ');
grid
axis([0 180 0 22])
xlabel('Omega-Alpha', 'FontWeight', 'bold');
ylabel('F', 'FontWeight', 'bold');
title('Fig 6 Case 3, Standard Case', 'FontWeight', 'bold');

end

%% Solve Case 2 Example Using Equations from Appendix I (Figs 7 & 8)

if group == 1

% Compute quadratic coefficients
for i=1:N

MRaa(i) = R5(i)*R9(i) - R6(i)*R8(i) - kinv(i)*kinv(i)*(I15(i)*I19(i)-
I16(i)*I18(i));
MIaa(i) = R5(i)*I19(i) - R6(i)*I18(i) + I15(i)*R9(i) - I16(i)*R8(i);

A(i) = MRaa(i)*I19(i)*I19(i) - MIaa(i)*R9(i)*I19(i);
B(i) = -MIaa(i)*(R6(i)*I18(i)+ I16(i)*R8(i)) + 2*MRaa(i)*I15(i)*I19(i);
C(i) = MRaa(i)*I15(i)*I15(i) - MIaa(i)*R5(i)*I15(i);

```

```

end

% Solve quadratic equation
for i=2:N

    Quad = [A(i) B(i) C(i)];
    r = roots(Quad);
    OmegaBeta1(i) = r(1);
    OmegaBeta2(i) = r(2);
    X1(i) = -MIaa(i)/(OmegaBeta1(i)*I19(i)+I15(i));
    X2(i) = -MIaa(i)/(OmegaBeta2(i)*I19(i)+I15(i));

    F1(i) = kinv(i)*kinv(i)/X1(i); % This is actually the square of F
    F2(i) = kinv(i)*kinv(i)/X2(i); % This is actually the square of F

end

figure(7)
plot(kinv, OmegaBeta1, 'r.', kinv, OmegaBeta2, 'b. ');
grid
axis([0 4 -0.008 0.014])
xlabel('1/k', 'FontWeight', 'bold');
ylabel('Omega-Beta', 'FontWeight', 'bold');
title('Fig 7, Case 2, Standard Case', 'FontWeight', 'bold');
annotation('textbox', 'String', [{'xb = ', num2str(xb)}], 'FontWeight', 'bold',
'FontSize', 10, ...
'BackgroundColor', [1 1 1]);

figure(8)
plot(OmegaBeta1, F1, 'r.', OmegaBeta2, F2, 'b. ');
grid
axis([0 0.014 0 1.5])
xlabel('Omega-Beta', 'FontWeight', 'bold');
ylabel('F', 'FontWeight', 'bold');
title('Fig 8, Case 2, Standard Case', 'FontWeight', 'bold');
annotation('textbox', 'String', [{'xb = ', num2str(xb)}], 'FontWeight', 'bold',
'FontSize', 10, ...
'BackgroundColor', [1 1 1]);

end

%% Solve Case 1 Example Using Equations from Appendix I (Figs 9 & 10)

if group == 1

% Compute quadratic coefficients
for i=1:N

MRbb(i) = R9(i)*R1(i) - R7(i)*R3(i) - kinv(i)*kinv(i)*(I19(i)*I11(i)-
I17(i)*I13(i));
MIbb(i) = R9(i)*I11(i) - R7(i)*I13(i) + I19(i)*R1(i) - I17(i)*R3(i);

A(i) = MRbb(i)*I11(i)*I11(i) - MIbb(i)*R1(i)*I11(i);

```

```

B(i) = -MIbb(i)*(R7(i)*I13(i)+ I17(i)*R3(i)) + 2*MRbb(i)*I19(i)*I11(i);
C(i) = MRbb(i)*I19(i)*I19(i) - MIbb(i)*R9(i)*I19(i);

end

% Solve quadratic equation
for i=2:N

    Quad = [A(i) B(i) C(i)];
    r = roots(Quad);
    OmegaH1(i) = r(1);
    OmegaH2(i) = r(2);
    X1(i) = -MIbb(i)/(OmegaH1(i)*I11(i)+I19(i));
    X2(i) = -MIbb(i)/(OmegaH2(i)*I11(i)+I19(i));

    F1(i) = kinv(i)*kinv(i)/X1(i); % This is actually the square of F
    F2(i) = kinv(i)*kinv(i)/X2(i); % This is actually the square of F

end

figure(9)
plot(kinv, OmegaH1, 'r.', kinv, OmegaH2, 'b. ');
grid
axis([0 10 -30 120])
xlabel('1/k', 'FontWeight', 'bold');
ylabel('Omega-H', 'FontWeight', 'bold');
title('Fig 9, Case 1, Standard Case', 'FontWeight', 'bold');

figure(10)
plot(OmegaH1, F1, 'r.', OmegaH2, F2, 'b. ');
grid
axis([0 22 0 1.5])
xlabel('Omega-H', 'FontWeight', 'bold');
ylabel('F', 'FontWeight', 'bold');
title('Fig 10, Case 1, Standard Case', 'FontWeight', 'bold');

end

%% Solve Case 1 Example Using Equations from Appendix I (Fig 11)

if group == 2

% Compute quadratic coefficients
for i=1:N

MRbb(i) = R9(i)*R1(i) - R7(i)*R3(i) - kinv(i)*kinv(i)*(I19(i)*I11(i)-
I17(i)*I13(i));
MIbb(i) = R9(i)*I11(i) - R7(i)*I13(i) + I19(i)*R1(i) - I17(i)*R3(i);

A(i) = MRbb(i)*I11(i)*I11(i) - MIbb(i)*R1(i)*I11(i);
B(i) = -MIbb(i)*(R7(i)*I13(i)+ I17(i)*R3(i)) + 2*MRbb(i)*I19(i)*I11(i);
C(i) = MRbb(i)*I19(i)*I19(i) - MIbb(i)*R9(i)*I19(i);


```

```

end

% Solve quadratic equation
for i=2:N

    Quad = [A(i) B(i) C(i)];
    r = roots(Quad);
    OmegaH1(i) = r(1);
    OmegaH2(i) = r(2);
    X1(i) = -MIbb(i)/(OmegaH1(i)*I11(i)+I19(i));
    X2(i) = -MIbb(i)/(OmegaH2(i)*I11(i)+I19(i));

    F1(i) = kinv(i)/sqrt(X1(i)); % F as defined on pp. 14-15
    F2(i) = kinv(i)/sqrt(X2(i)); % F as defined on pp. 14-15

    omlom21(i) = ra*sqrt(OmegaH1(i));
    omlom22(i) = ra*sqrt(OmegaH2(i));

end

figure(11)
plot(omlom21, F1, 'r.', omlom22, F2, 'b. ');
grid
axis([0 1.66666666667 0 1.75])
xlabel('omega-1 / omega-2','FontWeight','bold');
ylabel('F','FontWeight','bold');
title('Fig 11, Case 1, Standard Case (but with kappa = 1/400)','FontWeight','bold');

end

%% Solve Case 1 Example Using Equations from Appendix I (Fig 15)

if group == 3

% Compute quadratic coefficients
for i=1:N

MRbb(i) = R9(i)*R1(i) - R7(i)*R3(i) - kinv(i)*kinv(i)*(I19(i)*I11(i)-
I17(i)*I13(i));
MIbb(i) = R9(i)*I11(i) - R7(i)*I13(i) + I19(i)*R1(i) - I17(i)*R3(i);

A(i) = MRbb(i)*I11(i)*I11(i) - MIbb(i)*R1(i)*I11(i);
B(i) = -MIbb(i)*(R7(i)*I13(i)+ I17(i)*R3(i)) + 2*MRbb(i)*I19(i)*I11(i);
C(i) = MRbb(i)*I19(i)*I19(i) - MIbb(i)*R9(i)*I19(i);

end

% Solve quadratic equation
for i=2:N

    Quad = [A(i) B(i) C(i)];
    r = roots(Quad);

```

```

OmegaH1(i) = r(1);
OmegaH2(i) = r(2);
X1(i) = -MIbb(i)/(OmegaH1(i)*I11(i)+I19(i));
X2(i) = -MIbb(i)/(OmegaH2(i)*I11(i)+I19(i));

F1(i) = kinv(i)/sqrt(X1(i)); % F as defined on pp. 14-15
F2(i) = kinv(i)/sqrt(X2(i)); % F as defined on pp. 14-15

fac1 = b*omegaa*ra/sqrt(kappa);
fac2 = 12/39.37; % convert from fps to mps

vell(i) = F1(i)*fac1*fac2;
vel2(i) = F2(i)*fac1*fac2;

omlom21(i) = ra*sqrt(OmegaH1(i));
omlom22(i) = ra*sqrt(OmegaH2(i));

end

figure(15)
plot(omlom21, vell, 'r.', omlom22, vel2, 'b. ');
grid
axis([0 1.5 0 50])
xlabel('omega-h / omega-alpha','FontWeight','bold');
ylabel('Velocity, meters per sec','FontWeight','bold');
title('Fig 15, Case 1, Wing A','FontWeight','bold');
annotation('textbox','String',{['xa = ', num2str(xa)]},'FontWeight','bold',
'FontSize',10,...
'BackgroundColor',[1 1 1]);

end

%% Solve Case 2 Example Using Equations from Appendix I (Fig 16)

if group == 4

% Compute quadratic coefficients
for i=1:N

MRaa(i) = R5(i)*R9(i) - R6(i)*R8(i) - kinv(i)*kinv(i)*(I15(i)*I19(i)-
I16(i)*I18(i));
MIaa(i) = R5(i)*I19(i) - R6(i)*I18(i) + I15(i)*R9(i) - I16(i)*R8(i);

A(i) = MRaa(i)*I19(i)*I19(i) - MIaa(i)*R9(i)*I19(i);
B(i) = -MIaa(i)*(R6(i)*I18(i)+ I16(i)*R8(i)) + 2*MRaa(i)*I15(i)*I19(i);
C(i) = MRaa(i)*I15(i)*I15(i) - MIaa(i)*R5(i)*I15(i);

end

% Solve quadratic equation
for i=2:N

Quad = [A(i) B(i) C(i)];

```

```

r = roots(Quad);
OmegaBeta1(i) = r(1);
OmegaBeta2(i) = r(2);
X1(i) = -MIaa(i)/(OmegaBeta1(i)*I19(i)+I15(i));
X2(i) = -MIaa(i)/(OmegaBeta2(i)*I19(i)+I15(i));

F1(i) = kinv(i)/sqrt(X1(i)); % F as defined on pp. 14-15
F2(i) = kinv(i)/sqrt(X2(i)); % F as defined on pp. 14-15

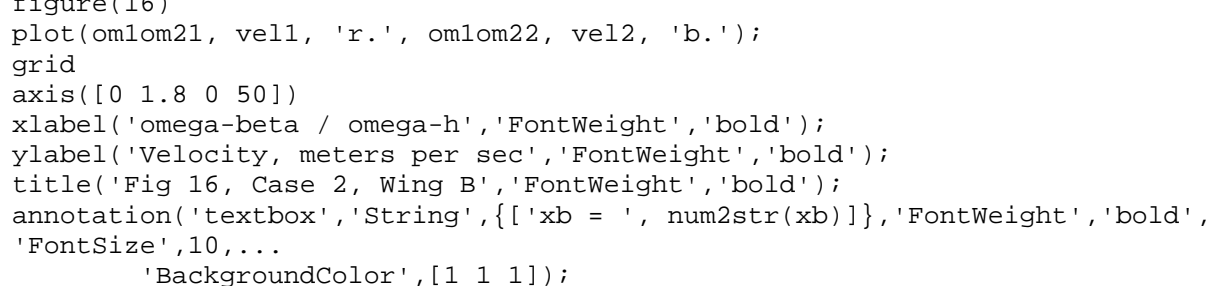
fac1 = b*omegah/sqrt(kappa);
fac2 = 12/39.37; % convert from fps to mps

vell(i) = F1(i)*fac1*fac2;
vel2(i) = F2(i)*fac1*fac2;

omlom21(i) = sqrt(OmegaBeta1(i))/rb;
omlom22(i) = sqrt(OmegaBeta2(i))/rb;

end

figure(16)
plot(omlom21, vell, 'r.', omlom22, vel2, 'b.');
```



```

grid
axis([0 1.8 0 50])
xlabel('omega-beta / omega-h','FontWeight','bold');
ylabel('Velocity, meters per sec','FontWeight','bold');
title('Fig 16, Case 2, Wing B','FontWeight','bold');
annotation('textbox','String',{['xb = ', num2str(xb)]},'FontWeight','bold',
'FontSize',10,...
'BackgroundColor',[1 1 1]);

end

%% Solve Case 3 Example Using Equations from Appendix I (Fig 17)

if group == 4

% Compute quadratic coefficients

for i=1:N

MRch(i) = R1(i)*R5(i) - R2(i)*R4(i) - kinv(i)*kinv(i)*(I11(i)*I15(i)-
I12(i)*I14(i));
MICH(i) = R1(i)*I15(i) - R2(i)*I14(i) + I11(i)*R5(i) - I12(i)*R4(i);

A(i) = MRch(i)*I15(i)*I15(i) - MICH(i)*R5(i)*I15(i);
B(i) = -MICH(i)*(R2(i)*I14(i)+ I12(i)*R4(i)) + 2*MRch(i)*I11(i)*I15(i);
C(i) = MRch(i)*I11(i)*I11(i) - MICH(i)*R1(i)*I11(i);

end

% Solve quadratic equation
for i=2:N

```

```

Quad = [A(i) B(i) C(i)];
r = roots(Quad);
OmegaAlpha1(i) = r(1);
OmegaAlpha2(i) = r(2);
X1(i) = -M1ch(i)/(OmegaAlpha1(i)*I15(i)+I11(i));
X2(i) = -M1ch(i)/(OmegaAlpha2(i)*I15(i)+I11(i));

F1(i) = kinv(i)/sqrt(X1(i)); % F as defined on pp. 14-15
F2(i) = kinv(i)/sqrt(X2(i)); % F as defined on pp. 14-15

fac1 = b*omegab*rb/sqrt(kappa);
fac2 = 12/39.37; % convert from fps to mps

vell1(i) = F1(i)*fac1*fac2;
vel2(i) = F2(i)*fac1*fac2;

omlom21(i) = sqrt(OmegaAlpha1(i))*(rb/ra);
omlom22(i) = sqrt(OmegaAlpha2(i))*(rb/ra);

end

figure(17)
plot(omlom21, vell1, 'r.', omlom22, vel2, 'b. ');
grid
axis([0 2.8 0 40])
xlabel('omega-alpha / omega-beta','FontWeight','bold');
ylabel('Velocity, meters per sec','FontWeight','bold');
title('Fig 17, Case 3, Wing B','FontWeight','bold');

end

```

APPENDIX C

ALTERNATE TWO-DEGREE-OF-FREEDOM SOLUTION METHODS

Three alternate solution methods are offered, all of which are based on the two-degree-of-freedom flutter equations of *NACA 496*. Compared to the number of computations involved in the *NACA 496* solution method, these alternate solution methods are much more computationally intensive and would have been excluded from consideration in 1934 for that reason. But with today's computational resources, these alternate solution methods require only a few seconds of execution time on a desktop computer. The solution methods will be presented in order of increasing complexity.

Although these alternate solution methods are appropriate for all three subcases mentioned in *NACA 496*, the equations for Subcase 1, flexure – torsion, are chosen to illustrate the methods. The starting point for each alternate solution method is equation (XXIV) on page 12 of *NACA 496*, quadratic in X with complex coefficients, re-written here

$$\Omega_h \Omega_\alpha X^2 + (\Omega_h A_{a\alpha} + \Omega_\alpha A_{ch})X + M_{b\beta} = 0 \quad (C1)$$

with companion equations

$$X = \frac{1}{\kappa} \left(\frac{b r_r \omega_r}{v k} \right)^2 \quad (C2)$$

$$\Omega_h = \left(\frac{\omega_h}{\omega_r r_r} \right)^2 \quad (C3)$$

$$\Omega_\alpha = \left(\frac{\omega_\alpha r_\alpha}{\omega_r r_r} \right)^2 \quad (C4)$$

where, for Subcase 1, the reference quantities, ω_r and r_r , are chosen to be ω_α and r_α , respectively.

An illustrative example will be presented for each alternate solution method. The problem-specific quantities chosen for the example are those employed in *NACA 496* for its “standard case”:

$$\kappa = 0.1; \quad c = 0.5; \quad a = -0.4; \quad x_\alpha = 0.2; \quad r_\alpha^2 = 0.25;$$

$$\text{and with } \omega_\alpha = 100, \quad \omega_h = 50, \text{ and } b = 1$$

Using the appropriate values in equations (C3) and (C4), the values of Ω_h and Ω_α are both 1.

Because equation (C1) is quadratic, zero, one, or two flutter solutions are possible. However, for the problem-specific quantities chosen, only one flutter solution is obtained.

As expected and as will be seen, all three alternate solution methods will yield almost exactly the same value of flutter velocity, v_f , and almost exactly the same value of flutter reduced frequency, k_f , as those predicted by the two-degree-of-freedom solution method of *NACA 496*. The family of solutions for Subcase 1 for the standard case already exists in figures 9 and 10. When $\Omega_h = 1$ is used in these figures

the problem-specific solution is obtained: $v_f = 173.26$ feet per second (fps) and $k_f = 0.4355$. The first row of Table C1 contains this result.

On occasion throughout this appendix, the abbreviation ASM will be used to denote “alternate solution method.”

Alternate Solution Method No. 1

This alternate solution method is directly analogous to the three-degree-of-freedom solution method discussed in *NACA 496*. It employs the computational shortcut of creating two equations, each with real coefficients, by separating the real and imaginary parts of equation (C1), thereby eliminating complex arithmetic. The right-hand side of both new equations is zero.

$$\Omega_h \Omega_\alpha X^2 + (\Omega_h R_{a\alpha} + \Omega_\alpha R_{ch})X + M_{b\beta}^R = 0 \quad (C5)$$

$$(\Omega_h I_{a\alpha} + \Omega_\alpha I_{ch})X + M_{b\beta}^I = 0 \quad (C6)$$

The first equation, (C5), is quadratic in X and is obtained from the real parts of $A_{a\alpha}$, A_{ch} , and $M_{b\beta}$; the second equation, (C6), is linear in X and is obtained from the imaginary parts.

At this point in ASM No. 1, the artifice of treating X as a parameter, rather than as a known quantity, is employed. Equations (C5) and (C6) are each solved for their roots, identified herein as X_{R1} , X_{R2} and X_I , for a large number of reduced frequencies. But, because from equation (C2), it is seen that X is proportional to the inverse square of velocity, only the real positive values of X_{R1} , X_{R2} and X_I are retained.

Next, the real positive roots are plotted as functions of the inverse of reduced frequency on the same set of axes. The intersection of either of the X_R 's with the X_I identifies the value of X and the value of reduced frequency that simultaneously solve equations (C5) and (C6), and therefore also solves the original quadratic equation with complex coefficients, equation (C1). These values are the flutter values - X_f and k_f .

With X_f and k_f known, the artifice of treating X as a parameter is abandoned and equation (C2) is employed, which when re-written to solve for flutter velocity, becomes

$$v_f = \frac{1}{\sqrt{X_f}} \frac{1}{\sqrt{\kappa}} \frac{b \omega_\alpha r_\alpha}{k_f} \quad (C7)$$

Plugging X_f , k_f , and the other quantities into equation (C7) yields the flutter velocity.

Illustrative Example for Alternate Solution Method No. 1. – ASM No. 1 was implemented in Matlab® where equations (C5) and (C6) were solved 10,000 times for values of the inverse of reduced frequency ranging from 0.001 to 10 in increments of 0.001. Figure C1 presents the results from this implementation: the ordinate represents the real positive roots of equations (C5) and (C6); the abscissa

is the inverse of reduced frequency. The solid black line represents the locus of the X_{R_1} , the first real positive root of equation (C5); the dashed black line represents the locus of the X_{R_2} , the second real positive root of equation (C5); and the solid red line represents the locus of the X_I , the real positive root of equation (C6). The circle represents the intersection of the X_{R_1} locus with the X_I locus and was obtained using an interpolation scheme.

By inverting the horizontal coordinate of the intersection, the flutter reduced frequency is obtained. By using it and the vertical coordinate in equation (C7), the flutter velocity is obtained. Both results are contained in the second row of Table CI and are seen to agree extremely well with the *NACA 496* results.

Alternate Solution Method No. 2

This alternate solution method is closely related to ASM No. 1 and also eliminates complex arithmetic via the same computational shortcut. But, rather than initially treating X as a parameter, as was done in ASM No. 1, in this solution method, X is assigned values and the flutter solution is obtained via systematic trial and error.

ASM No. 2 employs an outer loop on velocity and an inner loop on reduced frequency and, using equation (C2), it computes a value of X at each passing. These X 's are then substituted into the following equations

$$\Omega_h \Omega_\alpha X^2 + (\Omega_h R_{a\alpha} + \Omega_\alpha R_{ch})X + M_{b\beta}^R = Z_1 \quad (C8)$$

$$(\Omega_h I_{a\alpha} + \Omega_\alpha I_{ch})X + M_{b\beta}^I = Z_2 \quad (C9)$$

producing values of Z_1 and Z_2 at each passing.

Recall that the flutter condition is obtained when Z_1 and Z_2 are both zero for the same values of v and k . However, unless luck intervenes or infinitesimally small increments in v and k are chosen for the outer and inner loops, it is almost assured that no combination of v and k will be found, which results in Z_1 and Z_2 being exactly zero simultaneously. This being the case, two different interpolation schemes are employed to find the combination of v and k that does result in Z_1 and Z_2 being exactly zero simultaneously.

When each inner loop is complete (that is, for each velocity), curves of Z_1 and Z_2 as functions of reduced frequency are created. Because equation (C8) is quadratic, there can be zero, one, or two values of reduced frequency that cause Z_1 to be zero. Because equation (C9) is linear, there can be zero or one value of reduced frequency that causes Z_2 to be zero.

The Z_1 and Z_2 curves may or may not pass through zero. For curves that do pass through zero, a first interpolation scheme is employed to identify the values of reduced frequency at the zero crossings and these values and their corresponding velocity are potential solutions and are stored in arrays. There can

be up to three arrays: two for the Z_1 's and one for the Z_2 's. These identified reduced frequencies are defined as $k_{z_{11}}$, $k_{z_{12}}$ and k_{z_2} , respectively.

When the outer loop is complete, the reduced frequencies at the zero crossings, $k_{z_{11}}$, $k_{z_{12}}$ and k_{z_2} , are plotted as functions of velocity. Each point on the $k_{z_{11}}$ and $k_{z_{12}}$ curves (that is, each reduced frequency and its companion velocity) corresponds to Z_1 being exactly equal to zero. Likewise, each point on the k_{z_2} curve corresponds to Z_2 being exactly equal to zero. The flutter condition is obtained when either the $k_{z_{11}}$ curve or the $k_{z_{12}}$ curve intersects the k_{z_2} curve. Via a second interpolation scheme, the values of v and k at the intersection are determined. These values are v_f and k_f because they cause Z_1 and Z_2 to be zero simultaneously.

Illustrative Example for Alternate Solution Method No. 2. – This alternate solution method was also implemented in Matlab® where equations (C2), (C8), and (C9) were solved within nested loops. The inner loop varied reduced frequency from 0.01 to 2 in increments of 0.01; the outer loop varied velocity from 160 fps to 185 fps in increments of 0.5 fps. (The limits of the outer loop were chosen based on the knowledge of flutter velocity gained from the previous illustrative example.)

Figure C2 presents a plot of Z_1 and Z_2 as functions of reduced frequency for a velocity of 160 fps, well below the flutter velocity. As can be seen Z_1 , the solid curve, intersects zero at two points, $k_{z_{11}} = 0.3706$ and $k_{z_{12}} = 0.5317$, and Z_2 , the dashed curve, intersects zero at one point, $k_{z_2} = 0.4740$. These values of reduced frequency are combined with similar reduced frequencies for the other velocities to form the arrays that are plotted in the next figure.

Figure C3 presents a plot of $k_{z_{11}}$, $k_{z_{12}}$, and k_{z_2} as functions of velocity. As can be seen $k_{z_{12}}$, the dashed curve, intersects the k_{z_2} , the dashed-dotted curve, at the values of velocity and reduced frequency indicated in the third row of Table CI. As with the results for ASM No. 1, those for ASM No. 2 are in excellent agreement with the results from *NACA 496*.

Alternate Solution Method No. 3

This alternate solution method is very straightforward, but uses complex arithmetic. It also initially employs the artifice of treating X as a parameter and later abandons it.

Treating X as a parameter, equation (C1), quadratic in X with complex coefficients, is solved for X directly for a large number of reduced frequencies. Because the coefficients are complex the resulting X 's are also complex, but the X 's are not complex conjugates. These complex X 's are designated X_1 and X_2 .

With X_1 and X_2 and their corresponding reduced frequencies known, the artifice is abandoned and equation (C10)

$$v = \frac{1}{\sqrt{X}} \frac{1}{\sqrt{\kappa}} \frac{b\omega_\alpha r_\alpha}{k} \quad (C10)$$

is employed, yielding velocities, v_1 corresponding to X_1 , and v_2 , corresponding to X_2 , that are also complex and also not complex conjugates.

All the complex X 's, and therefore all the complex v 's and their corresponding k 's, satisfy equation (C1) and are therefore all flutter solutions. However, because in actual practice the flutter velocity is real, not complex, the task now is to examine all of the complex v 's to determine if any have a zero imaginary part, that is to determine if any are real.

A convenient way to perform this examination is to plot the imaginary part of v_1 against the real part of v_1 and the imaginary part of v_2 against the real part of v_2 , yielding two curves in the complex plain. Each point on each curve corresponds to a different value of reduced frequency. If one of the curves crosses the real axis, at the crossing, the imaginary part is zero, the real part is the flutter velocity, and the examination is complete. Interpolation is then employed, taking the complex velocities immediately before and immediately after the crossing to determine the value of the corresponding real part at the crossing, which is v_f , and the corresponding value of reduced frequency at the crossing, which is k_f .

Illustrative Example for Alternate Solution Method No. 3. – This alternate solution method was also implemented in Matlab® where equations (C1) and (C10) were solved 10,000 times for reduced frequencies ranging from 0.005 to 50 in increments of 0.005.

Figure C4 presents plots of the imaginary parts of v_1 and v_2 as functions of their respective real parts. The solid line is v_1 ; the dashed line, v_2 . By the nature of the curves, it is apparent that, as stated above, v_1 and v_2 are not complex conjugates. As can be seen in the figure, the dashed curve crosses the real axis and the interpolated values of velocity and reduced frequency at the crossing are indicated in the fourth row of Table CI. The results for ASM No. 3 are in perfect agreement with the results from NACA 496.

Table CI
Comparison of Flutter Predictions for
Standard Case

Solution Method	v_f fps	k_f
NACA 496	173.26	0.4355
Alt. Soln. Meth. No. 1	173.22	0.4356
Alt. Soln. Meth. No. 2	173.21	0.4358
Alt. Soln. Meth. No. 3	173.26	0.4355

APPENDIX D

THREE-DEGREE-OF-FREEDOM SOLUTION METHOD

This appendix provides a solution to the three-degree-of-freedom flutter equation following the procedure recommended in *NACA 496*. Equation (XXI) on page 12 of *NACA 496*, re-written here as equation (D1), is the three-degree-of-freedom flutter equation

$$\begin{aligned} \Omega_\alpha \Omega_\beta \Omega_h X^3 + (\Omega_\alpha \Omega_\beta A_{ch} + \Omega_\beta \Omega_h A_{a\alpha} + \Omega_h \Omega_\alpha A_{b\beta}) X^2 \\ + (\Omega_\alpha M_{a\alpha} + \Omega_\beta M_{b\beta} + \Omega_h M_{ch}) X + D = 0 \end{aligned} \quad (D1)$$

with companion equations

$$X = \frac{1}{\kappa} \left(\frac{b r_r \omega_r}{v k} \right)^2 \quad (D2)$$

$$\Omega_\alpha = \left(\frac{\omega_\alpha r_\alpha}{\omega_r r_r} \right)^2 \quad (D3)$$

$$\Omega_\beta = \left(\frac{\omega_\beta r_\beta}{\omega_r r_r} \right)^2 \quad (D4)$$

$$\Omega_h = \left(\frac{\omega_h}{\omega_r r_r} \right)^2 \quad (D5)$$

In equation (D1) the A 's, M 's, and D are complex quantities, making equation (D1) cubic in X with complex coefficients.

The subsection entitled "Solution Methods" within section III of the main body of the present paper outlines the three-degree-of-freedom solution method. To recap, this solution method involves the artifice of treating X as a parameter and the computational shortcut of creating two equations, each with real coefficients, by separating the real and imaginary parts of equation (D1), shown here as equations (D6) and (D7)

$$\begin{aligned} \Omega_\alpha \Omega_\beta \Omega_h X^3 + (\Omega_\alpha \Omega_\beta R_{ch} + \Omega_\beta \Omega_h R_{a\alpha} + \Omega_h \Omega_\alpha R_{b\beta}) X^2 \\ + (\Omega_\alpha M_{a\alpha}^R + \Omega_\beta M_{b\beta}^R + \Omega_h M_{ch}^R) X + D^R = 0 \end{aligned} \quad (D6)$$

$$\begin{aligned} (\Omega_\alpha \Omega_\beta I_{ch} + \Omega_\beta \Omega_h I_{a\alpha} + \Omega_h \Omega_\alpha I_{b\beta}) X^2 \\ + (\Omega_\alpha M_{a\alpha}^I + \Omega_\beta M_{b\beta}^I + \Omega_h M_{ch}^I) X + D^I = 0 \end{aligned} \quad (D7)$$

Equations (D6) and (D7) are each solved for their roots, identified herein as $X_{R_1}, X_{R_2}, X_{R_3}, X_{I_1}$ and X_{I_2} , for a large number of reduced frequencies. But, because from equation (D2), it is seen that X is proportional to the inverse square of velocity, only the real positive values of $X_{R_1}, X_{R_2}, X_{R_3}, X_{I_1}$ and X_{I_2} are of interest.

Next, all of the real positive roots are plotted as functions of the inverse of reduced frequency on the same set of axes. The intersection(s) of any of the X_R 's with any of the X_I 's identify(ies) the value(s) of X and the value(s) of reduced frequency that simultaneously solve equations (D6) and (D7), and therefore, also solves the original cubic equation with complex coefficients, equation (D1). These values are the flutter values - X_f and k_f .

With X_f and the k_f known, the artifice of treating X as a parameter is abandoned and equation (D2) is employed, which when re-written to solve for flutter velocity, becomes

$$v_f = \frac{1}{\sqrt{X_f}} \frac{1}{\sqrt{\kappa}} \frac{b \omega_r r_r}{k_f} \quad (D8)$$

Plugging X_f , k_f , and the other quantities into equation (D8) yields the flutter velocity.

The three-degree-of-freedom solution method is capable of finding zero, one, two, or three flutter modes, depending on the problem-specific quantities chosen.

Illustrative Example for Three-Degree-of-Freedom Solution Method

The problem-specific quantities chosen for this example are those employed in *NACA 496* for its "standard case":

$$\kappa = 0.1; \quad c = 0.5; \quad a = -0.4; \quad x_\alpha = 0.2; \quad r_\alpha^2 = 0.25; \quad x_\beta = 1/80; \quad r_\beta^2 = 1/160;$$

$$\text{and with } \omega_\alpha = 100; \quad \omega_\beta = 125; \quad \omega_h = 50; \quad b = 1; \quad \omega_r = 1; \quad r_r = 1$$

This solution method was implemented in Matlab® where equations (D6) and (D7) were solved 10,000 times for values of the inverse of reduced frequency ranging from 0.0005 to 5 in increments of 0.0005.

Figure D1 presents the results from this implementation: the ordinate represents the real roots of equations (D6) and (D7); the abscissa is the inverse of reduced frequency. The three black lines (solid, dashed, dotted) represent the loci of the roots of equation (D6); the two red lines (solid, dashed) represent the loci of the roots of equation (D7); the open blue circle indicates the intersection of the locus of X_{R2} with the locus of X_{I1} and is the flutter solution (a single flutter mode) for the quantities chosen.

By inverting the horizontal coordinate of the intersection point, the flutter reduced frequency is obtained. By using it and the vertical coordinate of the intersection point in equation (D8), the flutter velocity is obtained. The results are contained in Table D1.

Table DI
3DOF Flutter Prediction for
Standard Case

v_f fps	k_f
179.49	0.4476

The problem-specific quantities for the illustrative examples in Appendices C and D of the present paper are the same, including the dimensional values of ω_α and ω_h . As stated in Appendix C of the present paper, alternate solution method no. 1 for the two-degree-of-freedom (2DOF) flutter equation is directly analogous to the three-degree-of-freedom (3DOF) solution method. Thus, in comparing these two illustrative examples, one might expect their results to be similar in some ways, which is, in fact, the case.

Comparing first the values of flutter velocity and flutter reduced frequency from the two illustrative examples, from Tables CI and DI, it is seen that the respective values of v_f and k_f differ by only 3.5% and 2.7%. These differences are attributed, obviously, to the presence of the third degree of freedom in the 3DOF solution.

Comparing next the loci of the roots in figures C1 and D1, an obvious difference is the number of loci in each figure – three in the former and five in the latter. However, in figure D1, if one ignores the loci of the third “real” root, X_{R_3} , and the second “imaginary” root, X_{I_2} , (those attributed to the presence of the third degree of freedom), the remaining loci agree very well in their general character with the loci in figure C1. In each figure: (1) with increasing values of the inverse of reduced frequency, the loci of the first and second roots from the higher-order (“real”) equation (shown in solid and dashed black) approach each other; (2) the locus of the root from the lower-order (“imaginary”) equation (shown in solid red) lies between the other two loci; and (3) the locus of the “imaginary” root intersects the locus of the second “real” root.

Results from 3DOF Solution Method Asymptotically Approach Results from 2DOF Solution Method

Three examples are presented for the 3DOF solution method. In each example, two of the three modal frequencies (ω_α , ω_β , ω_h) are fixed and the third is varied from its initial value to a very high value. In the limit, each example corresponds to one of the three subcases discussed in the main body of the present paper. For example, for Subcase 1, which has as degrees of freedom α and h , ω_α and ω_h are fixed while

ω_β is varied. With the value of the third modal frequency at least an order of magnitude higher than the highest value of the other two, the expectation is that the flutter velocities (v_f) and flutter reduced frequencies (k_f) obtained using the 3DOF solution method will asymptotically approach those quantities obtained using the appropriate 2DOF solution method.

Results from 2DOF solution method. – The 2DOF solution methods are solved as described in the main body of this paper with quantities ω_r and r_r defined according to which of the three 2DOF solution methods is employed.

Each of these examples employs the problem-specific quantities from the *NACA 496* “standard case”:

$$\kappa = 0.1; \quad c = 0.5; \quad a = -0.4; \quad x_\alpha = 0.2; \quad r_\alpha^2 = 0.25; \quad x_\beta = 1/80; \quad r_\beta^2 = 1/160$$

The following table contains the natural frequencies and the corresponding values of frequency ratios for the three subcases.

Table DII
Summary of Natural Frequencies and Frequency Ratios for Examples

	ω_α rps	ω_β rps	ω_h rps	Ω_α	Ω_β	Ω_h
Subcase 1	100	x	50	1	x	1
Subcase 2	x	44.721	50	x	0.005	1
Subcase 3	100	75	x	71.111	1	x

To obtain the 2DOF flutter solutions for Subcase 1, figures 9 and 10 are used with $\Omega_h = 1$; for Subcase 2, figures 7 and 8 are used with $\Omega_\beta = 0.005$; and for Subcase 3, figures 5 and 6 are used with $\Omega_\alpha = 71.111$.

Figures D2(a) and D2(b) contain close-up views of portions of figures 9 and 10; figures D3(a) and D3(b) contain close-up views of portions of figures 7 and 8; and figures D4(a) and D4(b) contain expanded views of figures 5 and 6. Following the convention established in the main body of the present paper, these curves are red, indicating they were created using present calculations. In each figure, the solid black line indicates the target value of its particular Ω . Intersections of the solid black line with the red curves produce the dashed black lines, which indicate the corresponding values of $1/k_f$ and F , from which k_f and v_f , respectively, are obtained. (Recall that in figures 6, 8, and 10, although labelled “ F ” the quantity plotted is actually the square of the defined quantity, which has ramifications on the extraction of v_f from F .)

In figures D2(a) and D2(b), there is only a single intersection of the black line with the red curves, indicating only one flutter mode is predicted for Subcase 1; but in figures D3(a) and D3(b) and in figures

D4(a) and D4(b), because there are two intersections of the black line with the red curves, two flutter modes each are predicted for Subcases 2 and 3.

The following table presents a summary of the 2DOF flutter predictions:

Table DIII
2DOF Flutter Predictions for Standard Case

	Mode 1		Mode 2	
	v_f	k_f	v_f	k_f
	fps		fps	
Subcase 1	173.26	0.4355	x	x
Subcase 2	19.521	2.587	120.65	0.4727
Subcase 3	14.668	8.045	234.05	0.4458

Results from 3DOF solution method. – Figures D5, D6, and D7 contain the results of many 3DOF flutter solutions. These figures are comprised of semi-log plots of v_f and k_f as functions of the ω appropriate to the subcase. The solid blue circles represent the values of v_f and k_f predicted using the 3DOF solution method, where each corresponding pair came directly from an intersection such as the one indicated by the open blue circle in figure D1. The dashed red lines in the figures represent the values of v_f and k_f predicted using the 2DOF solution method and contained in Table DIII.

The nominal starting value for variable frequencies ω_β , ω_α , and ω_h in figures D5 through D7 was 100 rps. However, for Subcases 1 and 3, the fixed value of ω_α is also 100 rps. For these two subcases, the flutter modes that ultimately became the asymptotic solutions did not develop until their respective variable frequencies were above 100 rps: 125 rps for Subcase 1; 175 rps for Subcase 3.

As can be seen in figure D5, the 3DOF solution method predicts a single flutter mode, as did the 2DOF solution method. Also, with increasing values of ω_β , the circles approach the dashed lines, indicating that, in the limit, the values of v_f and k_f predicted by the 3DOF solution method approach those predicted by the 2DOF solution method, thereby confirming the initial expectation.

As can be seen in figure D6, the 3DOF solution method predicts two flutter modes, as did the 2DOF solution method. In each plot, with increasing values of ω_α , the circles approach the dashed lines, again indicating that, in the limit, the values of v_f and k_f predicted by the 3DOF solution method approach those predicted by the 2DOF solution method, and again confirming the initial expectation. The

comparatively higher density of circles for this subcase between $\omega_\alpha = 100$ rps and $\omega_\alpha = 250$ rps was necessary in order to capture the region of high curvature and the inflection in figure D6(c).

As can be seen in figure D7, the 3DOF solution method again predicts two flutter modes, as did the 2DOF solution method. In each plot, with increasing values of ω_h , the circles approach the dashed lines, once again indicating that, in the limit, the values of v_f and k_f predicted by the 3DOF solution method approach those predicted by the 2DOF solution method, and once again confirming the initial expectation.

For each subcase, in the limit, the 3DOF solution method predicts the same number of flutter modes and the same values of flutter velocity and flutter reduced frequency as did the 2DOF solution method.

REFERENCES

1. Zeiler, Thomas A.: *Results of Theodorsen and Garrick Revisited*. Journal of Aircraft. Vol. 37, No. 5, Sept-Oct 2000, pp 918-920.
2. Theodorsen, Theodore: *General Theory of Aerodynamic Instability and the Mechanism of Flutter*. NACA Report No. 496, 1940.
3. Theodorsen, Theodore; and Garrick, I. E.: *Mechanism of Flutter, a Theoretical and Experimental Investigation of the Flutter Problem*. NACA Report No. 685, 1940.
4. Theodorsen, Theodore; and Garrick, I. E.: *Flutter Calculations in Three Degrees of Freedom*. NACA Report No. 741, 1942.
5. Bisplinghoff, R. L.; Ashley, H.; and Halfman, R. L.: *Aeroelasticity*, Addison-Wesley-Longman, Reading, MA, 1955.
6. Bisplinghoff, R. L.; and Ashley, H.: *Principles of Aeroelasticity*, Dover, New York, 1975.

TABLE I. - TRIPPING POINTS IN NACA 496

No.	Tripping Point	Identified herein on page -	Occurs in NACA 496 -
1	Three versions of <i>NACA 496</i> dated 1934, 1940, and 1949.	4	--
2	No errata for some of the errors in 1934 version that were corrected in 1940 and 1949 versions.	4	--
3	Assignment of the same equation numbers, (1) - (9) and (11) - (19), to different expressions.	12	pp. 12, 14, 15
4	The use of the same symbol, l_{ij} , to represent a quantity and that quantity divided by reduced frequency.	13	pp. 12 & 14
5	The use of the same symbol, F , to represent a quantity and the square of that quantity.	16	figs 6, 8, 10 – the square of the quantity -- figs 11-14 – the quantity
6	Quantity D is never defined.	18	D is plotted in fig 12
7	Omission of values for ω_h and ω_β .	23	these values required to produce figs 16 and 17

TABLE II. – IDENTIFIED ERRORS IN NACA 496

No.	Identified Error	Identified herein on page(s) -	Occurs in NACA 496 on page -
1	The R''_{ah} row of Table III corresponding to $a = -0.4$ and $c = 0.5$ is in error.	15	17
2	Expression $v_D = v_R \frac{1}{\frac{1}{2}+a}$ is incorrect. Should be $v_D = v_R \frac{1}{\sqrt{1+2a}}$.	19	16
3	As presented in figure 13, the values comprising curve B are the square roots of the proper values.	20	20
4	Transcription errors: As presented in figure 14, correct values of F were paired with non-corresponding values of x_a – that led to incorrect curves A, B, and C.	22	20

TABLE III. – COMPUTATIONAL SHORTCUTS IN *NACA 496*

No.	Computational Shortcut	Benefit	Identified herein on page(s) -	Occurs in <i>NACA 496</i> on page(s) -
1	Separating an equation with complex coefficients into its real and imaginary parts, yielding two equations with real coefficients.	Avoids complex arithmetic.	9, 10, 66, 67, and 70	12 and 13
2	Eliminating the factor $1/b$ from equation (10/C), resulting in equations (12/3), (12/6), (12/9), (12/13), (12/16), and (12/19).	Relieves engineers of extra, but unnecessary, multiplications in the hand-calculation of these expressions	12	12
3	Eliminating the factor $1/k$ from equations (12/11) through (12/19), resulting in equations (14/11) through (14/19).	Relieves engineers of extra, but unnecessary, multiplications in the hand-calculation of these expressions	12	14

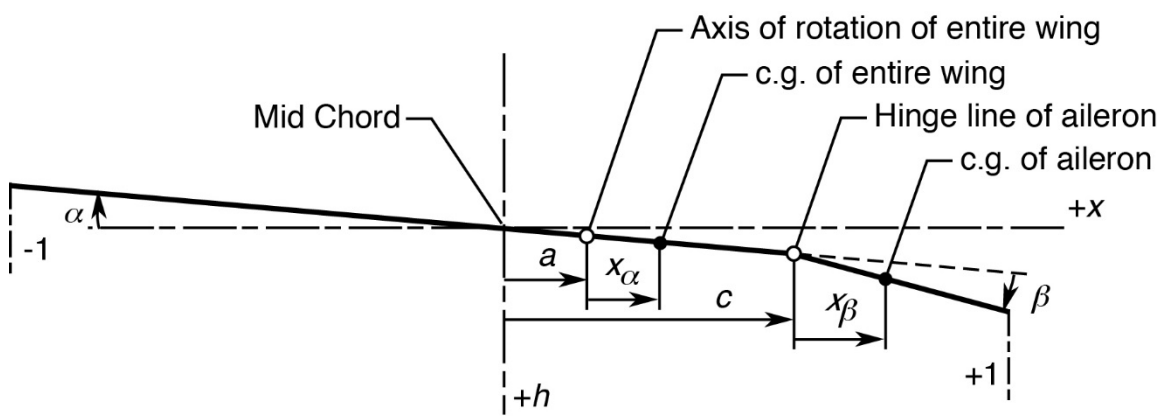


Figure 1. – Parameters of the airfoil-aileron combination

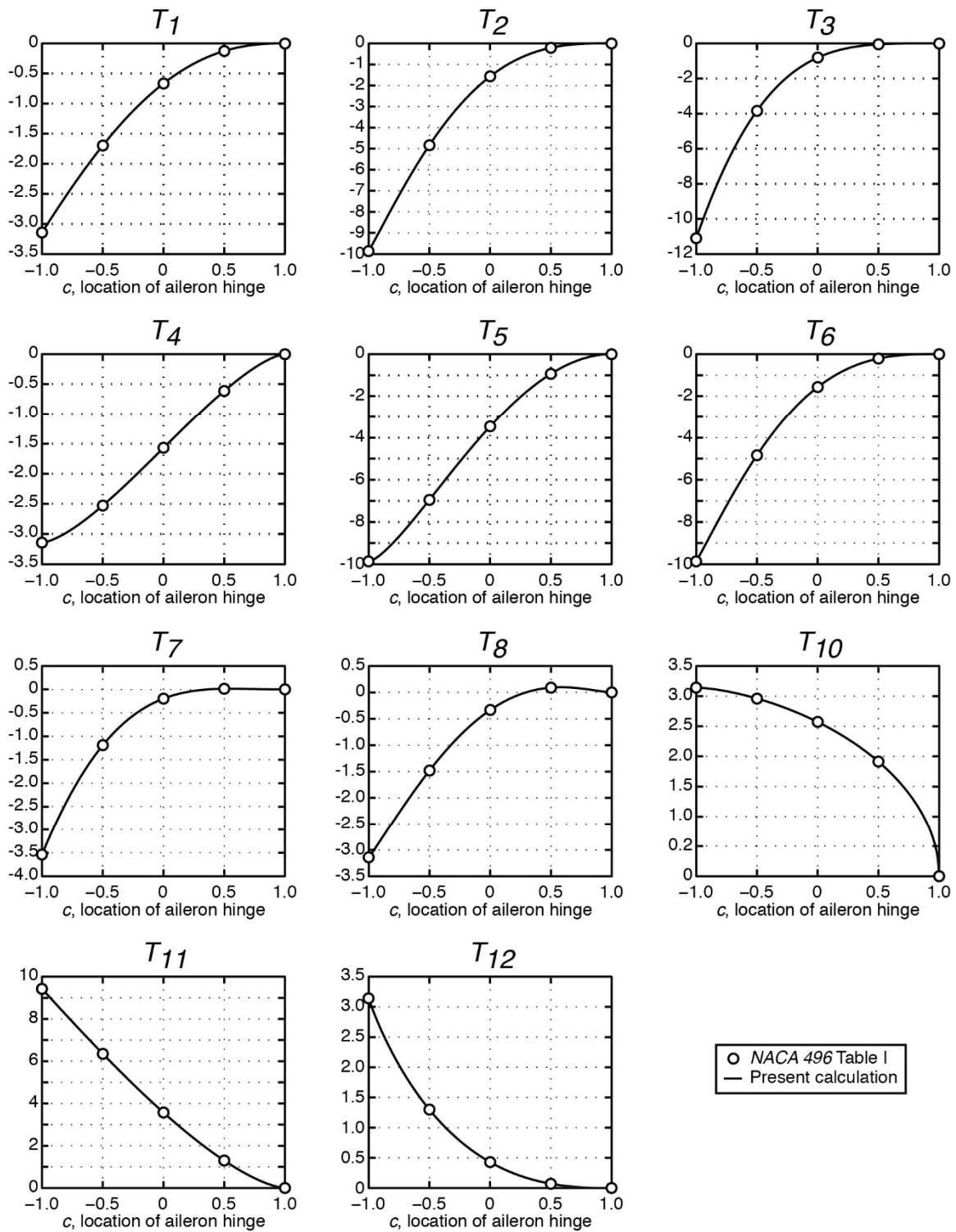


Figure 2. – Constants resulting from the integration of velocity potentials.

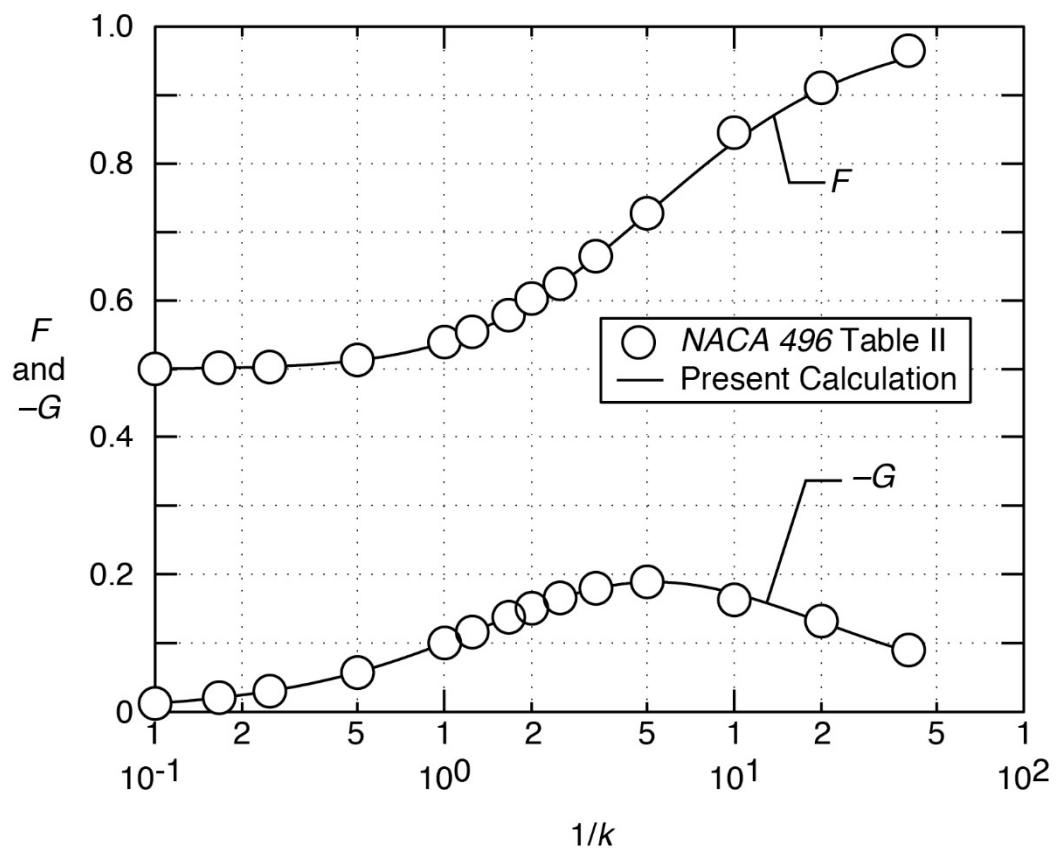
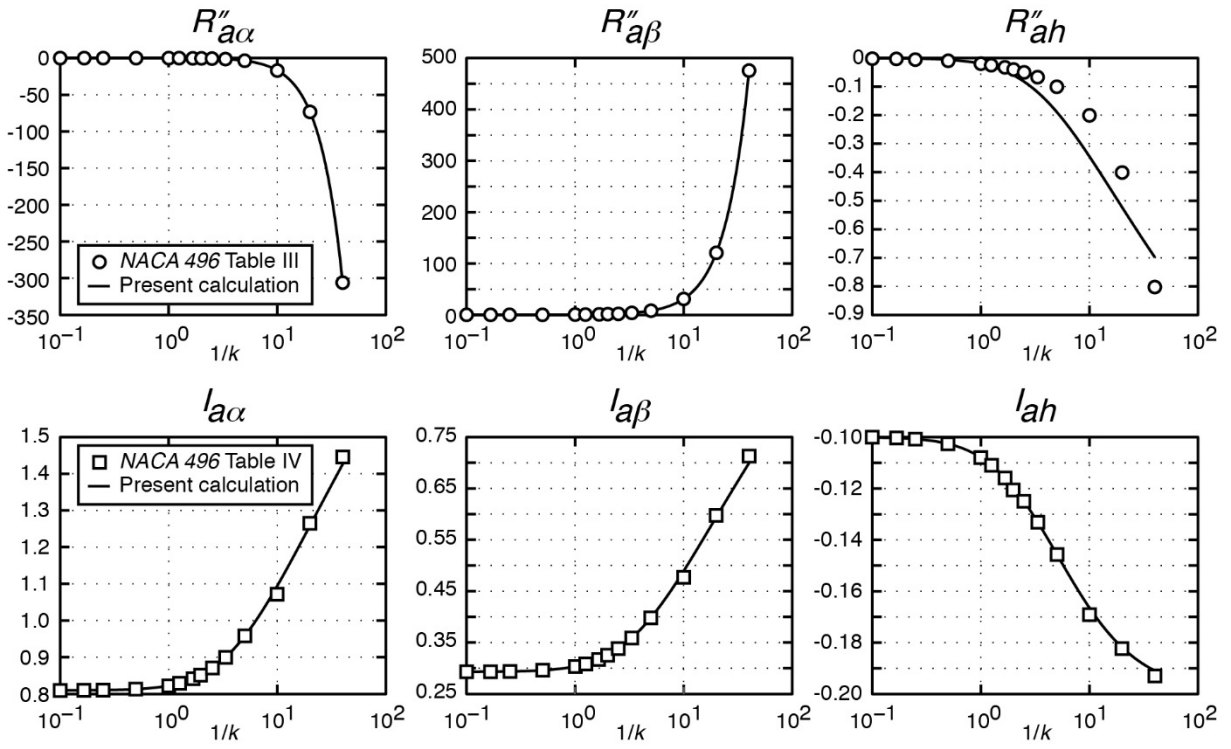
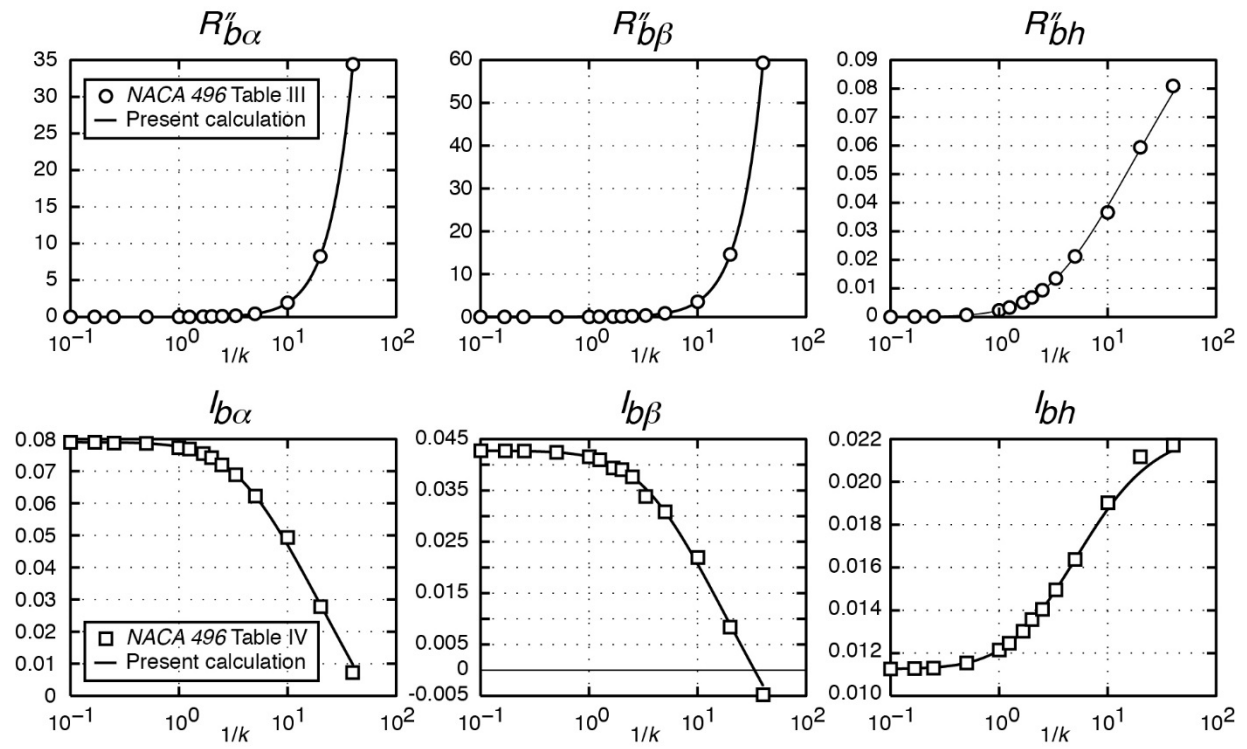


Figure 3. – Elements of the Theodorsen circulation function.



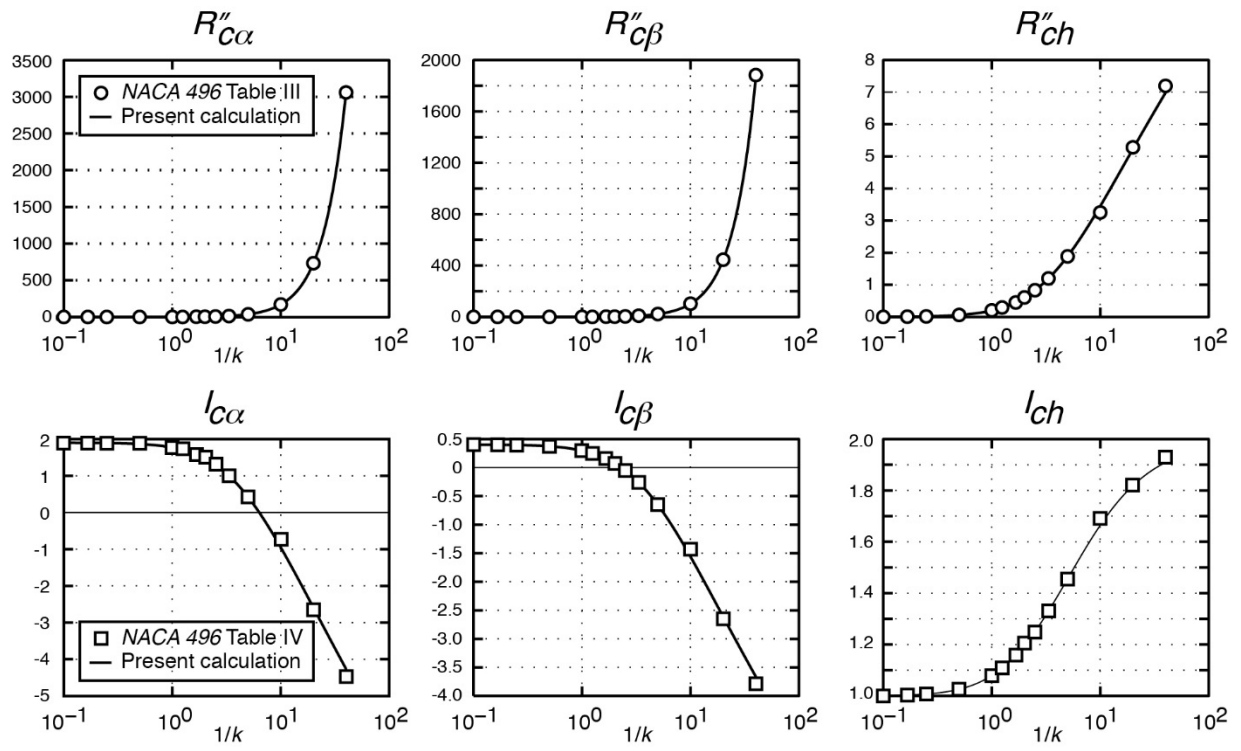
(a) Elements from pitching moment equation.

Figure 4. – Reduced-frequency-dependent portions of the elements of the equations of motion.



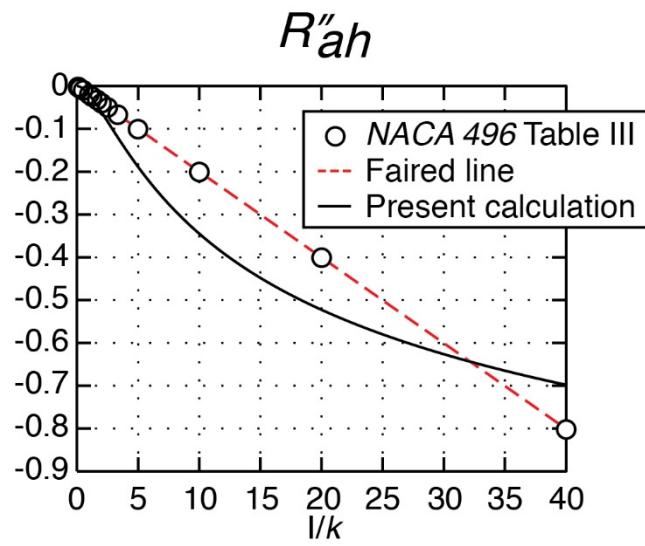
(b) Elements from hinge moment equation.

Figure 4. – Reduced-frequency-dependent portions of the elements of the equations of motion.



(c) Elements from vertical force equation.

Figure 4. – Reduced-frequency-dependent portions of the elements of the equations of motion.



(d) Element R''_{ah} re-drawn.

Figure 4. – Reduced-frequency-dependent portions of the elements of the equations of motion.

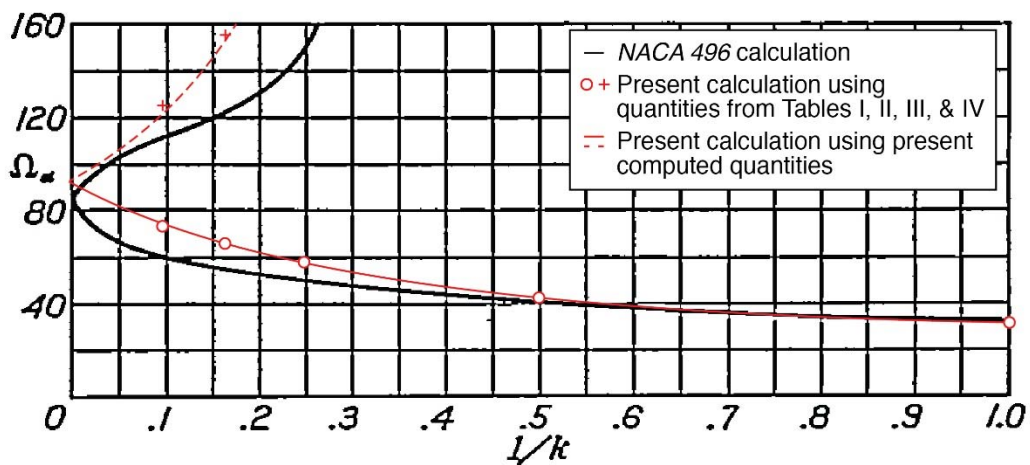


FIGURE 5. – Case 3, Torsion-aileron (α, β): Standard case. Showing Ω_α against $1/k$.

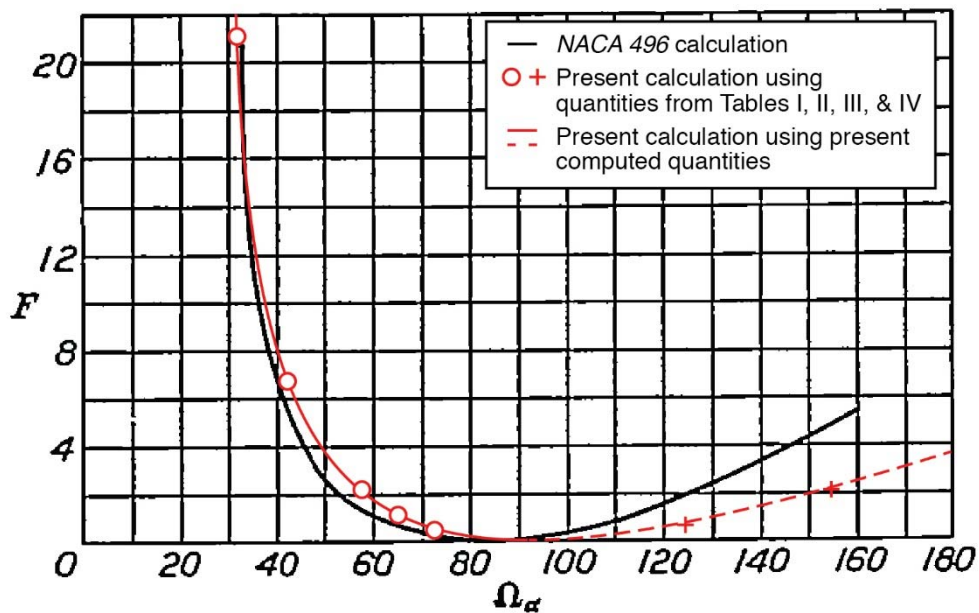


FIGURE 6. – Case 3, Torsion-aileron (α, β): Standard case. Showing flutter factor F against Ω_α .

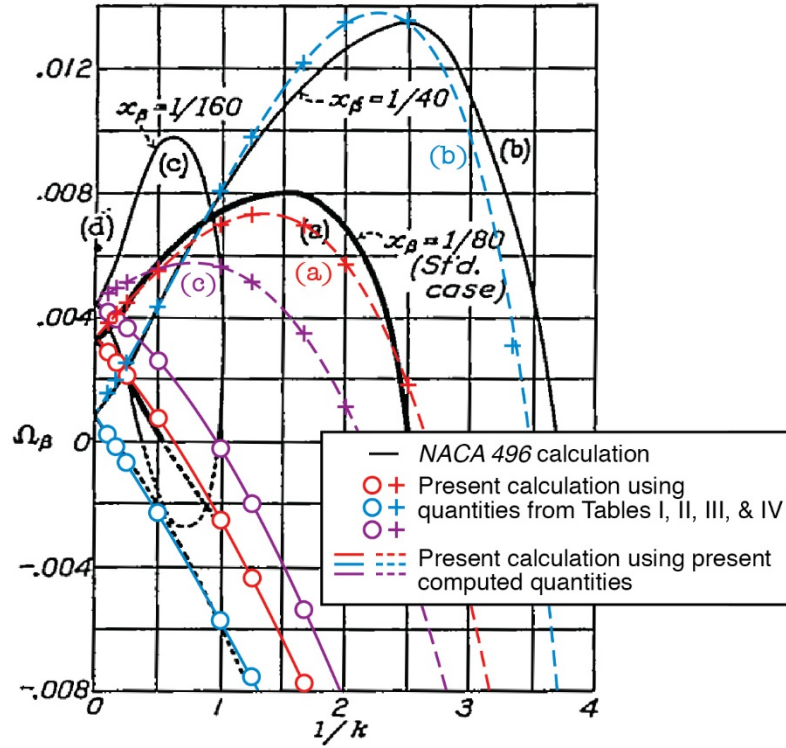


FIGURE 7. – Case 2, Aileron-deflection (β, h): (a) Standard case. (b), (c), (d) indicate dependency on x_β . Case (d), $x_\beta = -0.004$, reduces to a point.

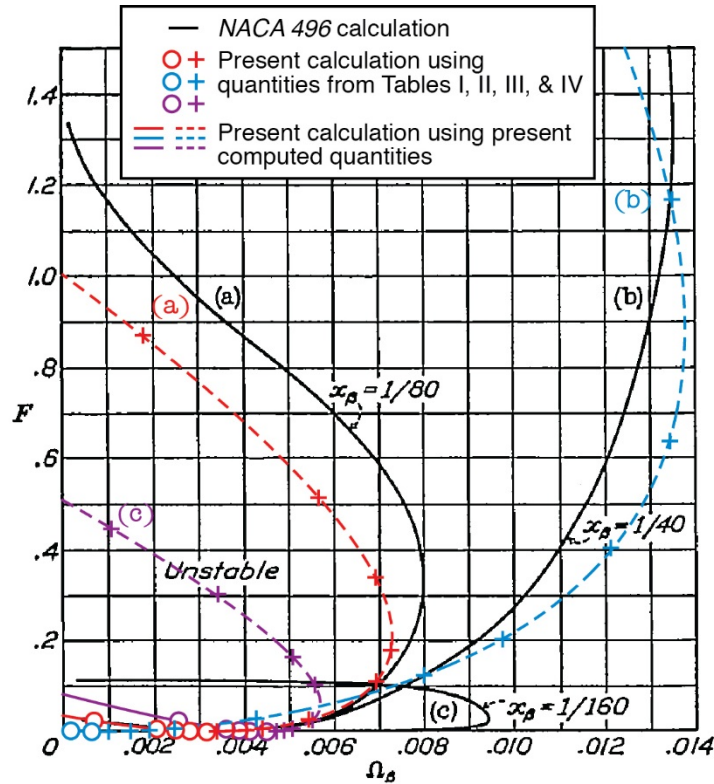


FIGURE 8. – Case 2, Aileron-deflection (β, h): Final curves giving flutter factor F against Ω_β corresponding to cases shown in figure 7.

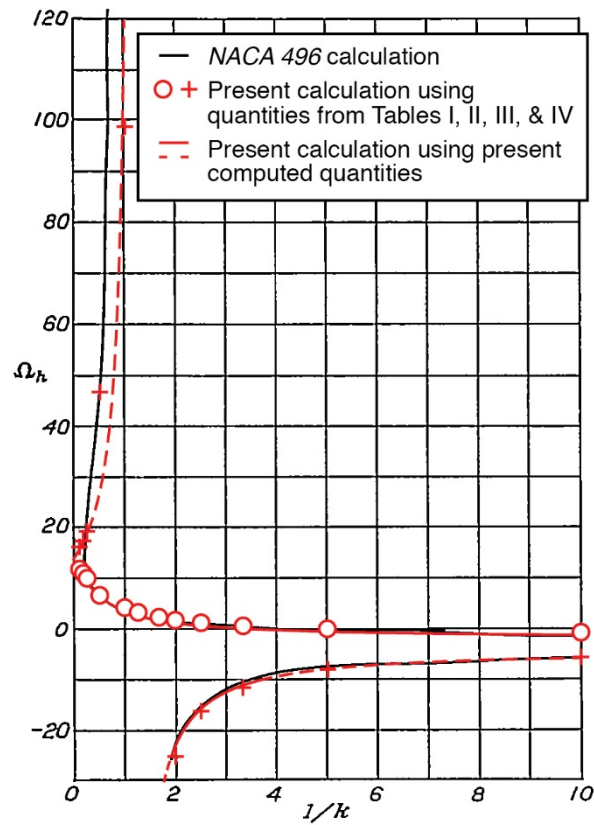


FIGURE 9. – Case 1, Flexure-torsion (h, α): Standard case. Showing Ω_h against $1/k$.

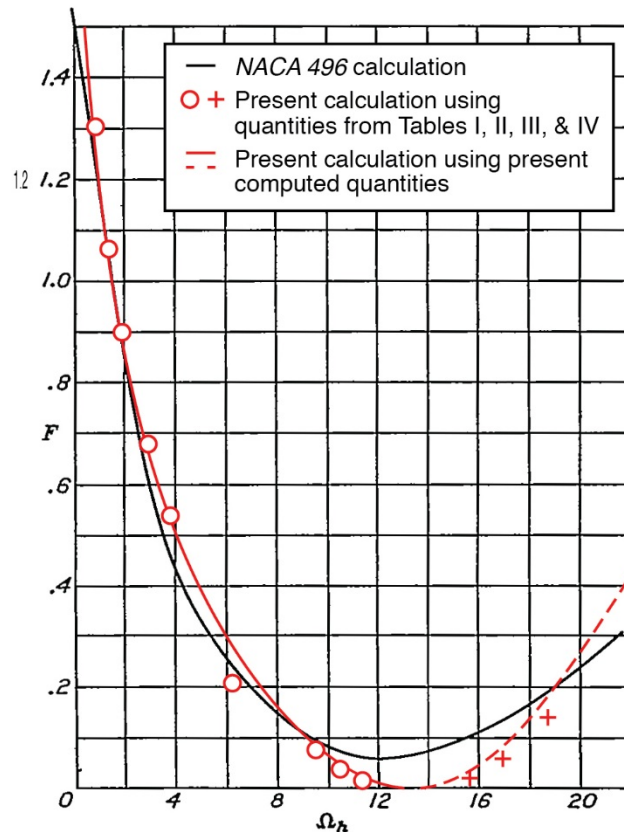


FIGURE 10. – Case 1, Flexure-torsion (h, α): Standard case. Showing flutter factor F against Ω_h .

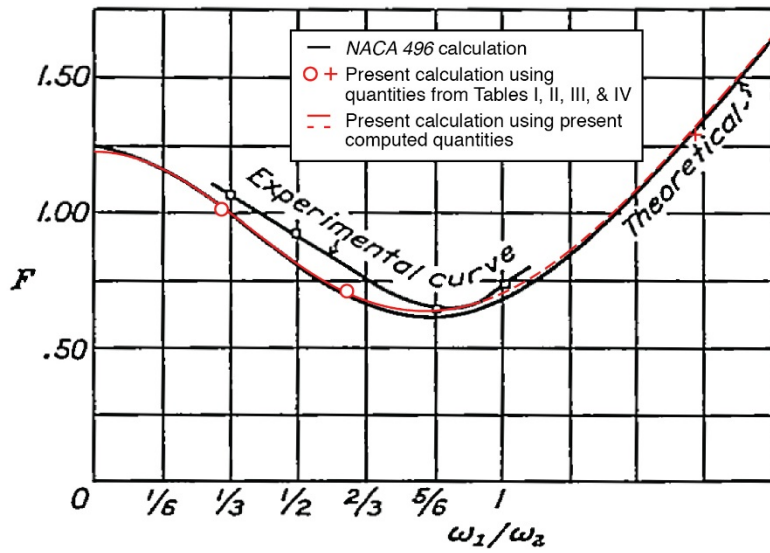


FIGURE 11. – Case 1, Flexure-torsion (h, α): Showing dependency of F on ω_1/ω_α . The upper curve is experimental. Airfoil with $r = 1/2$; $a = -0.4$; $x = 0.2$; $4\kappa = 0.01$; ω_1/ω_2 variable.

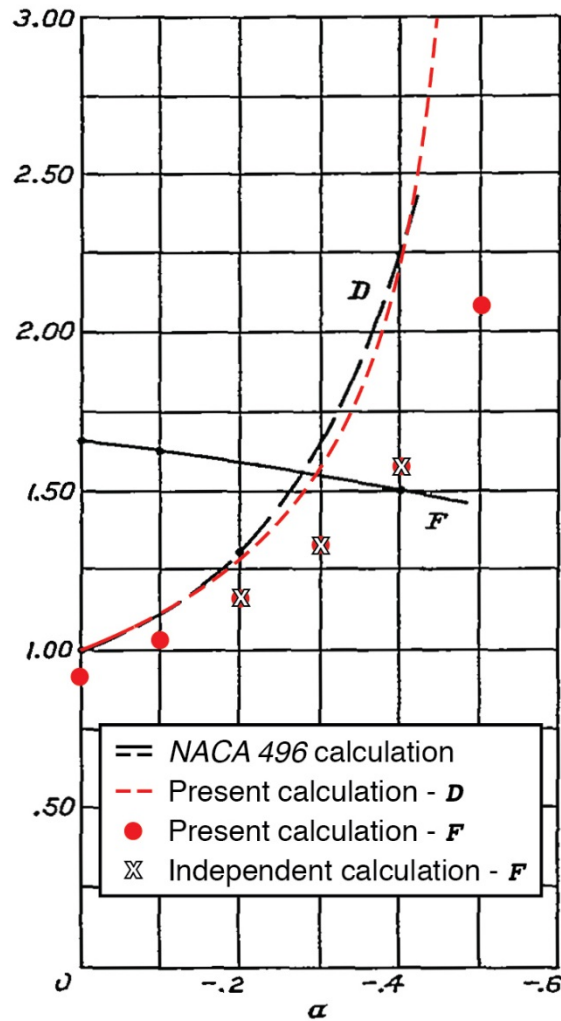


FIGURE 12. – Case 1, Flexure-torsion (h, α): Showing dependency of F on location of axis of rotation α . Airfoil with $r = 1/2$; $x = 0.2$; $\kappa = 1/4$; $\omega_1/\omega_2 = 1/6$; α variable.

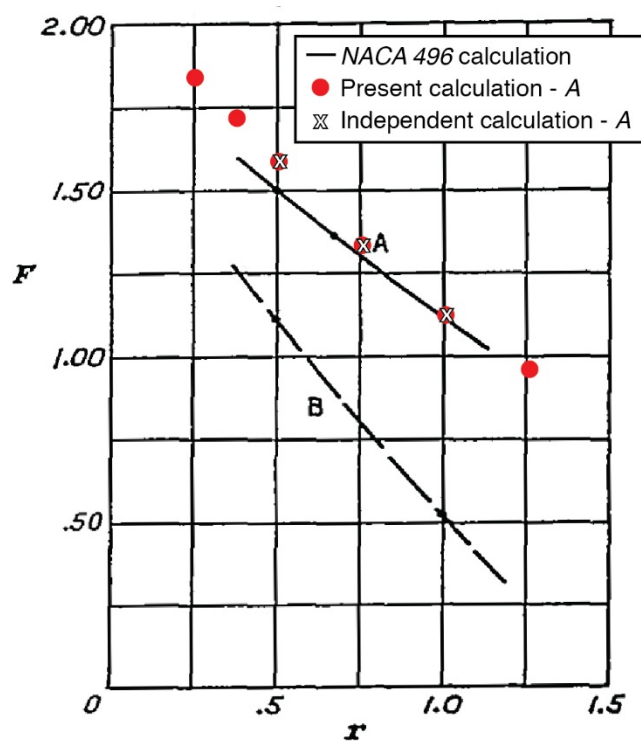


FIGURE 13. – Case 1, Flexure-torsion (h, α): Showing dependency of F on the radius of gyration $r_\alpha = r$.

A, airfoil with $a = -0.4$; $\kappa = \frac{1}{4}$; $x = 0.2$; $\omega_1/\omega_2 = \frac{1}{6}$; r variable.

B, airfoil with $a = -0.4$; $\kappa = \frac{1}{4}$; $x = 0.2$; $\omega_1/\omega_2 = 1.00$; r variable.

Figure 13A. – Curve A

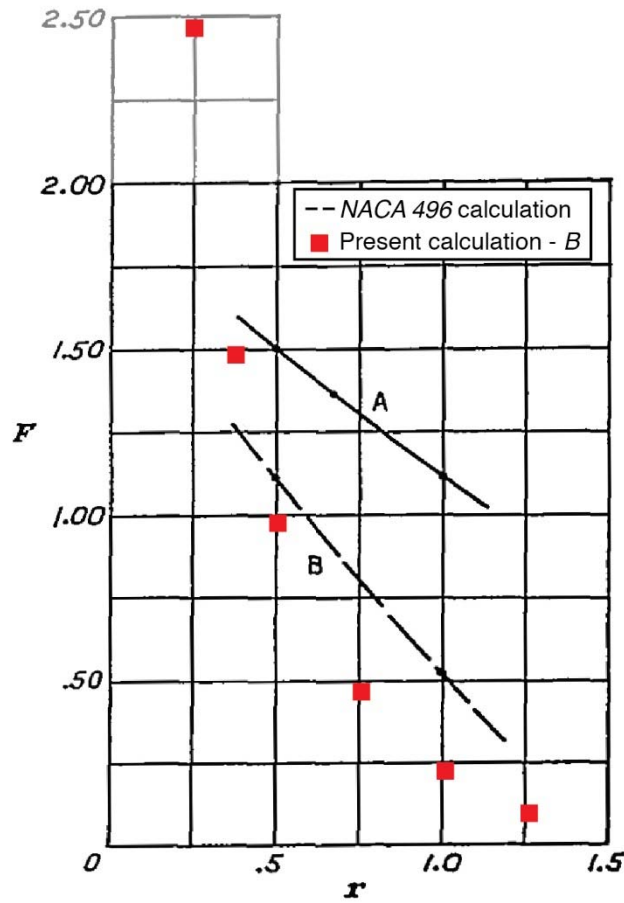


FIGURE 13. – Case 1, Flexure-torsion (h, α): Showing dependency of F on the radius of gyration $r_\alpha = r$.

A, airfoil with $a = -0.4$; $\kappa = \frac{1}{4}$; $x = 0.2$; $\omega_1/\omega_2 = \frac{1}{6}$; r variable.

B, airfoil with $a = -0.4$; $\kappa = \frac{1}{4}$; $x = 0.2$; $\omega_1/\omega_2 = 1.00$; r variable.

(a) Comparison of present calculation and Curve B of *NACA 496*

Figure 13B. – Curve B

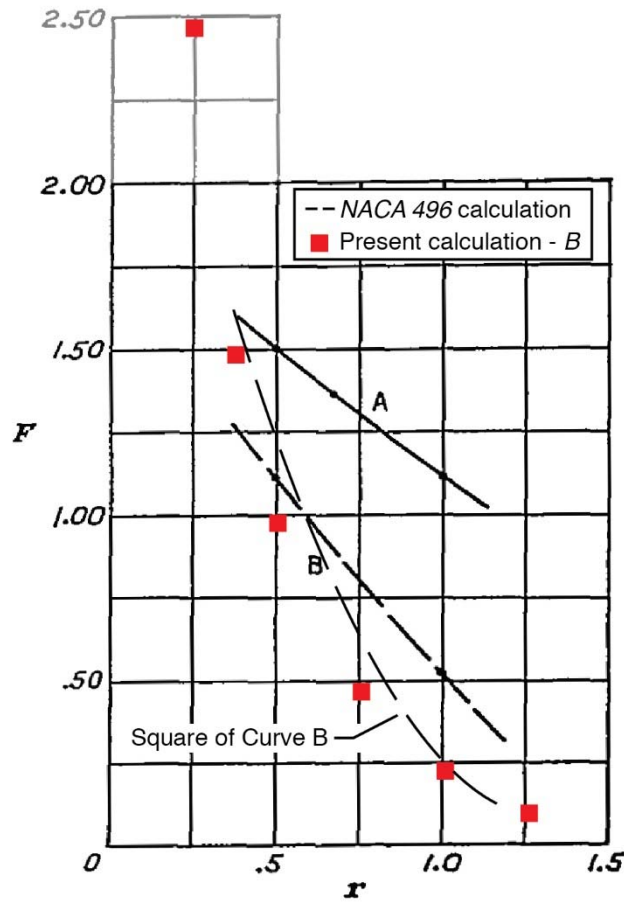


FIGURE 13. – Case 1, Flexure-torsion (h, α): Showing dependency of F on the radius of gyration $r_\alpha = r$.

A, airfoil with $a = -0.4$; $\kappa = \frac{1}{4}$; $x = 0.2$; $\omega_1/\omega_2 = \frac{1}{6}$; r variable.

B, airfoil with $a = -0.4$; $\kappa = \frac{1}{4}$; $x = 0.2$; $\omega_1/\omega_2 = 1.00$; r variable.

(b) Comparison of present calculation and square of Curve B of NACA 496

Figure 13B. – Curve B

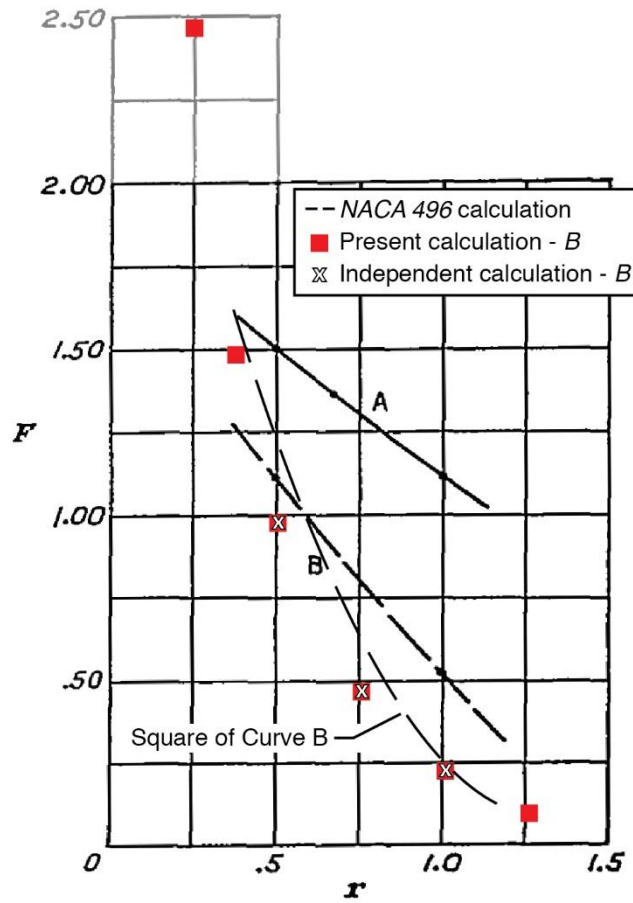


FIGURE 13. – Case 1, Flexure-torsion (h, α): Showing dependency of F on the radius of gyration $r_\alpha = r$.

A, airfoil with $a = -0.4$; $\kappa = \frac{1}{4}$; $x = 0.2$; $\omega_1/\omega_2 = \frac{1}{6}$; r variable.

B, airfoil with $a = -0.4$; $\kappa = \frac{1}{4}$; $x = 0.2$; $\omega_1/\omega_2 = 1.00$; r variable.

(c) Comparison of present calculation, independent calculation, and square of Curve B of NACA 496

Figure 13B. – Curve B

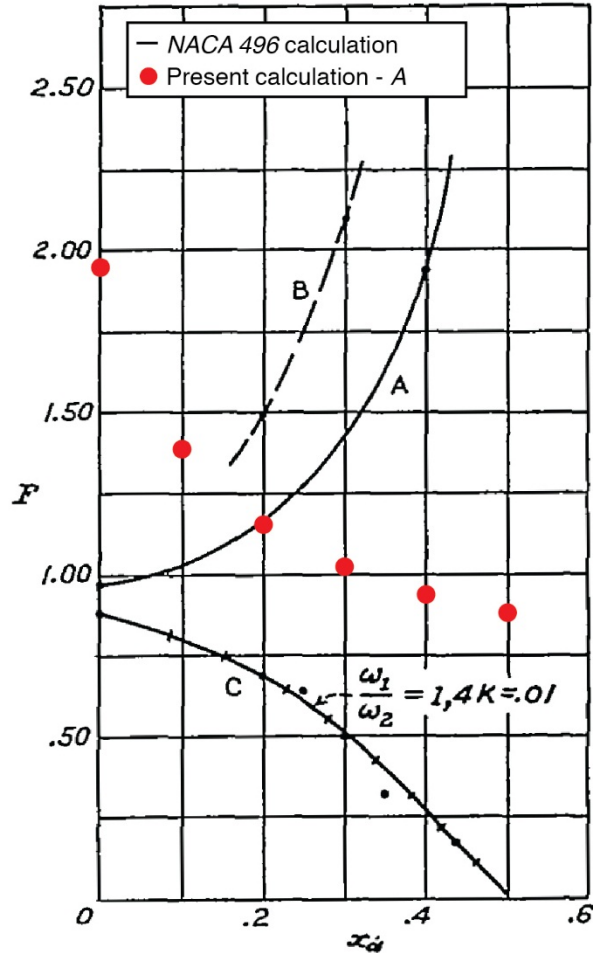


FIGURE 14. – Case 1, Flexure-torsion (h, α): Showing dependency of F on x_α , the location of the center of gravity.

A, airfoil with $r = 1/2$; $a = -0.4$; $\kappa = 1/400$; $\omega_1/\omega_2 = 1/6$; x variable.

B, airfoil with $r = 1/2$; $a = -0.4$; $\kappa = 1/4$; $\omega_1/\omega_2 = 1/6$; x variable.

C, airfoil with $r = 1/2$; $a = -0.4$; $\kappa = 1/100$; $\omega_1/\omega_2 = 1$; x variable.

(a) Comparison of present calculation and Curve A of NACA 496

Figure 14A. – Curve A

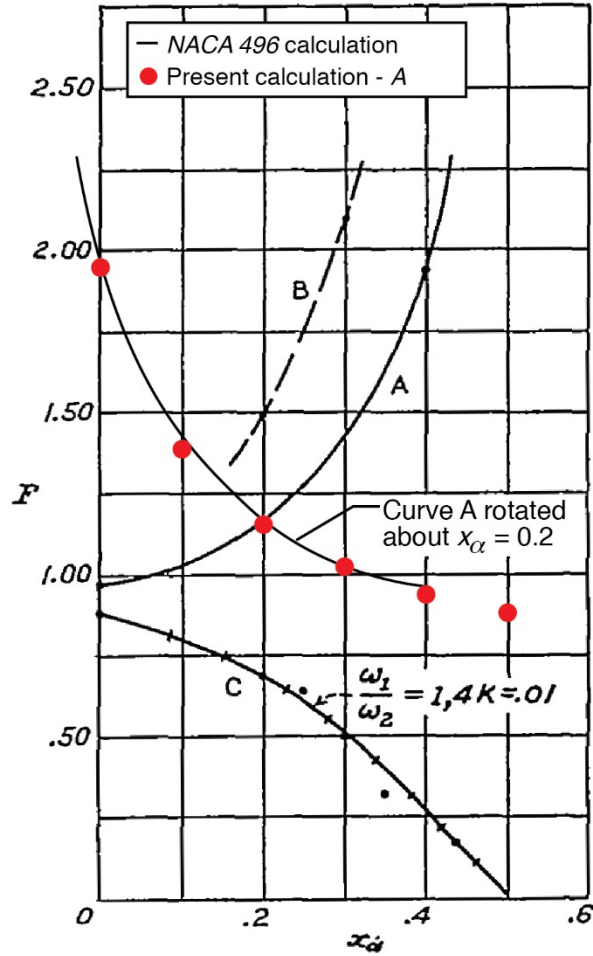


FIGURE 14. – Case 1, Flexure-torsion (h, α): Showing dependency of F on x_α , the location of the center of gravity.

A, airfoil with $r = 1/2$; $a = -0.4$; $\kappa = 1/400$; $\omega_1/\omega_2 = 1/6$; x variable.

B, airfoil with $r = 1/2$; $a = -0.4$; $\kappa = 1/4$; $\omega_1/\omega_2 = 1/6$; x variable.

C, airfoil with $r = 1/2$; $a = -0.4$; $\kappa = 1/100$; $\omega_1/\omega_2 = 1$; x variable.

(b) Comparison of present calculation and rotated Curve A of NACA 496

Figure 14A. – Curve A

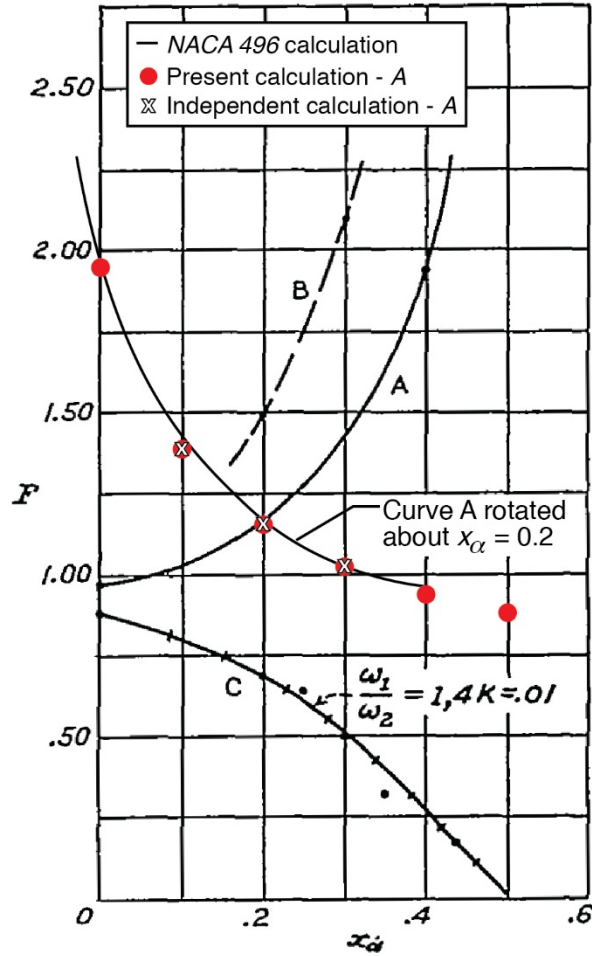


FIGURE 14. – Case 1, Flexure-torsion (h, α): Showing dependency of F on x_α , the location of the center of gravity.

A, airfoil with $r = 1/2$; $a = -0.4$; $\kappa = 1/400$; $\omega_1/\omega_2 = 1/6$; x variable.

B, airfoil with $r = 1/2$; $a = -0.4$; $\kappa = 1/4$; $\omega_1/\omega_2 = 1/6$; x variable.

C, airfoil with $r = 1/2$; $a = -0.4$; $\kappa = 1/100$; $\omega_1/\omega_2 = 1$; x variable.

(c) Comparison of present calculation, independent calculation, and rotated Curve A of NACA 496

Figure 14A. – Curve A

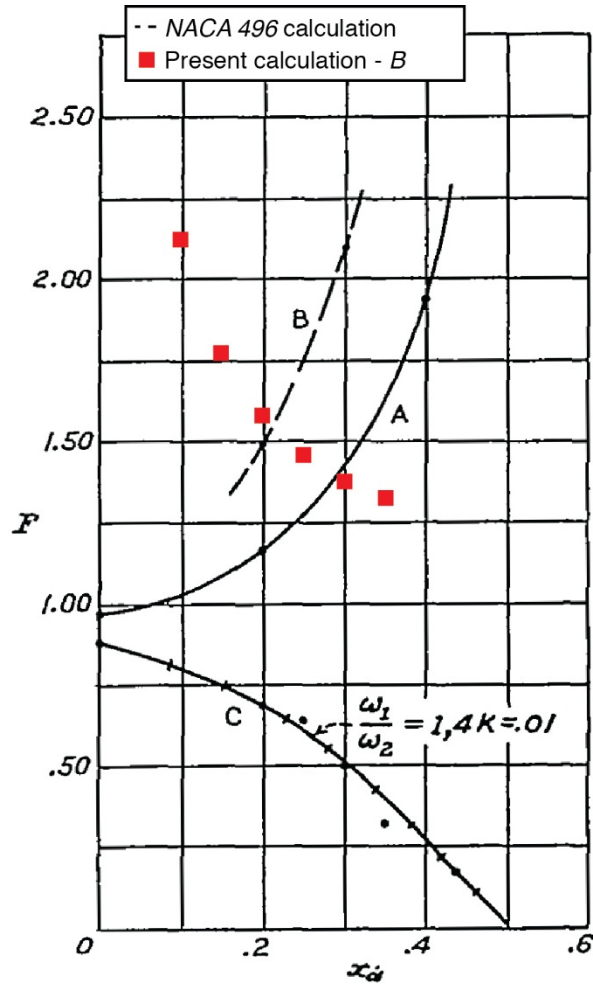


FIGURE 14. – Case 1, Flexure-torsion (h, α): Showing dependency of F on x_α , the location of the center of gravity.

A, airfoil with $r = 1/2$; $a = -0.4$; $\kappa = 1/400$; $\omega_1/\omega_2 = 1/6$; x variable.

B, airfoil with $r = 1/2$; $a = -0.4$; $\kappa = 1/4$; $\omega_1/\omega_2 = 1/6$; x variable.

C, airfoil with $r = 1/2$; $a = -0.4$; $\kappa = 1/100$; $\omega_1/\omega_2 = 1$; x variable.

(a) Comparison of present calculation and Curve B of NACA 496

Figure 14B. – Curve B

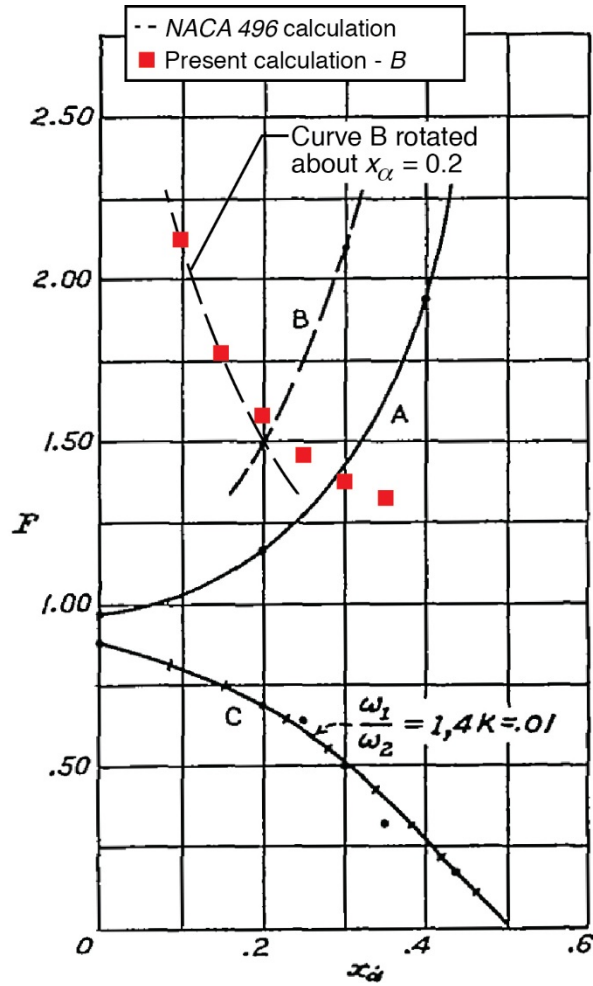


FIGURE 14. – Case 1, Flexure-torsion (h, α): Showing dependency of F on x_α , the location of the center of gravity.

A, airfoil with $r = 1/2$; $a = -0.4$; $\kappa = 1/400$; $\omega_1/\omega_2 = 1/6$; x variable.

B, airfoil with $r = 1/2$; $a = -0.4$; $\kappa = 1/4$; $\omega_1/\omega_2 = 1/6$; x variable.

C, airfoil with $r = 1/2$; $a = -0.4$; $\kappa = 1/100$; $\omega_1/\omega_2 = 1$; x variable.

(b) Comparison of present calculation and rotated Curve B of NACA 496

Figure 14B. – Curve B

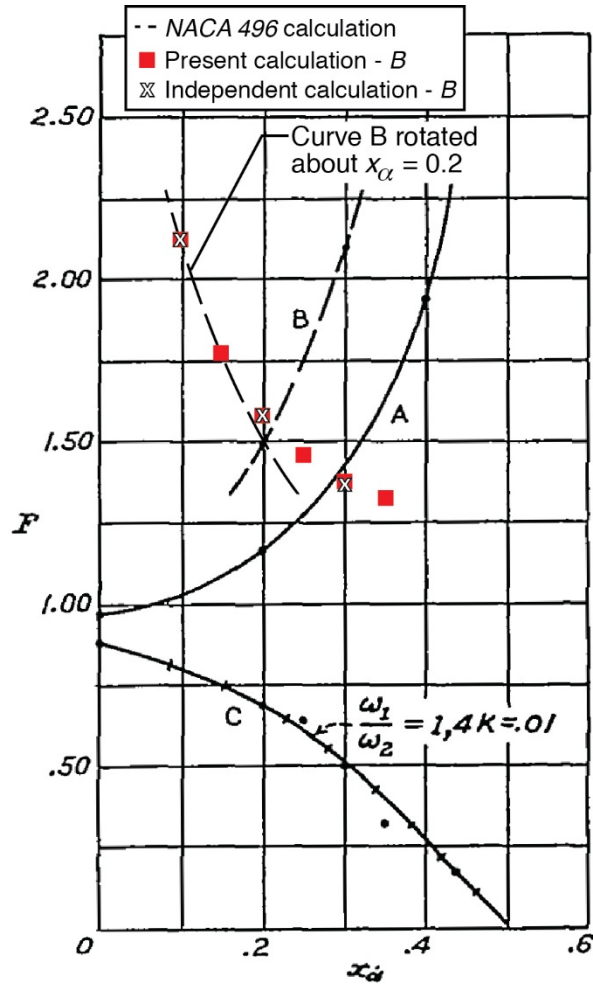


FIGURE 14. – Case 1, Flexure-torsion (h, α): Showing dependency of F on x_α , the location of the center of gravity.

A, airfoil with $r = 1/2$; $a = -0.4$; $\kappa = 1/400$; $\omega_1/\omega_2 = 1/6$; x variable.

B, airfoil with $r = 1/2$; $a = -0.4$; $\kappa = 1/4$; $\omega_1/\omega_2 = 1/6$; x variable.

C, airfoil with $r = 1/2$; $a = -0.4$; $\kappa = 1/100$; $\omega_1/\omega_2 = 1$; x variable.

(c) Comparison of present calculation, independent calculation, and rotated Curve B of NACA 496

Figure 14B. – Curve B

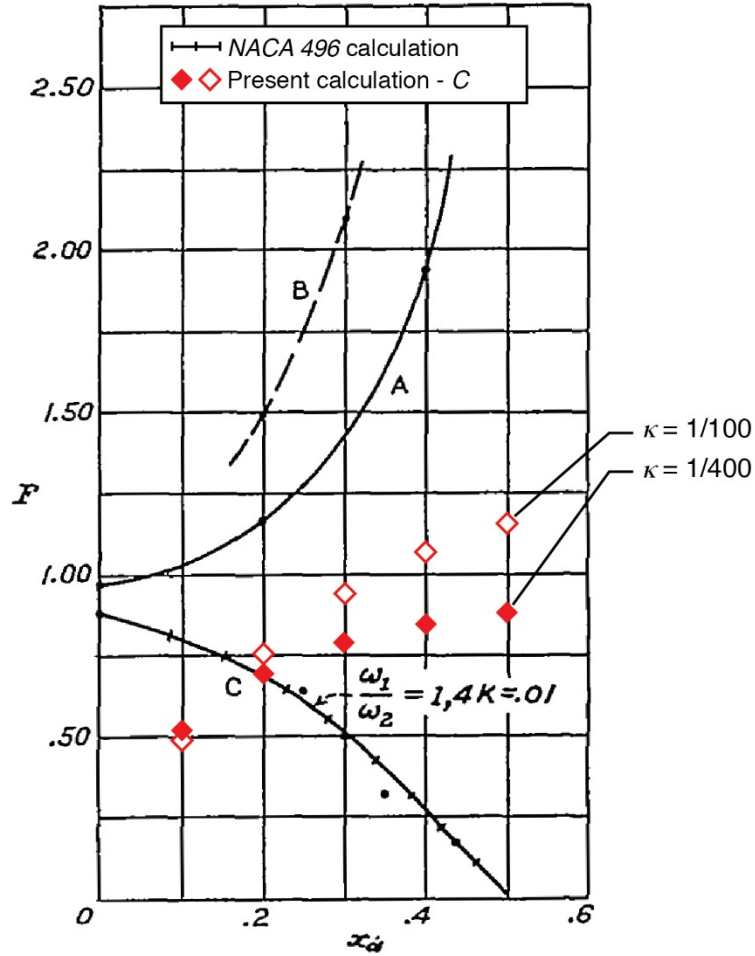


FIGURE 14. – Case 1, Flexure-torsion (h, α): Showing dependency of F on x_α , the location of the center of gravity.

A, airfoil with $r = 1/2$; $a = -0.4$; $\kappa = 1/400$; $\omega_1/\omega_2 = 1/6$; x variable.

B, airfoil with $r = 1/2$; $a = -0.4$; $\kappa = 1/4$; $\omega_1/\omega_2 = 1/6$; x variable.

C, airfoil with $r = 1/2$; $a = -0.4$; $\kappa = 1/100$; $\omega_1/\omega_2 = 1$; x variable.

(a) Comparison of present calculation and Curve C of NACA 496

Figure 14C. – Curve C

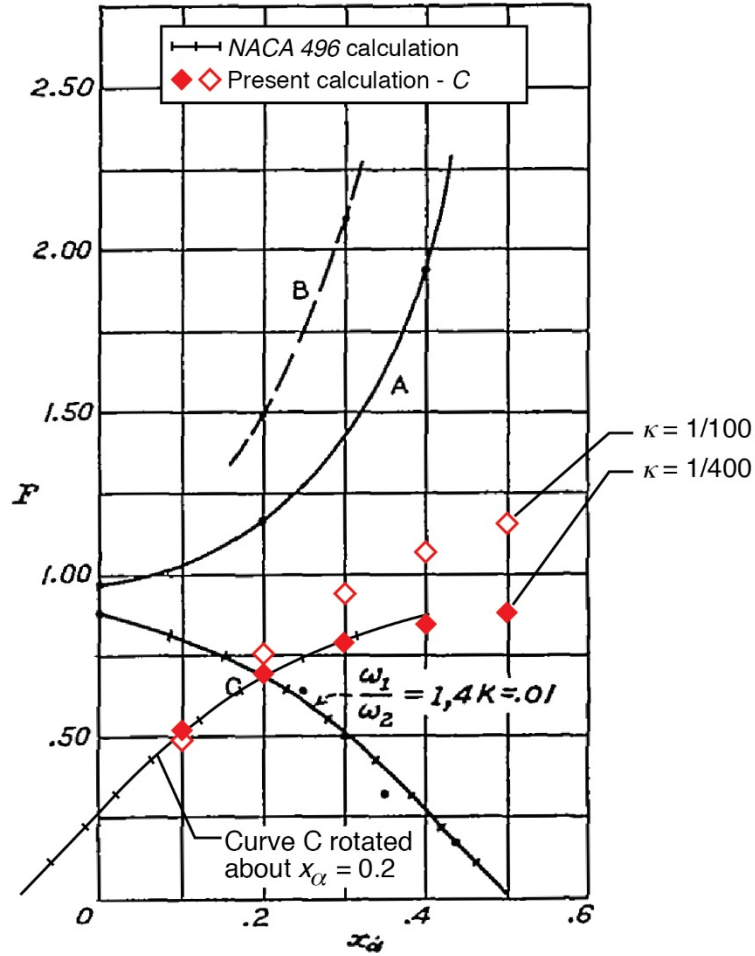


FIGURE 14. – Case 1, Flexure-torsion (h, α): Showing dependency of F on x_α , the location of the center of gravity.

A, airfoil with $r = 1/2$; $a = -0.4$; $\kappa = 1/400$; $\omega_1/\omega_2 = 1/6$; x variable.

B, airfoil with $r = 1/2$; $a = -0.4$; $\kappa = 1/4$; $\omega_1/\omega_2 = 1/6$; x variable.

C, airfoil with $r = 1/2$; $a = -0.4$; $\kappa = 1/100$; $\omega_1/\omega_2 = 1$; x variable.

(b) Comparison of present calculation and rotated Curve C of NACA 496

Figure 14C. – Curve C

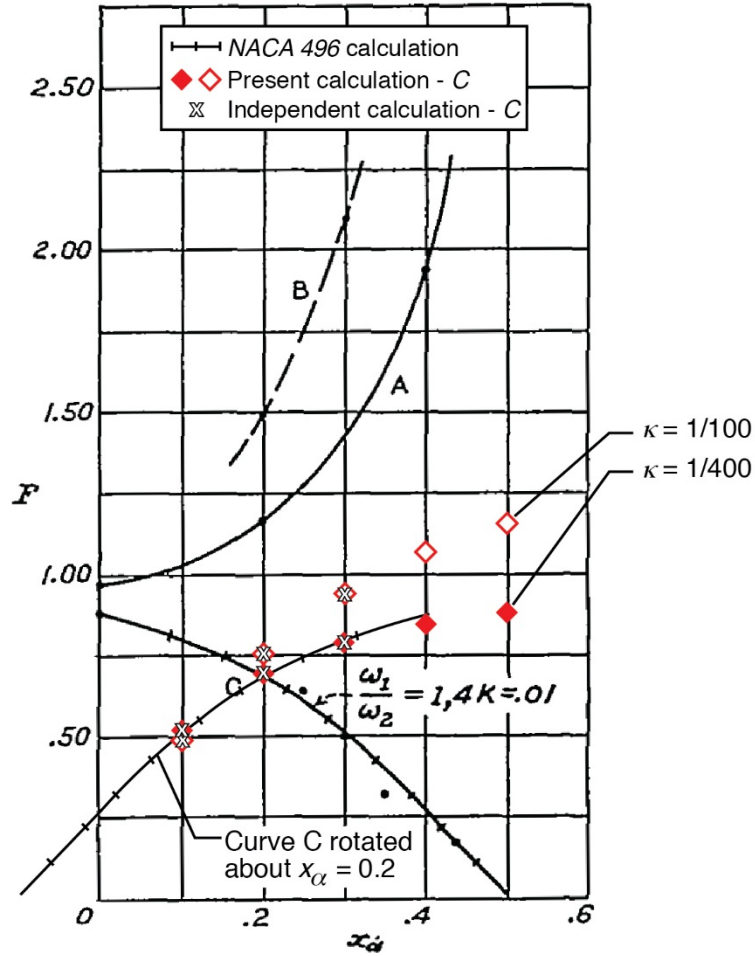


FIGURE 14. – Case 1, Flexure-torsion (h, α): Showing dependency of F on x_α , the location of the center of gravity.

A, airfoil with $r = 1/2$; $a = -0.4$; $\kappa = 1/400$; $\omega_1/\omega_2 = 1/6$; x variable.

B, airfoil with $r = 1/2$; $a = -0.4$; $\kappa = 1/4$; $\omega_1/\omega_2 = 1/6$; x variable.

C, airfoil with $r = 1/2$; $a = -0.4$; $\kappa = 1/100$; $\omega_1/\omega_2 = 1$; x variable.

(c) Comparison of present calculation, independent calculation, and rotated Curve C of NACA 496

Figure 14C. – Curve C

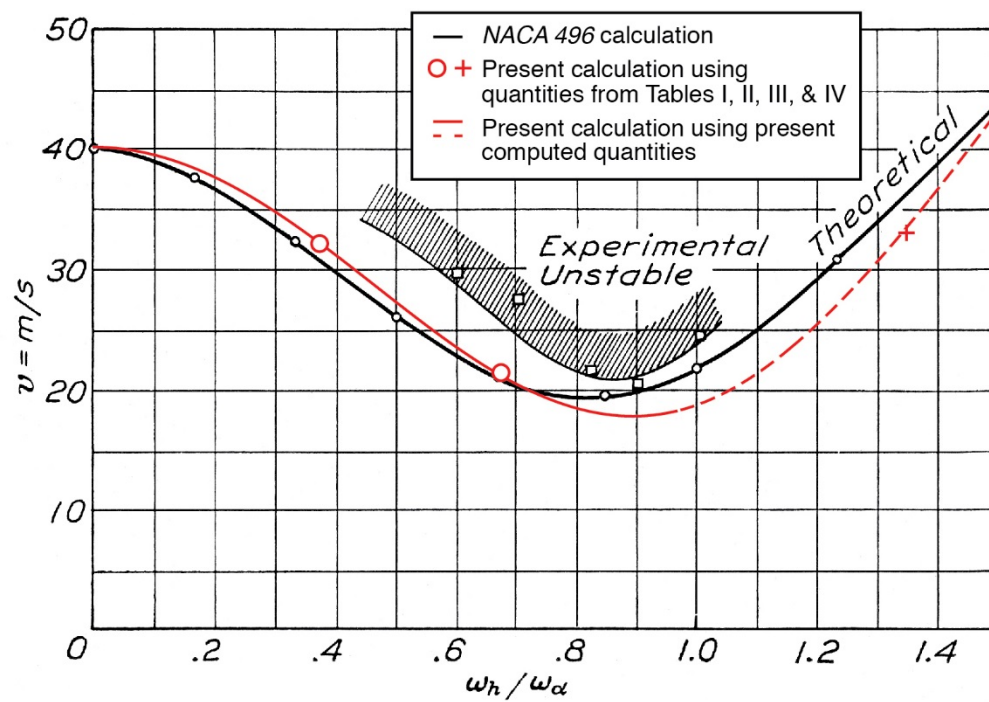


FIGURE 15. – Case 1. Wing A. Theoretical and experimental curves giving flutter velocity v against frequency ratio ω_h / ω_α . Deflection-torsion.

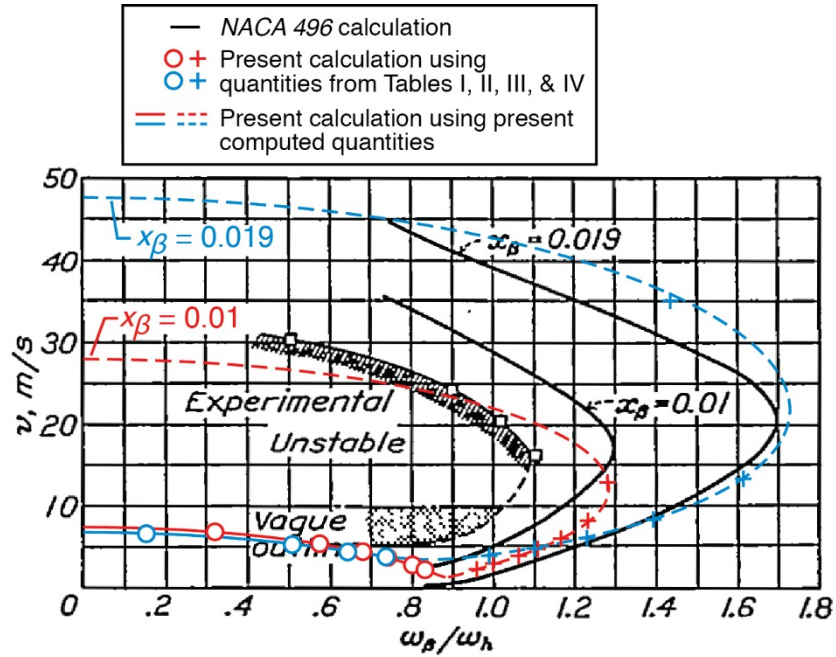


FIGURE 16. – Case 2. Wing B. Theoretical and experimental curves giving flutter velocity v against frequency ratio ω_β/ω_h . Aileron-deflection (βh).

-- with assumed value of $\omega_h = 5.8 \times 2\pi$ --

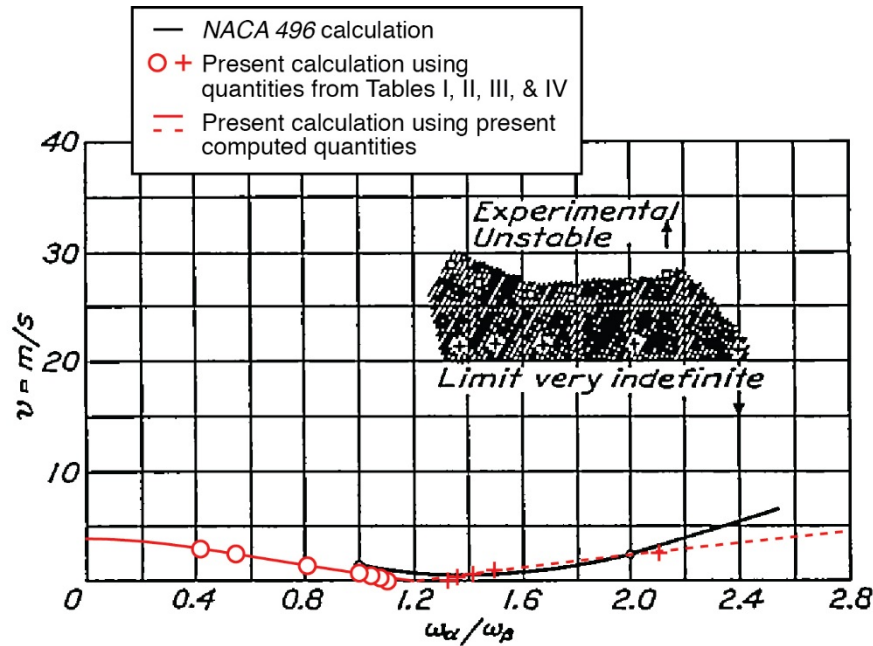


FIGURE 17. – Case 3. Theoretical curve giving flutter velocity against the frequency ratio $\omega_\alpha/\omega_\beta$. The experimental unstable are is indefinite due to the importance of internal friction at very small velocities. Torsion-aileron (α, β).

-- with assumed value of $\omega_\beta = 4.4 \times 2\pi$ --

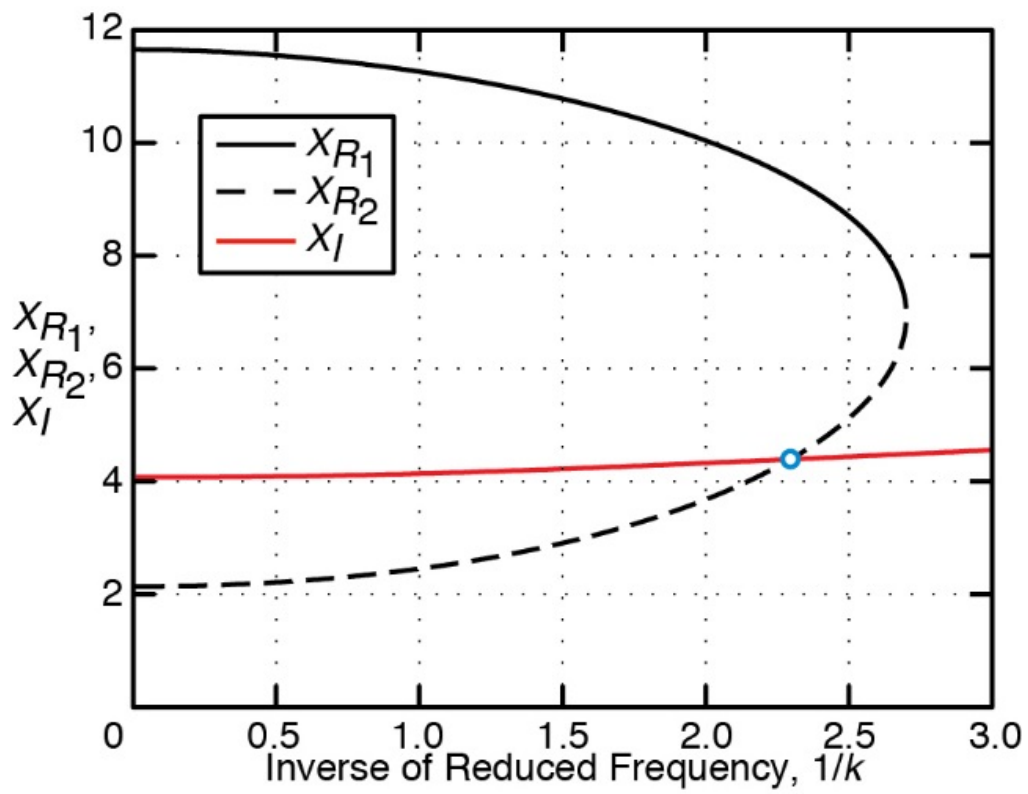


Figure C1 – Illustrative example for Alternate Solution Method No. 1.

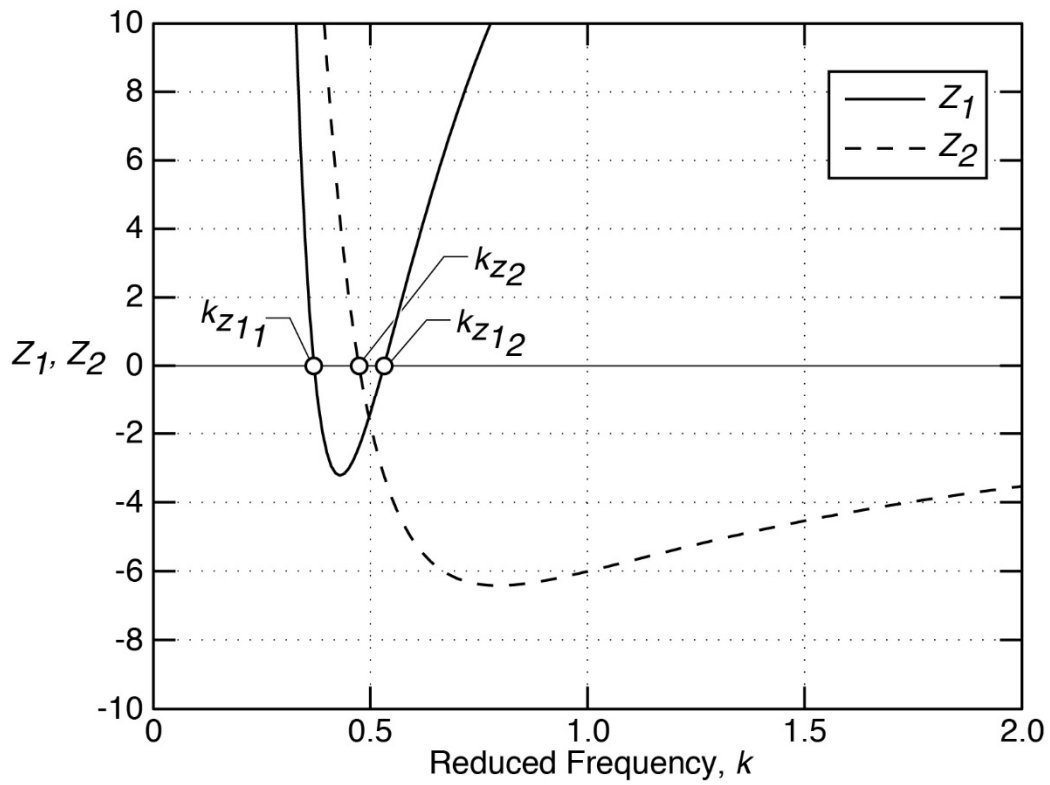


Figure C2 – Illustrative example for Alternate Solution Method No. 2
– Z_1 and Z_2 as functions of reduced frequency at a velocity of 160 fps.

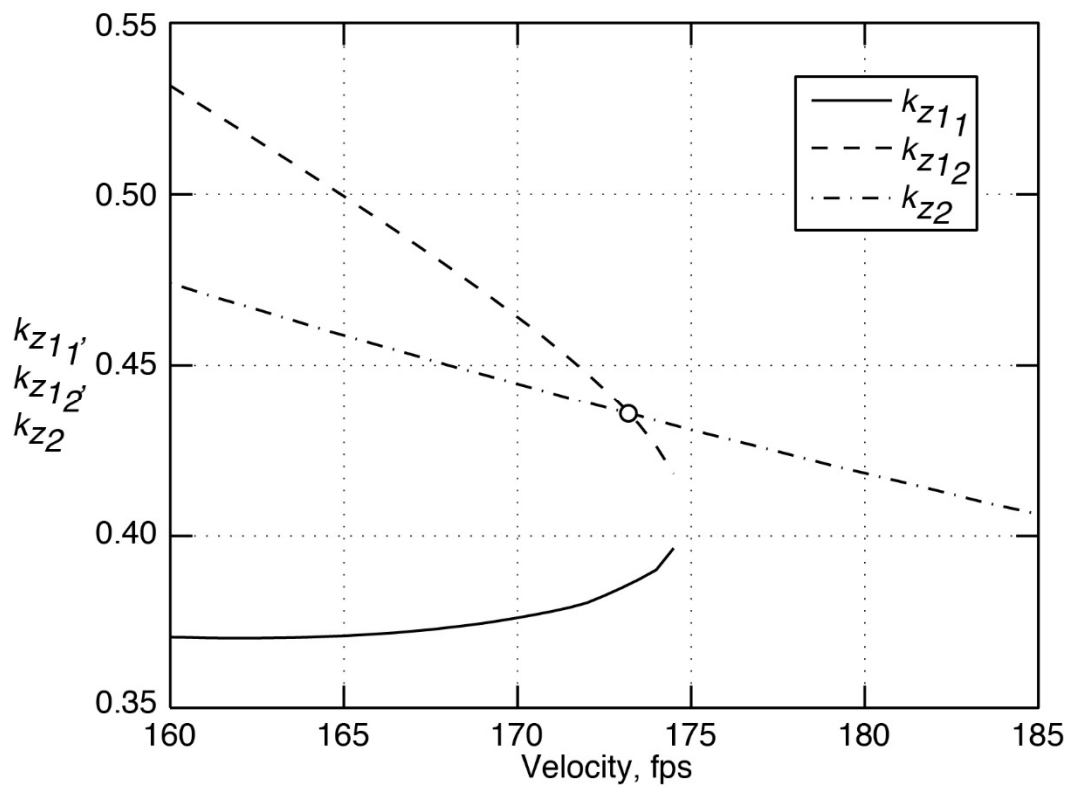


Figure C3 – Illustrative example for Alternate Solution Method No. 2
– Reduced frequencies as a function of velocity.

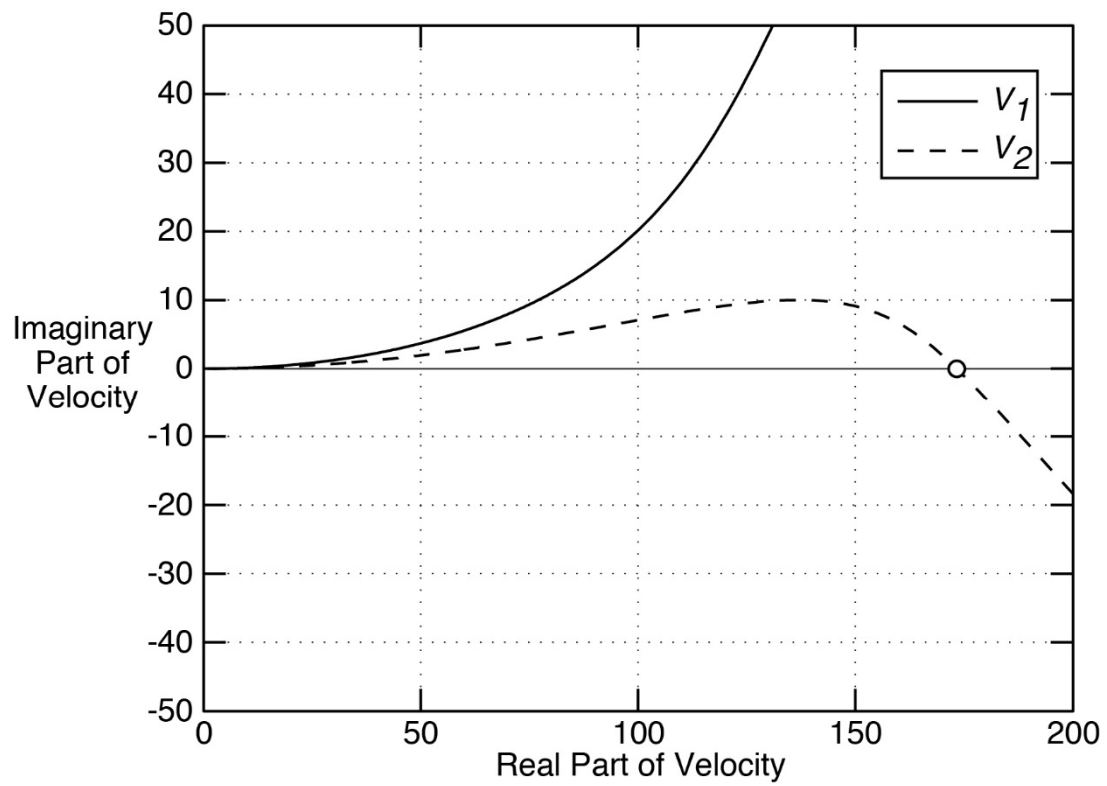


Figure C4 – Illustrative example for Alternate Solution Method No. 3.

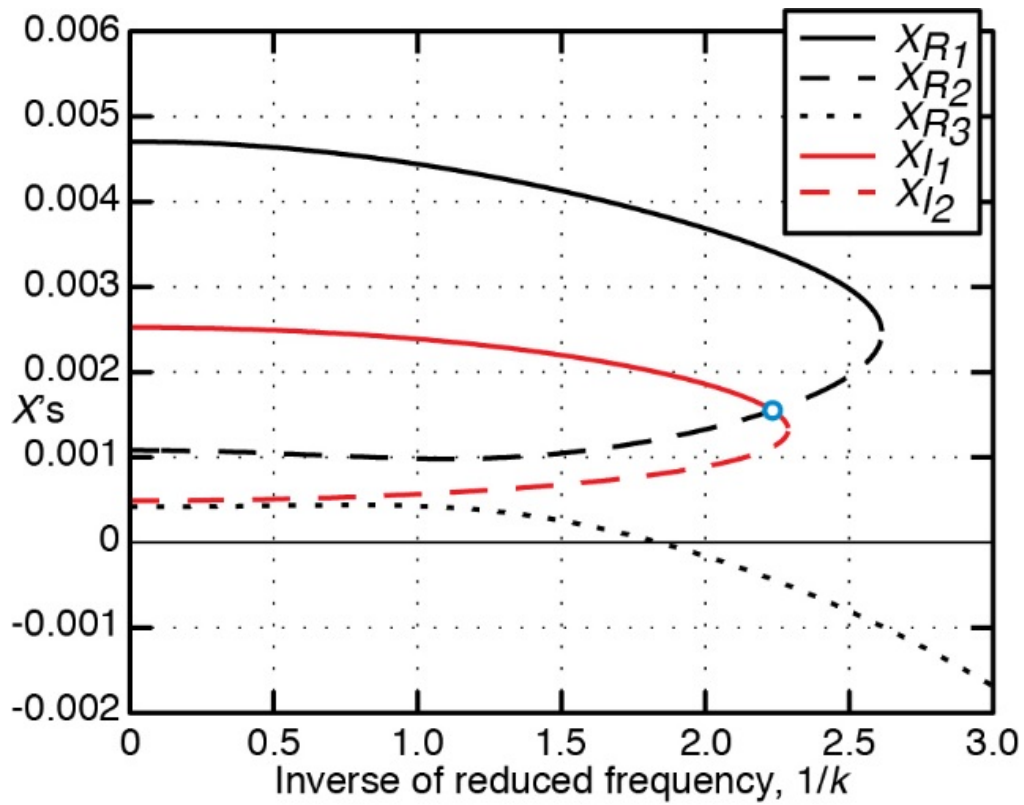
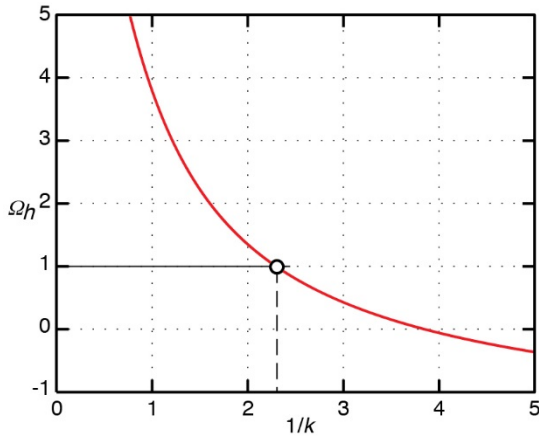
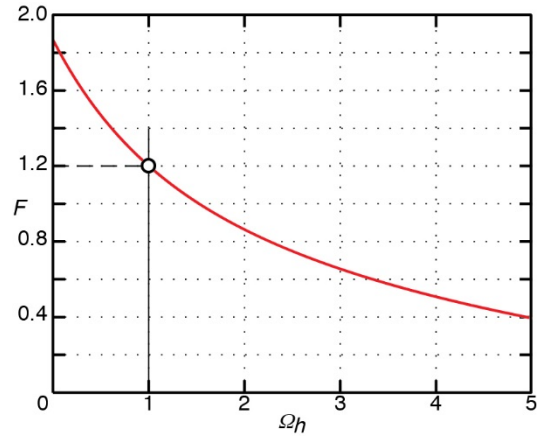


Figure D1 – Illustrative example for Three-Degree-of-Freedom Solution Method; “standard case” quantities chosen, with $\omega_\alpha = 100$, $\omega_\beta = 125$, $\omega_h = 50$.



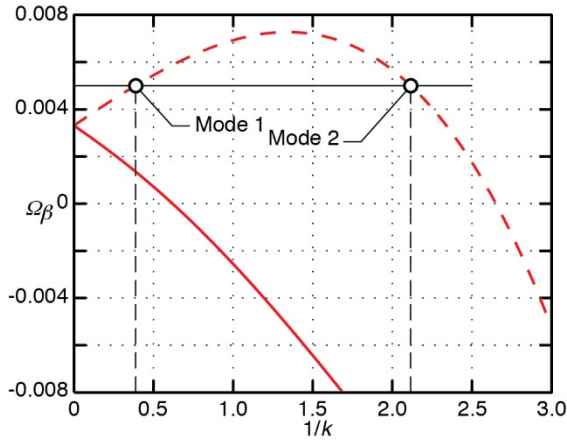
(a) Recreation of Figure 9



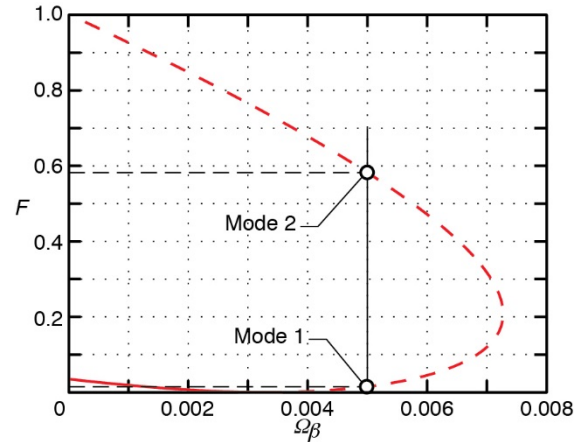
(b) Recreation of Figure 10

Figure D2 – Results from 2DOF Solution Method, Subcase 1;

$$\omega_\alpha = 100, \omega_h = 50, r_\alpha^2 = 0.25, \Omega_h = 1.$$



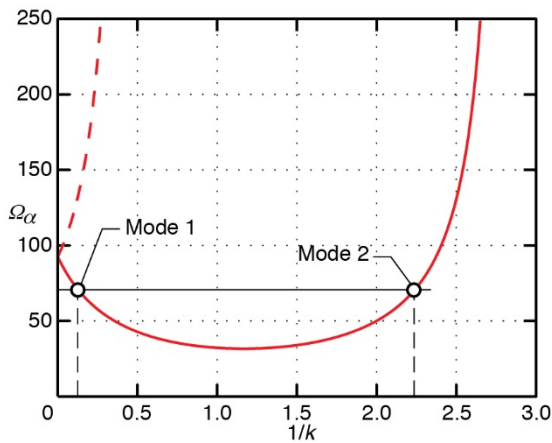
(a) Recreation of Figure 7



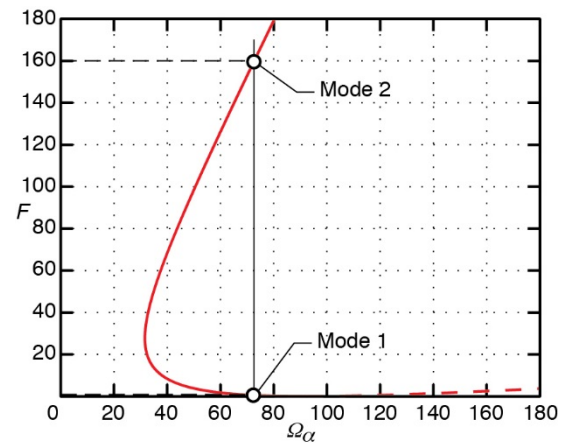
(b) Recreation of Figure 8

Figure D3 – Results from 2DOF Solution Method, Subcase 2;

$$\omega_\beta = 44.721, \omega_h = 50, r_\beta^2 = 1/160, x_\beta = 1/80, \Omega_\beta = 0.005.$$



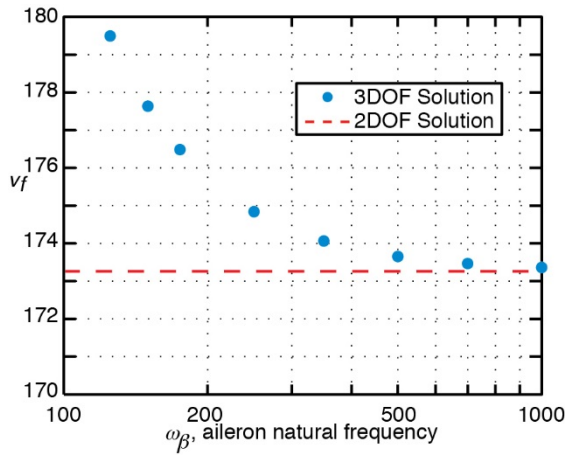
(a) Recreation of Figure 5



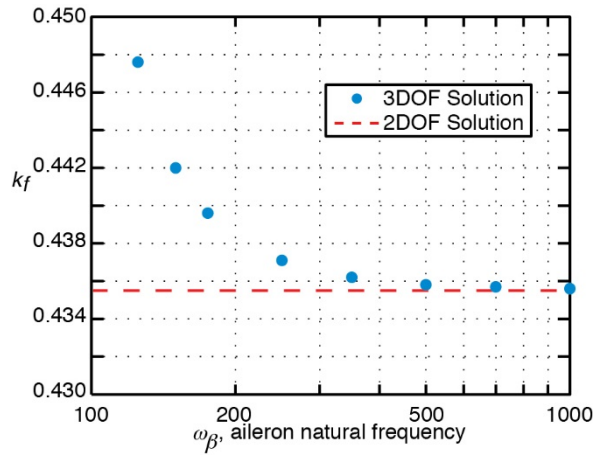
(b) Recreation of Figure 6

Figure D4 – Results from 2DOF Solution Method, Subcase 3;

$$\omega_\alpha = 100, \omega_\beta = 75, r_\alpha^2 = 0.25, r_\beta^2 = 1/160, x_\beta = 1/80, \Omega_\alpha = 71.111.$$

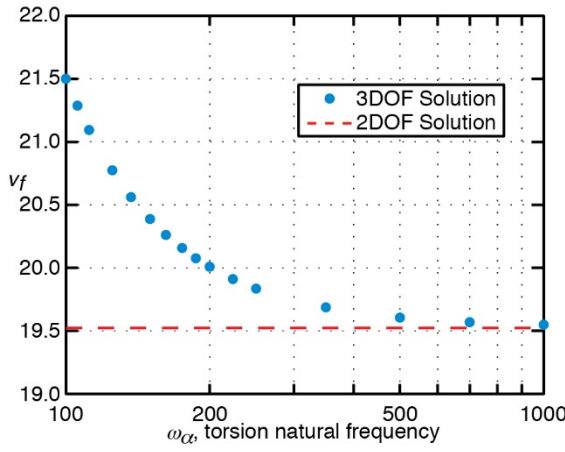


(a) Flutter velocity vs ω_β

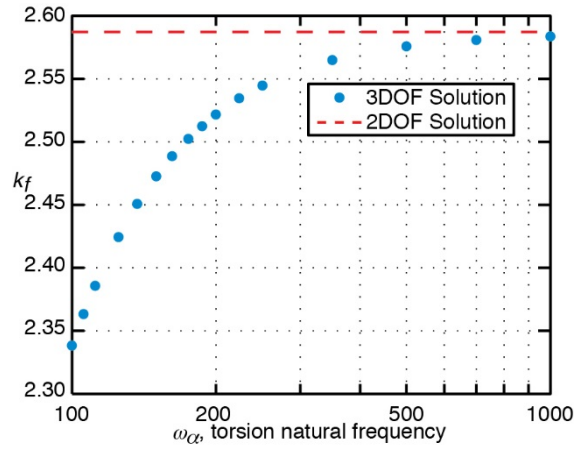


(b) Flutter reduced frequency vs ω_β

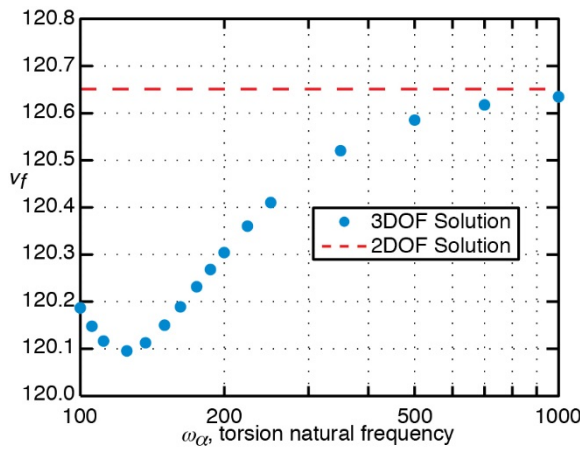
Figure D5 – Results from 3DOF Solution Method, “Subcase 1”;
 $\omega_\alpha = 100$, $\omega_h = 50$, ω_β variable, “standard case”.



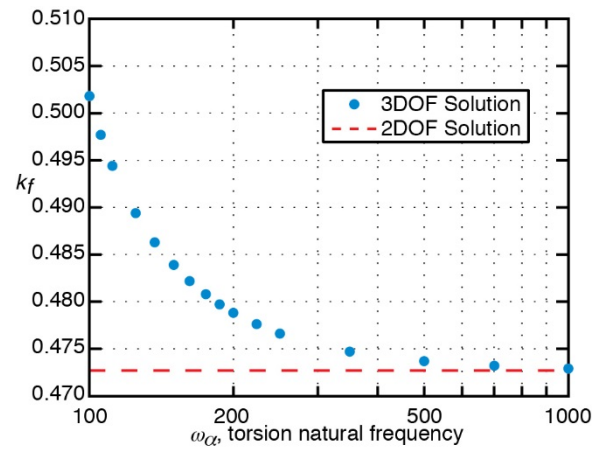
(a) Mode 1 flutter velocity vs ω_α



(b) Mode 1 flutter reduced frequency vs ω_α

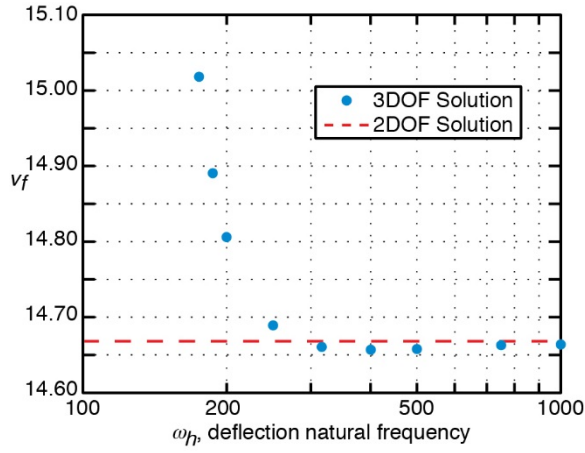


(c) Mode 2 flutter velocity vs ω_α

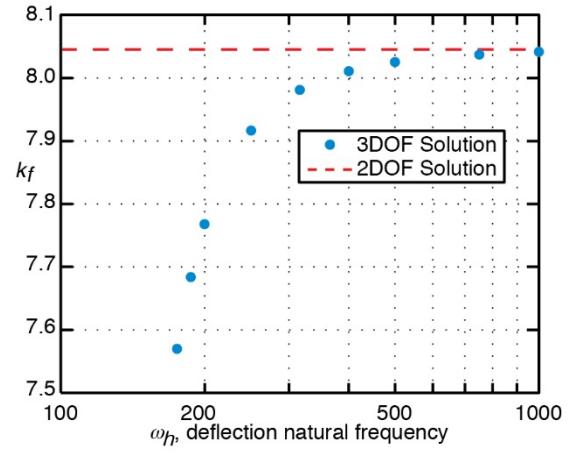


(d) Mode 2 flutter reduced frequency vs ω_α

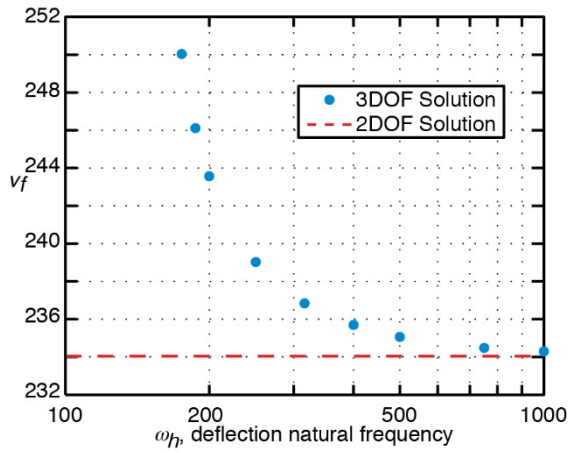
Figure D6 – Results from 3DOF Solution Method, “Subcase 2”;
 $\omega_\beta = 44.721$, $\omega_h = 50$, $r_\beta^2 = 1/160$, $x_\beta = 1/80$, ω_α variable.



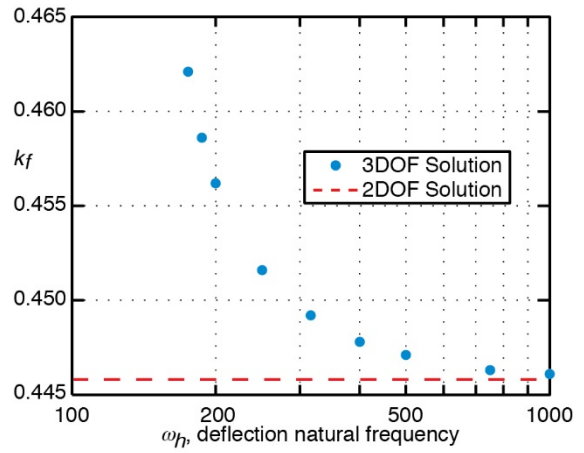
(a) Mode 1 flutter velocity vs ω_h



(b) Mode 1 flutter reduced frequency vs ω_h



(c) Mode 2 flutter velocity vs ω_h



(d) Mode 2 flutter reduced frequency vs ω_h

Figure D7 – Results from 3DOF Solution Method, “Subcase 3”;
 $\omega_\alpha = 100$, $\omega_\beta = 75$, $r_\alpha^2 = 0.25$, $r_\beta^2 = 1/160$, $x_\beta = 1/80$, ω_h variable.

REPORT DOCUMENTATION PAGE					Form Approved OMB No. 0704-0188	
<p>The public reporting burden for this collection of information is estimated to average 1 hour per response, including the time for reviewing instructions, searching existing data sources, gathering and maintaining the data needed, and completing and reviewing the collection of information. Send comments regarding this burden estimate or any other aspect of this collection of information, including suggestions for reducing this burden, to Department of Defense, Washington Headquarters Services, Directorate for Information Operations and Reports (0704-0188), 1215 Jefferson Davis Highway, Suite 1204, Arlington, VA 22202-4302. Respondents should be aware that notwithstanding any other provision of law, no person shall be subject to any penalty for failing to comply with a collection of information if it does not display a currently valid OMB control number.</p> <p>PLEASE DO NOT RETURN YOUR FORM TO THE ABOVE ADDRESS.</p>						
1. REPORT DATE (DD-MM-YYYY)		2. REPORT TYPE			3. DATES COVERED (From - To)	
01-06 - 2015		Technical Publication				
4. TITLE AND SUBTITLE Re-Computation of Numerical Results Contained in NACA Report No. 496				5a. CONTRACT NUMBER		
				5b. GRANT NUMBER		
				5c. PROGRAM ELEMENT NUMBER		
6. AUTHOR(S) Perry, Boyd, III				5d. PROJECT NUMBER		
				5e. TASK NUMBER		
				5f. WORK UNIT NUMBER 432938.11.01.07.43.40.08		
7. PERFORMING ORGANIZATION NAME(S) AND ADDRESS(ES) NASA Langley Research Center Hampton, VA 23681-2199				8. PERFORMING ORGANIZATION REPORT NUMBER L-20554		
9. SPONSORING/MONITORING AGENCY NAME(S) AND ADDRESS(ES) National Aeronautics and Space Administration Washington, DC 20546-0001				10. SPONSOR/MONITOR'S ACRONYM(S) NASA		
				11. SPONSOR/MONITOR'S REPORT NUMBER(S) NASA/TP-2015-218765		
12. DISTRIBUTION/AVAILABILITY STATEMENT Unclassified - Unlimited Subject Category 08 Availability: STI Program (757) 864-9658						
13. SUPPLEMENTARY NOTES						
14. ABSTRACT An extensive examination of NACA Report No. 496 (NACA 496), "General Theory of Aerodynamic Instability and the Mechanism of Flutter," by Theodore Theodorsen, is described. The examination included checking equations and solution methods and re-computing interim quantities and all numerical examples in NACA 496. The checks revealed that NACA 496 contains computational shortcuts (time- and effort-saving devices for engineers of the time) and clever artifices (employed in its solution methods), but, unfortunately, also contains numerous tripping points (aspects of NACA 496 that have the potential to cause confusion) and some errors. The re-computations were performed employing the methods and procedures described in NACA 496, but using modern computational tools. With some exceptions, the magnitudes and trends of the original results were in fair-to-very-good agreement with the re-computed results. The exceptions included what are speculated to be computational errors in the original in some instances and transcription errors in the original in others. Independent flutter calculations were performed and, in all cases, including those where the original and re-computed results differed significantly, were in excellent agreement with the re-computed results. Appendix A contains NACA 496; Appendix B contains a Matlab ® program that performs the re-computation of results; Appendix C presents three alternate solution methods, with examples, for the two-degree-of-freedom solution method of NACA 496; Appendix D contains the three-degree-of-freedom solution method (outlined in NACA 496 but never implemented), with examples.						
15. SUBJECT TERMS Aeroelastic stability; Flutter; NACA Report No. 496; Theodore Theodorsen						
16. SECURITY CLASSIFICATION OF:			17. LIMITATION OF ABSTRACT	18. NUMBER OF PAGES	19a. NAME OF RESPONSIBLE PERSON	
a. REPORT	b. ABSTRACT	c. THIS PAGE			STI Help Desk (email: help@sti.nasa.gov)	
U	U	U	UU	117	19b. TELEPHONE NUMBER (Include area code) (757) 864-9658	